AD

USAAVLABS TECHNICAL REPORT 65-80

INVESTIGATION OF AN ISOLATED MONOCYCLIC V/STOL PROPELLER PERFORMANCE AND OSCILLATORY STRESS

By

R. W. de Decker

12.60 C.75 122 cy

February 1966

Code 1

U. S. ARMY AVIATION MATERIEL LABORATORIES
FORT EUSTIS, VIRGINIA

CONTRACT DA 44-177-AMC-319(T)
VERTOL DIVISION
THE BOEING COMPANY
MORTON, PENNSYLVANIA

DISCLAIMERS

The findings in this report are not to be construed as an
official Department of the Army position, unless so designated
by other authorized documents.

When Government drawings, specifications, or other data are
used for any purpose other than in connection with a definitely
related Government procurement operation, the United States
Government thereby incurs no responsibility nor any obligation
whatsoever; and the fact that the Government may have formu-
lated, furnished, or in any way supplied the said drawings,
specifications, or other data is not to be regarded by impli-
cation or otherwise as in any manner licensing the holder or
any other person or corporation, or conveying any rights or
permission, to manufacture, use, or sell any patented invention
that may in any way be related thereto.

DISPOSITION INSTRUCTIONS

Destroy this report when it is no longer needed. Do not return
it to the originator.

This report has been reviewed by the U. S. Army Aviation
Materiel Laboratories and is considered to be technically
sound.

This work was performed under Contract DA 44-177-AMC-319(T)
and was undertaken to investigate the monocyclic propeller
control concept with respect to its practicality and effective-
ness as a longitudinal control device for propeller-driven V/STOL
aircraft.

INVESTIGATION OF AN ISOLATED MONOCYCLIC

V/STOL PROPELLER PERFORMANCE AND

OSCILLATORY STRESS

R-432

by

R. W. de Decker

Prepared by

VERTOL DIVISION
THE BOEING COMPANY
Morton, Pennsylvania

for

U.S. ARMY AVIATION MATERIEL LABORATORIES
FORT EUSTIS, VIRGINIA

SUMMARY

Previous tests have shown longitudinal control of tilt-wing
aircraft by means of single-axis cyclic control of rigid pro-
pellers (monocyclic pitch control) to be practical and effec-
tive. However, three aspects remained to be investigated.
These were: (1) the limitations on control power due to blade
stall, (2) the effect of control application on the power
required to hover, and (3) the effect of control system stiff-
ness on the dynamic behavior of the blades and control system.
A static test was therefore conducted, utilizing a high-solidity
monocyclic propeller model with control systems of different
stiffnesses mounted on the Cornell Apparatus for Rotorcraft
Tests (CART).

The aerodynamic test data showed that 8 degrees of monocyclic
control will provide 25-percent thrust offset in the region of
optimum propeller efficiency. The resulting control moment is
more than adequate for trim and maneuver of an agile tilt-wing
aircraft. It was found that control power remained a linear
function of cyclic angle up to the maximum tested (10 degrees),
whether the blades were partially stalled or not. The variation
of power loss with cyclic pitch is a curve of square-order
characteristics. With 2 degrees of cyclic (center of gravity
control) at a β = 13.5 degrees (hover β), the increase in power
is approximately 1 percent. The large amount of control pro-
vided by 8 degrees of cyclic pitch is for maneuver purposes and
is normally a transient. Although the increase in power is
large (approximately 10 percent), this is not a steady-state
condition.

As a guide in assessing total thrust margins required, the
results of this study combined with data on thrust losses in-
duced by yaw and roll control were analyzed. The Advisory
Group for Aeronautical Research and Development (AGARD) of
NATO (Reference 8) suggests the following requirements:

   a. Full control about one axis and half control about the
       other axes with a thrust margin (T/W) of 1.00.

   b. Half control about all axes with a T/W of 1.05.

Applying these criteria to a typical tilt-wing aircraft in the
20,000-pound weight class, and assuming MIL-H-8501A control
powers, the thrust margins required are 12.5 and 11 percent
respectively.

The test data obtained were compared with previous test results and with theory. A comparison of pitching moment from unsteady aerodynamics theory with the test data indicated that the theory was conservative by about 10 percent. The results of this test confirmed observations made during previous monocyclic tests: (1) that there is an apparent phase shift of the monocyclic axis at high collective angle, caused by hysteresis in the airfoil's stall characteristics, and (2) that there is an increase in side force as collective angle is increased, caused by a nonlinear variation in airfoil drag with cyclic pitch.

The monocyclic propeller test program also included investigation of the effects of control system stiffness on the dynamic response of the propeller and control system. The results indicate that the use of cyclic-blade-pitch control reduces the harmonic content of control system oscillatory loads to basically a first-harmonic response. Higher harmonic loads are present, but their amplitudes are less than 10 percent of the resultant peak-to-peak load, and are therefore considered negligible. The results of the program also indicate that the increase of control system stiffness resulted in an increase in blade-pitch-link oscillatory loads.

CONTENTS

ILLUSTRATIONS

LIST OF SYMBOLS

A	Disc area, ft^2
a	Section lift curve slope, 1/rad
B	Number of blades
c	Blade chord, ft
D	Propeller diameter, ft
M	Pitching moment, ft-lb
M_b	Beam bending moment, in -lb
n	Propeller rotational speed, rps
R	Propeller radius, ft
r	Blade section radius, ft
V_T	Propeller tip speed, ft/sec
V_O	Hovering induced velocity at disc, ft/sec
β	Blade angle at 0.75 radius, deg
γ	Monocyclic pitch angle, deg
Ω	Azimuth angle, deg
ρ	Density, slug/ft^3
σ	Propeller solidity = 0.254
δ	Axial deflection of blade pitch link, in
λ_o	Hovering induced velocity ratio $\dfrac{V_O}{V_t}$
C_M	Pitching moment coeff $\dfrac{P.M. @ hub}{\rho n^2 D^5}$, balance axis system
C_ℓ	Rolling moment coeff $\dfrac{R.M. @ hub}{\rho n^2 D^5}$, balance axis system

C_x Long. force coeff $\dfrac{\text{Long. Force}}{\rho n^2 D^4}$, balance axis system

C_S Side-force coeff $\dfrac{\text{S.F.}}{\rho n^2 D^4}$, balance axis system

C_T Thrust coeff $\dfrac{T}{\rho n^2 D^4}$

C_P Power coeff. $\dfrac{P}{\rho n^3 D^5}$

F.M.   Figure of merit $= 0.798 \dfrac{(C_T)^{\frac{3}{2}}}{C_P}$

$\dfrac{r}{R}$ Thrust offset $= \dfrac{(\text{P.M. @ Hub})}{(T)\quad(R)}$

T/W   Thrust margin

E   Modulus of elasticity - lb/in ^{2}

I   Moment of inertia - in ^{4}

W   Running weight - lb/in

P   Axial load on pitch links - lb

L   Pitch link length - in

Y   Deflection of pitch link due to bending - in

x   Distance along pitch link - in

INTRODUCTION

Monocyclic propeller pitch is proposed for longitudinal control of tilt-wing aircraft during hover and transition. The theoretical effectiveness of this system was substantiated in previous tests (References 3 and 4). However, three areas were not fully investigated:

1. The absolute limit of control power due to blade stall.

   During previous tests, high cyclic angles combined with high collective angles were not tested owing to structural or power limitations. However, high cyclic and collective angles are required for control of tilt-wing aircraft during hover and transition. In addition, although the very limited test data from previous tests did not show it, theory had led to the expectation that control power would become a nonlinear function of cyclic angle at high collective angles.

2. The variation of power required for hover with control application.

   Data from previous tests were inadequate owing to balance incompatibility in one test and the absence of a torque measuring device in the other test. However, data in this area are necessary because any power losses associated with control application dictate an increase in installed thrust for hover at constant altitude.

3. The effect of control system stiffness on the dynamic behavior of the blades and control system.

   VTOL propeller controls with monocyclic features have control system stiffness variation as a function of azimuth angle. Such stiffness variations can result in the amplification of higher harmonic blade loads and/or the aggravation of stall flutter. It was anticipated that a two-per-rev control system stiffness variation existed in the Vertol monocyclic control used in its tilt-wing design. However, existing analytical techniques do not account for this stiffness variation. Therefore, prediction of its effect on control system dynamic response would be difficult without static and dynamic test data on control systems with varying stiffness.

1

The present static test provides an assessment of these aspects. In addition, data on control power, in-plane forces, figure of merit, and pitch link loads were obtained. A comparison with theory or previous tests was also made where applicable.

These tests were made on a Boeing propeller designed for mono-cyclic testing. The design is generally representative of the present state of the art in VTOL propellers, from the point of view of solidity and blade geometry, but some compromises were required to adapt the blades to the existing VZ-2 hub and to stay within the available power envelope of the test facility. The propeller was mounted on the Army-Cornell Apparatus for Rotorcraft Tests (CART). The CART balance has a sensitivity compatible with the measured forces and moments. The test was conducted from 30 April to 28 May 1965, in a building larger than that used for the test of Reference 3. Comparison of runs from the latter test, made inside and outside the building, showed no recirculation effects.

The several control systems investigated in the subject test program had characteristic azimuthal stiffness variations which are described in the body of this report as one-per-rev and two-per-rev control system stiffness variations. The one-per-rev system is characterized by a stiffness variation of one complete sine wave in a 360-degree sweep (see Figures 28a and 28b). The two-per-rev system is characterized by a second-harmonic wave in a 360-degree sweep (see Figures 28c and 28d). The terminology "one-per-rev and two-per-rev control systems" will be used in this context in the following pages.

MODEL, TEST FACILITY, AND INSTRUMENTATION DESCRIPTION

MODEL

A 6-foot-diameter propeller was designed to represent the aero-
dynamic characteristics of current state-of-the-art four-bladed
17.5-foot-diameter VTOL propellers. Therefore, the model pro-
peller has high solidity (0.254) and high blade twist (26 deg-
rees). However, a number of design compromises were necessary.
A three-way VZ-2 hub was available which had been modified for
monocyclic control (by restraining the flapping hinges and by
allowing manual adjustment of collective and cyclic blade angle)
and had been adapted to the CART facility. Therefore, a three-
bladed propeller was designed with a solidity equivalent to the
four-bladed propeller. In addition, the high solidity and the
power available dictated a 6-foot diameter for the model. The
small diameter combined with the relatively large VZ-2 hub
resulted in a hub/disc diameter ratio of 0.25. Also, maximum
allowable centrifugal force loads on the control system did not
permit operation at full-scale tip speed. The maximum tip
speed that could be attained was about 60 percent of full scale.
As a consequence of these compromises, a high figure of merit
and optimum C_T/σ were not obtained. The model was, however,
entirely adequate to fulfill the objectives of this test. The
propeller geometry is shown in Figure 1, while photographs of
the hub, propeller, and control system are shown in Figures 2
and 3.

Three control system configurations were evaluated in the stress
measurement phase of the test program. Two of the systems uti-
lized the modified VZ-2 pitch links shown in Figure 4. These
links are stiffer and stronger than those used on the VZ-2
control system. The two configurations which utilized the
modified VZ-2 pitch links differed only in the mechanism for
achieving blade cyclic-pitch control. One of the two systems
had a single, rigid cyclic control link for tilting the swash-
plate, as shown in Figure 5, while the other system had a multi-
link-bell-crank arrangement for swashplate tilt control, as
shown in Figure 6. Each of these systems had identical collec-
tive control components. The third control system, with the
VZ-2 blade pitch links shown in Figure 7, had the multi-linkage
cyclic control referred to above, and had the same collective
control as utilized in the other two control systems.

Table I summarizes and identifies the three control system
configurations with which this program is concerned.

TABLE I

Configuration	Blade Pitch Link	Cyclic Control Link
A	Modified VZ-2	Single, Rigid
B	Modified VZ-2	Multi-Link
C	VZ-2	Multi-Link

The stiffness characteristics of the three control systems, as a function of azimuth position, are shown in Figure 8. The pitch and cyclic links were strain-gauged to measure loads in the control system. Strain gauges were also mounted on the blades and the hub, as shown in the following sketch, to measure blade flap bending, chord bending, and torsional stresses:

STA. 1.8 in
(FLAP
BENDING)

STA. 10.75 in
(TORSION)

STA. 18 in
(FLAP
BENDING)

STA. 24 in
(CHORD
BENDING)
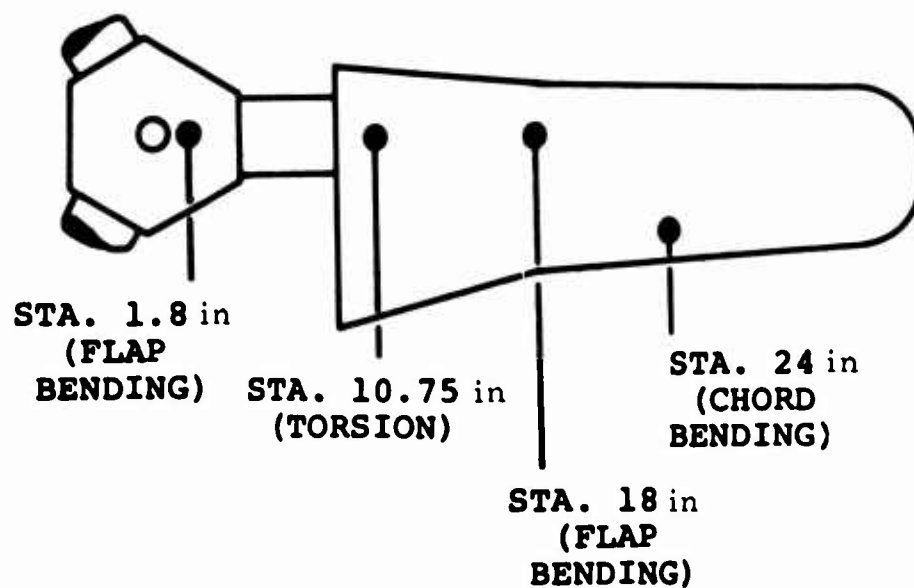
TEST FACILITY

The CART facility, on loan from USAAVLABS, was used for this test. The propeller and hub were mounted on the six-component strain gauge balances at the top of the tower which is carried on the platform of the trailer. The propeller is driven by a large automobile engine through a torque converter type transmission. The engine and transmission are located below the platform. A strain gauge Thomas coupling was inserted in the drive system to measure torque. The propeller was mounted 12 feet above the trailer and 14 feet aft of the forward end of the trailer. The trailer acts as a groundboard and measures 36 by 18 feet. For this static test the trailer was situated in a large building (100 feet wide, 100 feet high and several hundred feet long). A previous investigation (see Reference 3) has shown that recirculation is not a problem in a building of this size. General views of the CART facility are shown in Figure 9, and it is fully described in Reference 2.

INSTRUMENTATION

Force and moment data from the six-component balance and the torque flexure were recorded on the Vertol Mobile Test Facility data system. These data were recorded with both analog and digital facilities. The data system is fully described in Reference 10, and Figure 10 shows a photograph of the control console. Stress data from the blade and hub strain gauges and from the control system were recorded on oscillograph recorders. Also recorded were propeller rpm and collective and cyclic angles. Pressure and temperature were recorded to provide density correction information for aerodynamic data.

TEST PROCEDURE

Prior to the start of the test, the static spring rate of the control system with varying degrees of stiffness was determined. To accomplish this, a torque loading was imposed on the root end of a blade, which in turn was reacted by the specific control system. Figure 6 shows a typical test setup, with the rotor and the rotor controls fixed to a rigid stand, and with a wooden yoke for imposing a torque load installed on the root end of a propeller blade. When the blade was rotated to the specified azimuth position (through 360 degrees in 30 degree increments), the loading device was also rotated to maintain proper load alignment with the torque arm. Angular blade motions (about the blade pitch axis) were monitored at the 75-percent blade radius position with an inclinometer. The azimuth variation of control system stiffness was determined in the above mentioned manner for three torque loads: 600, 1200, and 1800 inch-pounds. For each of these torque loads, the effect of collective control settings was determined at 8, 12, and 16 degrees. Pitch control inputs were 0, 2, and 4 degrees, at each of the aforementioned collective settings.

In addition, the six-component strain gauge balance, the torque flexure, the hub and blade strain gauges, and the control system strain gauges were calibrated. Also, the blades were "tracked" to ensure that all blades were subjected to the same aerodynamic loading. This was accomplished by adjusting blade angle of attack (adjusting blade pitch link length) until the mean loads on the three pitch links (each of which was instrumented for this portion of the program) were approximately equal. After completing the blade tracking procedure, load data was acquired for only one blade pitch link so that the other two pitch link channels could be made available for monitoring additional blade cyclic stress data.

A data run consisted of one collective and one cyclic angle at various rpm up to 1900 rpm. At high collective angles, testing was limited to a maximum of 1700 rpm because of limited torque output of the engine and structural limitations of the control system. Collective angles from 8 to 22 degrees and monocyclic angles from -2 to +10 degrees were investigated during that part of the test for which both aerodynamic and stress data were obtained. During the other part of the test, for which only stress data were recorded, collective angles from 10 to 20 degrees and cyclic angles from 0 to 6 degrees were used.

6

The following two tables (II and III) summarize the combinations of parameters tested:

TABLE II		
Collective Blade Angle	Cyclic Blade Angle	Propeller RPM
8°, 10°, 12°, 14° 16°, 18°, 20°, 22°	-2°, 0°, 2°, 4°, 6°, 8°, 10°	1500, 1700 1900*
(Both aerodynamic and stress data were measured at these data points)		
*1900 RPM could not be attained at the highest collective blade angles, due to stress limitations.		

TABLE III		
Collective Blade Angle	Cyclic Blade Angle	Propeller RPM
10°, 14°, 18°, 20°	0°, 6°	1500 - 2300*
(Stress data only were measured at these data points)		
*Except as limited by available power and allowable stresses.		

During a data run, aerodynamic forces and moments were measured, as well as the torque required to drive the propeller. Pitch link cyclic loads were recorded, and data were monitored at critical blade stations about several mutually perpendicular

7

bending axes to ensure that the maximum safe stress limitations were not exceeded.

The collective and cyclic angles were set using an inclinometer and a template. The rpm was set with a tachometer attached to the rotor head, and was allowed to stabilize a few seconds before data were recorded.

Inspection of the forces and moments under no-load condition showed the presence of small cyclic in-plane forces. These were thought to be caused by imperfect alignment of the Thomas coupling in the final drive system. For this reason, four digital punch cards and four oscillograph recordings were taken under no-load conditions before and after each data run,with the number 1 blade at 0-, 90-, 180- and 270-degree azimuth angles. Dummy load resistors were used to check the calibration of the strain gauges before and after each run.

DISCUSSION OF RESULTS - AERODYNAMIC

GENERAL

The aerodynamic results of this test consist of moment, force, and power derivatives, due to the application of monocyclic pitch control. The range of collective pitch angles investigated was sufficient to include partial stall. The range of monocyclic angles investigated was sufficient to evaluate the effect on power requirements. The tests were made with the propeller plane two diameters above the ground board. As is indicated in Reference 5, ground effect is negligible at this height.

All moments and forces were nondimensionalized by the method outlined in Reference 4. Moment data are also presented in terms of thrust offset $\left(i.e., \dfrac{r}{R} = \dfrac{\text{Pitching Moment}}{(\text{Thrust})(\text{Radius})} \right)$

All moment data were resolved about the propeller hub. The relationship between the propeller axis system and the balance is shown in Figure 11.

A digital computer program (Reference 7) was used to reduce the raw data obtained from the data system.

BASIC PROPELLER CHARACTERISTICS

Data on the aerodynamic characteristics of the propeller were obtained at zero-degree monocyclic angle and at collective angles from 8 to 22 degrees. Curves of propeller power and thrust coefficient are presented in addition to a plot of figure of merit as a function of $C_T/_\sigma$, as shown in Figures 12, 13, and 14.

While the model propeller design was based on a full-scale propeller of high figure of merit and design $C_T/_\sigma$, the model propeller performance predicted with the recently developed method of Reference 6 (including the effect of the compromises discussed in the model description) was substantially below that of the full-scale propeller. This has been borne out by the test results. The optimum $C_T/_\sigma$ was found to be 0.575. The measured figure of merit at this $C_T/_\sigma$ was found to be 0.695. The preceding information is shown in Figure 14. The curvature of C_T versus β, as shown in Figure 12, indicates the onset of blade stall above approximately 17 to 18 degrees of collective angle.

9

A comparison was made with the previously mentioned theory. Theoretical characteristics, with a correction factor caused by the inboard shift of the tip vortexes, due to rounded blade tips, are optimistic by about 10 percent at optimum blade efficiency, as is shown in Figures 12 and 14. Theory predicted the correct C_T/σ for maximum figure of merit, as shown in Figure 14. However, theory did not indicate blade stall until 22 degrees collective was reached, as shown in Figure 12.

MONOCYCLIC CONTROL CHARACTERISTICS

Curves of pitching moment, rolling moment and side-force coefficient resolved about the propeller hub are shown in Figure 15 as a function of cyclic angle for each of the collective angles tested. Longitudinal force is not shown because it was found to be negligible, as predicted by theory and as shown in References 3 and 4. Thrust coefficient as a function of cyclic angle for each collective angle tested is shown in Figure 16. Power coefficients and figure of merit as functions of cyclic angle for each collective angle tested are given in Figures 17 and 18, respectively.

Pitching Moment

The pitching moment curves presented in Figure 15 show little scatter and good linearity. It should be noted that at high collective angles there is no decrease in pitching moment as cyclic angle is increased (i.e., control power is a linear function of cyclic angle throughout the range of collective angles tested), even though the blades are partially stalled, as is evidenced by the sharp drop in figure of merit at these high collective blade angles. This is contrary to expectation, although the same phenomenon was observed in the test of Reference 3. In an effort to explain this, it is hypothesized that the high-frequency variation of the blade angle of attack (approximately 30 cycles per second) delays the onset of stall of a blade section that is initially not stalled, but that a section that is initially stalled will remain stalled when cyclic control is applied. Thus, at high collective angles where the blades are partially stalled (as evidenced by Figure 12), blade sections remain in their original separated or unseparated flow state. As a consequence, control power is a linear function of cyclic angle, and the thrust remains unchanged throughout the cyclic angle range.

As good linearity was encountered, a plot of dC_M/d_γ versus $C_T/_\sigma$ is presented in Figure 19. This figure also shows a comparison with theory. The theory is derived in Appendix I of this report, using the unsteady aerodynamic factor derived in Reference 1.

As was shown in Reference 3, the theory is conservative in the present test by approximately 10 percent. Figure 20 presents a comparison of $C_{M\gamma}$ versus $C_T/_\sigma$ from the present test and the test reported in Reference 3. The general shape of the two curves is the same, as is the maximum value. A lack of available power prevented testing at values of $C_T/_\sigma$ where, as was shown in the test of Reference 3, $C_{M\gamma}$ starts dropping off very rapidly.

Monocyclic control cycles the blade angle once per revolution to increase the blade angle on one side of the axis about which a moment is desired and decrease the angle on the other. This produces an increase of thrust on one side of the propeller and a decrease on the other side, thus effectively offsetting the thrust towards the side of the maximum cyclic input. This offset may be expressed as a percentage of the radius. Thrust offset in percent radius as a function of cyclic angle is presented in Figure 21 for each collective angle tested, and summarized in Figure 22. These data were also derived from theoretical considerations in Appendix I, and are plotted in Figure 23. The desired 25-percent thrust offset can be attained with about 8 degrees of cyclic control in the optimum operating range of the propeller (14-degree collective angle). However, 25-percent offset can still be obtained at 20-degree collective blade angle, which is in the region where the blade has partially stalled. A comparison with theory indicates that the theory is very conservative.* There are two reasons for this. First, the moment is calculated from the theory of Reference 1 and is therefore about 10 percent lower than the actual moment measured.

---

* (This theory employs the theory used in developing the expression for $C_{M\gamma}$ and the one described in the Basic Propeller Characteristics section.)

Second, the thrust is calculated from the theory presented in Reference 6 which, without the blade tip correction factor, gives results about 20 percent higher than the test results, as shown in Figure 12. Then, dividing one by the other to obtain the moment offset, the theory may be expected to predict about 70 percent of the measured offset. This is indeed the case.

Rolling Moment

The rolling moment curves shown in Figure 15 depict good linearity, though some scatter is evident. The scatter is thought to be caused by side-to-side shaking of the tower. This is induced by imperfect alignment of the Thomas coupling in the final drive system. As reasonable linearity was found, the slopes (dC_ℓ/d_γ) were plotted against C_T/σ as shown in Figure 24. The presence of a rolling moment causes an effective shift in monocyclic axis phase angle. This is plotted in Figure 25 as a function of C_T/σ. This figure shows that there is no phase angle shift until blade stall is approached. Then, an apparent lead of the aerodynamic moment to the cyclic input develops. This is probably due to hysteresis in the blade's lift versus angle-of-attack characteristics. As blade angle increases from the zero cyclic position, stall occurs on a portion of the blade. However, as the disturbance is extremely rapid, stall is not fully developed until some time after the point of maximum cyclic input. Also, as the blade angle decreases after the maximum cyclic input is reached, the maximum lift coefficient is not reestablished. This results in an asymmetry of the cyclic blade lift and the apparent lead. The trend was also noted in Reference 3.

Side Force

The side-force coefficient is shown as a function of monocyclic angle in Figure 15. Considerable scatter, evident in this figure, is generated by the same misalignment that caused scatter in the rolling moment data. The slope of dC_s/d_γ is plotted against C_T/σ, as shown in Figure 26. This was done to establish the trend shown in Reference 3, and was predicted by theory. As was found in Reference 3, when the thrust is increased, side force increases too while magnitude of this side force is approximately 1 percent of the thrust per degree of cyclic. The side-force component is caused by the drag increase of the blade with increasing cyclic angle (and therefore the

12

blade lift) and the drag decrease of the blade with decreasing cyclic angle.

Thrust

Thrust coefficient as a function of cyclic angle is shown in Figure 16 for each collective angle tested. The considerable scatter was due to binding in the Thomas coupling splines which prevented free movement of the propeller in the vertical direction. It was found that increasing torque aggravated the binding. As a consequence, at high collective angles (which required high torque inputs) the thrust coefficient decreases as cyclic control is applied, because increased cyclic angle requires an increase in torque. This causes the C_T versus γ plot to behave as if monocyclic control causes thrust losses. Unfortunately, the true reason for this thrust decrease (i.e. binding of the splines) was not discovered until late in the test program. Therefore, it was possible to repeat only a limited number of test points. These test points are the solid symbols on the 16- and 18-degree collective curves of Figure 16.* An examination of these points and the test data for 20- and 22-degree collective angle (which were obtained after the binding splines were discovered) shows that at 16-degree collective, $dC_T/d_\gamma = +.0008$, at 18- and 20-degrees collective, $dC_T/d_\gamma = 0$, and at 22-degrees collective, $dC_T/d_\gamma = -.001$.

However, it should be noted that when testing at a 22-degree collective angle it was found impossible to eliminate all binding. Thus, on the basis of this somewhat limited data and the more complete data for 8-, 10-, 12-, and 14-degree collective angles, it must be concluded that the thrust is <u>not</u> affected by the application of monocyclic control (i.e. $dC_T/d_\gamma = 0$) at constant propeller rpm and collective angle. This confirms the test results of Reference 4.

Power Requirements

The effect of monocyclic control on power required is shown in Figure 17. This figure shows that power required increases

---

*Solid symbols are used here to distinguish test points obtained after the binding splines were discovered. However, as the binding splines did not affect any of the other quantities measured, solid symbols are not used elsewhere.

with control application. Also shown is the monocyclic angle
required to maintain 10-, 15-, 20-, and 25-percent radius thrust
offset. From this it can be seen that to maintain constant
thrust with a 25-percent thrust offset and 14-degree collective
blade angle (the approximate optimum blade angle), requires an
8-degree monocyclic angle and about a 16-percent power increase.
Figure 27 shows what this power requirement means in terms of
installed thrust margin required to maintain a thrust/weight
ratio of 1.0 (i.e. the thrust margin required to apply cyclic
control without losing altitude) as a function of β and desired
thrust offset. Figure 27 then shows that if 25-percent offset
is desired at the previously mentioned optimum collective blade
angle ($\beta = 14$ degrees), an 11.8-percent thrust margin is re-
quired to compensate for the power losses and remain at a con-
stant altitude. It also shows that to meet MIL-H-8501A pitch
requirements, a 5.8-percent thrust margin is required for a
typical tilt-wing aircraft in the 20,000-pound-design-gross-
weight class. The same increase in power required is also
reflected in a decrease of propeller figure of merit, as shown
in Figure 18. Scatter is present because there was scatter in
the thrust data for reasons explained previously. It can be
seen that if 25-percent thrust offset is demanded in the region
of optimum propeller efficiency, the figure of merit will
decrease from about 0.69 to about 0.55. This decrease is due
entirely to the increased power required, and not to a decrease
in thrust.

DISCUSSION OF RESULTS - STRESS

DISCUSSION

The data acquired during the static tests were plotted as applied torque versus blade angular deflection for each of the azimuth positions (0 to 360 degrees in 30-degree increments). The resultant curves were straight lines. This indicates that control system configurations A and B had linear spring rates, as shown in Figure 8. However, these straight lines did not pass through the origin (0 torque at 0 angular deflection). This may be explained by the fact that "slop" was present in each of the systems and that some pre-load was needed to eliminate this "slop".

The slopes of the straight lines were measured and plotted versus azimuth position. Since the slopes are measures of the spring rates, a relationship was obtained and plotted for the variation of spring rate as a function of azimuth position. The graphs of Figure 28 show the influence of cyclic-pitch link support of the swashplate at the 90-degree azimuth position, and the collective pitch trunnion support of the swashplate at the 0-degree and 180-degree azimuth positions.

Torque-displacement slopes versus azimuth position graphs for configuration B show that a two-per-rev is present. There are no definite trends due to collective- or cyclic-pitch settings. The scatter present is due to small differences between large numbers, since the spring rate has been measured in units of inch-pounds per degree of deflection, with the measured deflection of 20 minutes with an applied torque of 1200 inch-pounds. This explains why, in general, the spring rate at 0 degrees does not correspond with that at 360 degrees. These figures also show that the spring rate is higher at 90 degrees than at 270 degrees. The reason for this is that the expanse of unsupported swashplate is greater at 270 degrees than at 90 degrees and, therefore, has a greater tendency to deflect when under load. A harmonic analysis performed on a representative graph showed a dominant two-per-rev with a strong one- and four-per-rev.

HARMONIC	1	2	3	4	5	6
In-lb/Deg	255	1196	92	220	31	95

From the graphs of torque-displacement slopes for control con-
figuration A, it can be seen that a predominant one-per-rev is
present with a two-per-rev superimposed on it. A harmonic
analysis performed on a representative graph verified this, and
it also showed a strong three-, four-, and five-per-rev.

HARMONIC	1	2	3	4	5	6
In-lb/Deg	632	127	193	165	167	13

Again, there are no definite trends due to collective- or
cyclic-pitch settings. Scatter is present for the same reason
as for Configuration B. Comparison of the two control system
configurations shows Configuration A to be stiffer than Con-
figuration B. This can be attributed to the fact that the
relatively rigid single cyclic link is stiffer than the series
of seven links used to produce cyclic pitch in Configuration B.
It can also be seen that at 270 degrees both systems have about
the same stiffness. Since both systems use the same collective
link, this would be expected. However, from 0 to 180 degrees
the single cyclic linkage is stiffer because it is more effec-
tive in inhibiting the deflection of the swashplate than the
series of seven links used in the multi-linkage system. At
the 0-degree azimuth position, there is no significant differ-
ence between the two systems, since the spring rate of the
system is determined by the gimbal supporting the swashplate,
and it is identical for both cases.

PARAMETRIC STUDY

A parametric analysis was performed on the recorded pitch link
loads to determine the effect of collective pitch, cyclic pitch,
and rpm on pitch link loads. From past experience, it was
known that cyclic-pitch link loads varied with cyclic-pitch
setting and with propeller rotational speed in the following
manner:

$$\text{P.L.L.} = c \times (\gamma)^X \times (rpm)^Y$$

where c = constant

Pitch link loads were plotted versus γ on log-log graph paper
holding β and rpm constant. The resultant curve was a straight
line, and its slope was measured. Figure 29 shows typical
curves. This slope is the exponent "X" of γ in the equation
for pitch link load. This same procedure was carried out for
propeller rotational speed in order to determine the exponent

16

"Y". See Figure 30 for typical curves. Figure 31 shows that
β has no effect upon cyclical loads. This was done for the
three control system configurations. The expression above was
solved for the constant term, and the conditions of several
runs were substituted into the equation to obtain the value of
the constant term. For the cyclic loads, each run gave approx-
imately the same value of "c". The steady loads did not give
as good agreement. Resultant equations of cyclic pitch link
load for the three control systems are as follows:

1. Cyclic Pitch Link Loads

$$P.L.L. = 9.4 \times 10^{-6} \; (\theta_1)^{\frac{1}{2}} \times (rpm)^2 \quad \theta_1 > 0$$

<div align="right">Configuration C</div>

$$P.L.L. = 9.4 \times 10^{-6} \times (rpm)^2 \quad \theta_1 = 0$$

$$P.L.L. = 12.3 \times 10^{-6} \times (\theta_1)^{\frac{1}{2}} \times (rpm)^2 \quad \theta_1 > 0$$

<div align="right">Configuration B</div>

$$P.L.L. = 12.3 \times 10^{-6} \times (rpm)^2 \quad \theta_1 = 0$$

$$P.L.L. = 13.5 \times 10^{-6} \times (\theta_1)^{\frac{1}{2}} \times (rpm)^2 \quad \theta_1 > 0$$

<div align="right">Configuration A</div>

$$P.L.L. = 13.5 \times 10^{-6} \times (rpm)^2 \quad \theta_1 = 0$$

Since the constant "c" is a function of stiffness, it would be
expected that the values of "c" would increase with increasing
system stiffness. This is borne out in the final equations.

During the dynamic test, an attempt was made to induce stall
flutter. However, owing to stress and power limitations the
attempt was not successful.

BLADE PITCH LINK STIFFNESS

Both blade pitch link configurations used in the test were put
in compression in an axial load tester to determine their spring
constant. The maximum compression load applied was approxi-
mately equal to the maximum compression load experienced by the
pitch links in the dynamic test (mean plus cyclic). It was
determined that the spring constant of the VZ-2 pitch link was
67,000 pounds per inch, while that of the modified pitch link
was 117,000 pounds per inch. This means that if an axial load
of 300 pounds is applied to the pitch links, the VZ-2 pitch
link will deflect 0.0044 inch and the modified pitch link 0.0025
inch. The difference of 0.0019 inch is the additional deflec-
tion experienced by control system Configuration C in comparison

with Configuration B. It should be noted that, due to considerable "slop" in the modified pitch link, the spring constant is linear only when the "slop" has been removed. This occurs when the load is approximately 75 pounds. The results of the compression test on the pitch links are shown in Figure 32. Choosing a representative condition, such as 8-degree collective setting and 0-degree cyclic setting, the angular deflection from the static test is 24 minutes. This corresponds to a deflection of 0.0279 inch for the entire control system. The increase of deflection due to use of the VZ-2 pitch links is relatively insignificant when compared to the total deflection.

From this it could be concluded that the mean loads on the two systems (same lower controls) should be the same. However, this is not borne out in the results of the dynamic test program. The mean loads in the modified pitch links were considerably higher than those in the VZ-2 pitch links.

An analysis was made to determine the axial deflection of the two blade pitch links under consideration (VZ-2 and modified) when subjected to the centrifugal force experienced during a typical data run in the hover program. The analyses are shown in Appendix II of this report and are concerned with runs 220 and 328. Under the same hover conditions, the axial deflection of the VZ-2 pitch link was determined to be 0.016 inch, while the modified pitch link deflected only 0.006 inch. The differential blade angular rotation between the two pitch link configurations is approximately 0.15 degree, with the VZ-2 configuration being at a lower angle of attack than the modified configuration. This accounts for the lower mean load in the VZ-2 blade pitch links under the same operating condition as the modified pitch links.

A 24-point harmonic analysis was performed on the raw data of pitch link loading which had been recorded on tape by an oscillograph. The results of the analysis are shown in Figure 33, where percent harmonic load refers to the magnitude of the individual harmonic divided by the resultant oscillatory load. The charts show variation of harmonic content with rpm, cyclic pitch, and collective pitch. It can be seen that, with no cyclic control input, the harmonic loading in the blade pitch link is greatly influenced by azimuthal control system stiffness variation. A one-per-rev control system produces strong first-harmonic loads while a two-per-rev control system produces strong second-harmonic loads. Addition of cyclic-pitch blade control motions produces a predominantly one-per-rev harmonic

18

loading, even with a two-per-rev control system. Harmonic loads greater than the first are, for all practical purposes, unaffected by rotational speed, cyclic-pitch angle, and collective-pitch angle.

An analysis of the blade pitch link load data was made to determine modal response frequencies. The relative harmonic load content was studied as a function of rotational speed. A band of response frequencies was established for the first several elastic torsion modes of the control system shown in Figure 34. Included in the above figures are the upper and lower limits of the control system natural frequency. This was determined by a theoretical analysis utilizing the spring rate limits of the control systems with which this program is concerned.

The relative harmonic content of the blade pitch link load was considered on the basis of amplitude trends of each harmonic as functions of rotational speed. Also each harmonic was considered in relation to its magnitude relative to adjacent harmonics. If a particular harmonic load was of significant amplitude relative to the largest harmonic load (about 25-30 percent was considered significant), a vertical bar of influence was placed on the natural frequency spectrum chart at the proper operating rotational speed and the harmonic line under consideration. The length of the bar was dependent on the magnitude of adjacent harmonic loads in relation to the harmonic load under consideration. If significant influence is felt on second and third harmonic loads, then the bar would include these two harmonic lines on the spectrum chart.

All three control systems under consideration in this study were found to have a first torsional response mode of approximately the same frequency.

CONCLUSIONS

The principal conclusions of this investigation are:

1. Using a typical tilt-wing propeller, monocyclic
    control is an effective means of controlling pitch
    attitude, since at least 25-percent thrust offset
    could be maintained beyond the onset of blade stall,
    as shown in Figure 22.

2. The measured pitching moments substantiate those
    predicted by theory and, in fact, exceed the pre-
    diction by about 10 percent in the optimum opera-
    ting region of the propeller.

3. The propeller was tested well beyond the onset of
    blade stall and no serious reduction in control
    power was found, while control power available
    remained a linear function of monocyclic deflec-
    tion, as shown in Figure 22.

4. Application of monocyclic control does not affect
    thrust at constant propeller rpm and collective
    blade angle. However, an increase in power is
    required to maintain rpm. The total effect on net
    thrust of control application about all three
    axes is presented in Appendix III. The pitch
    control thrust loss referred to is that which occurs
    as a result of the reduction in collective blade
    angle required to maintain constant rpm at con-
    stant power, when cyclic is applied.

5. The findings of this test are substantially in
    agreement with all previous tests and relevant
    theory in the area of pitching moment, rolling
    moment, and side force derivatives due to mono-
    cyclic control application.

6. An increase in control system stiffness will
    produce a corresponding increase in the mean
    load response of the blade pitch link.

7. The harmonic loading in the blade pitch link is
    greatly influenced by the azimuthal control
    system stiffness variation with no cyclic control
    input. A one-per-rev control system produces strong

first-harmonic loads, while a two-per-rev
control system produces strong second-harmonic
loads.

8. The addition of cyclic-pitch blade-control motions
   produces a predominantly one-per-rev harmonic load-
   ing, even with a two-per-rev control system.

9. For the test blade-control system under consider-
   ation, the oscillatory pitch link loads vary as
   the square root of the cyclic blade angle and as
   the square of the rotational speed.
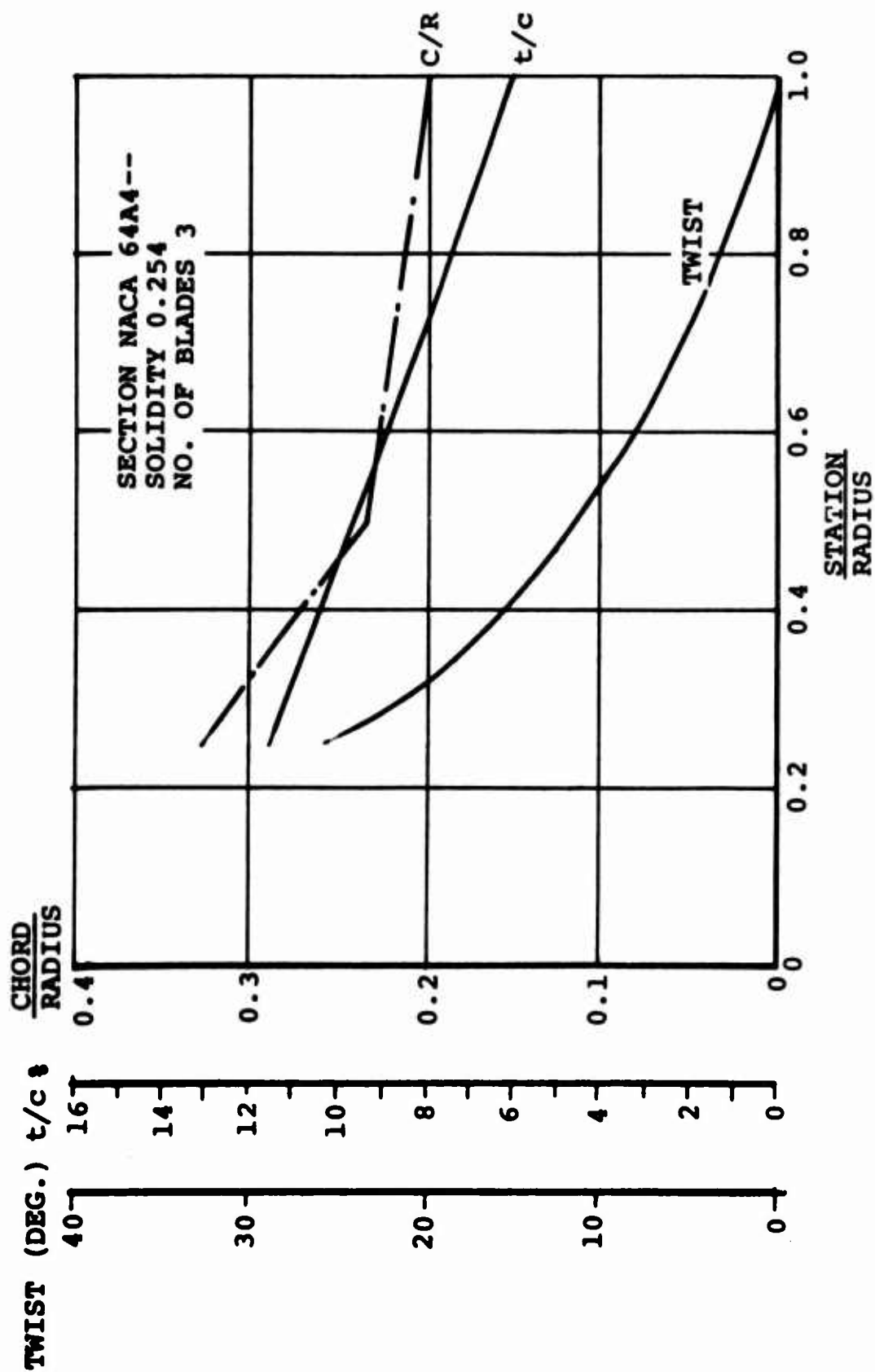
FIGURE 1. BLADE GEOMETRY.
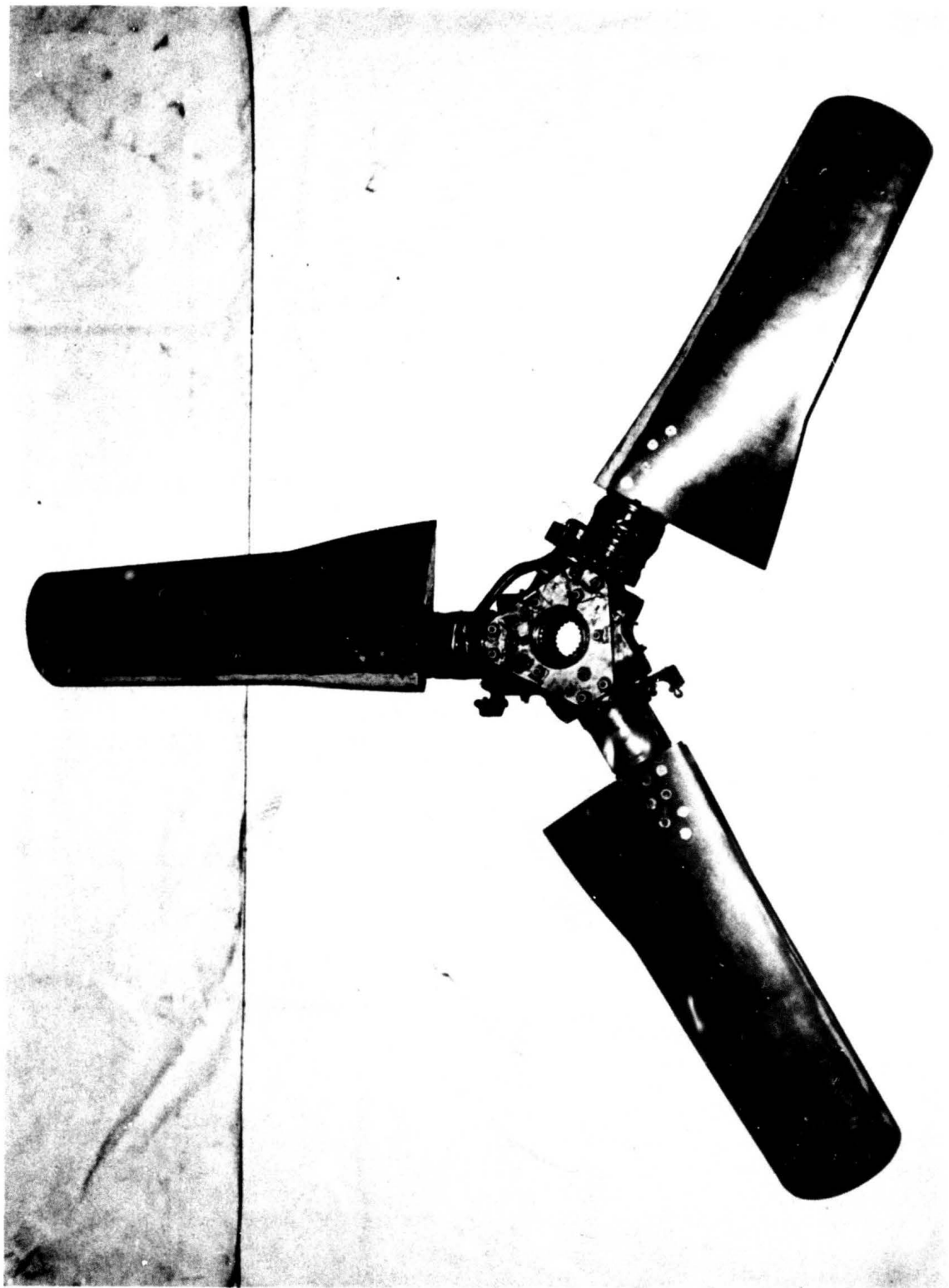
FIGURE 2. SIX-FOOT-DIAMETER MONOCYCLIC TEST PROPELLER.

23
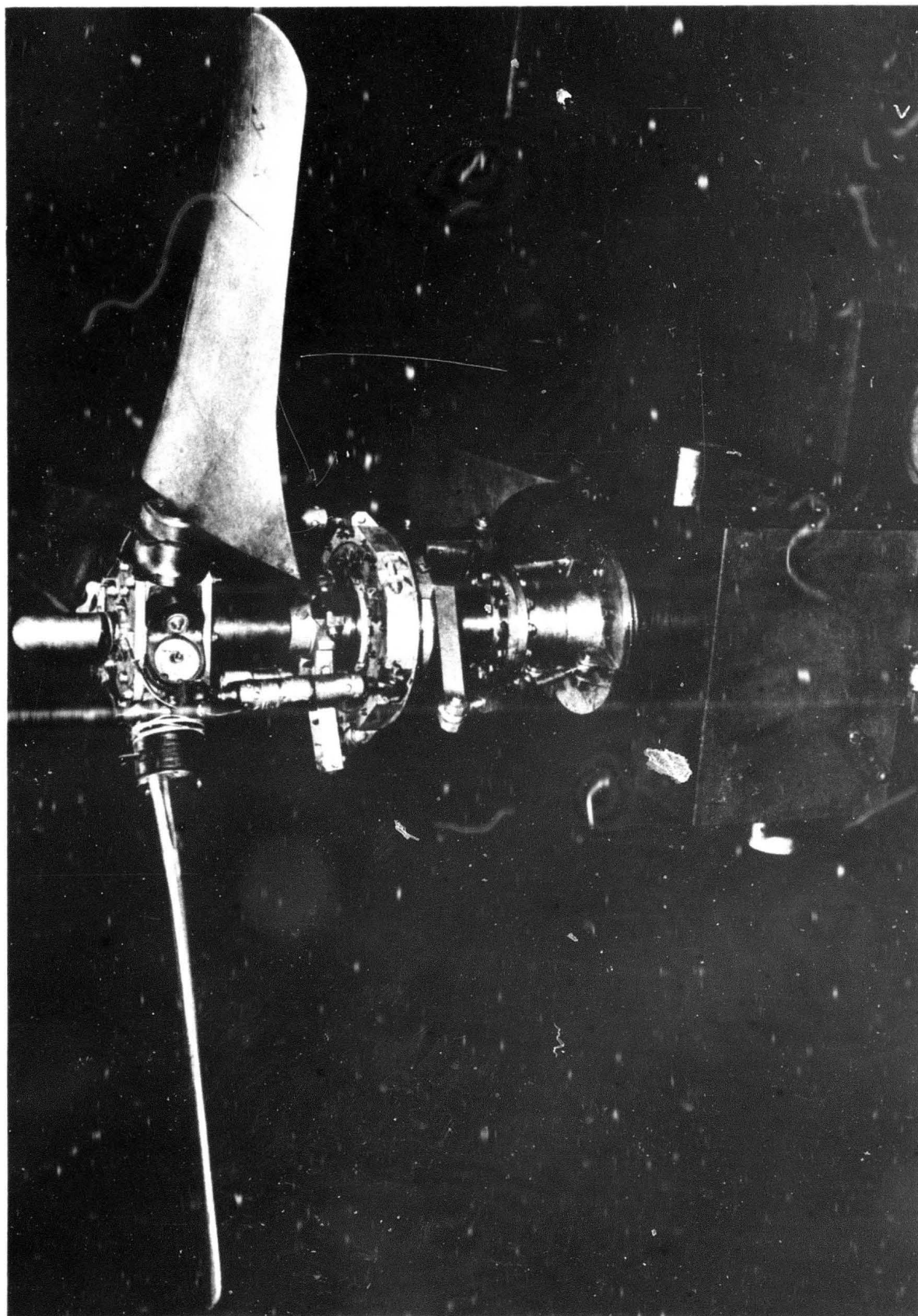
FIGURE 3. SIX-FOOT-DIAMETER MONOCYCLIC TEST PROPELLER, HUB, AND BALANCE.

24

NOT TO SCALE

6.25

$1\frac{1}{2}$ x .049

2024-T4
ALUM. TUBE

℄ P.L.
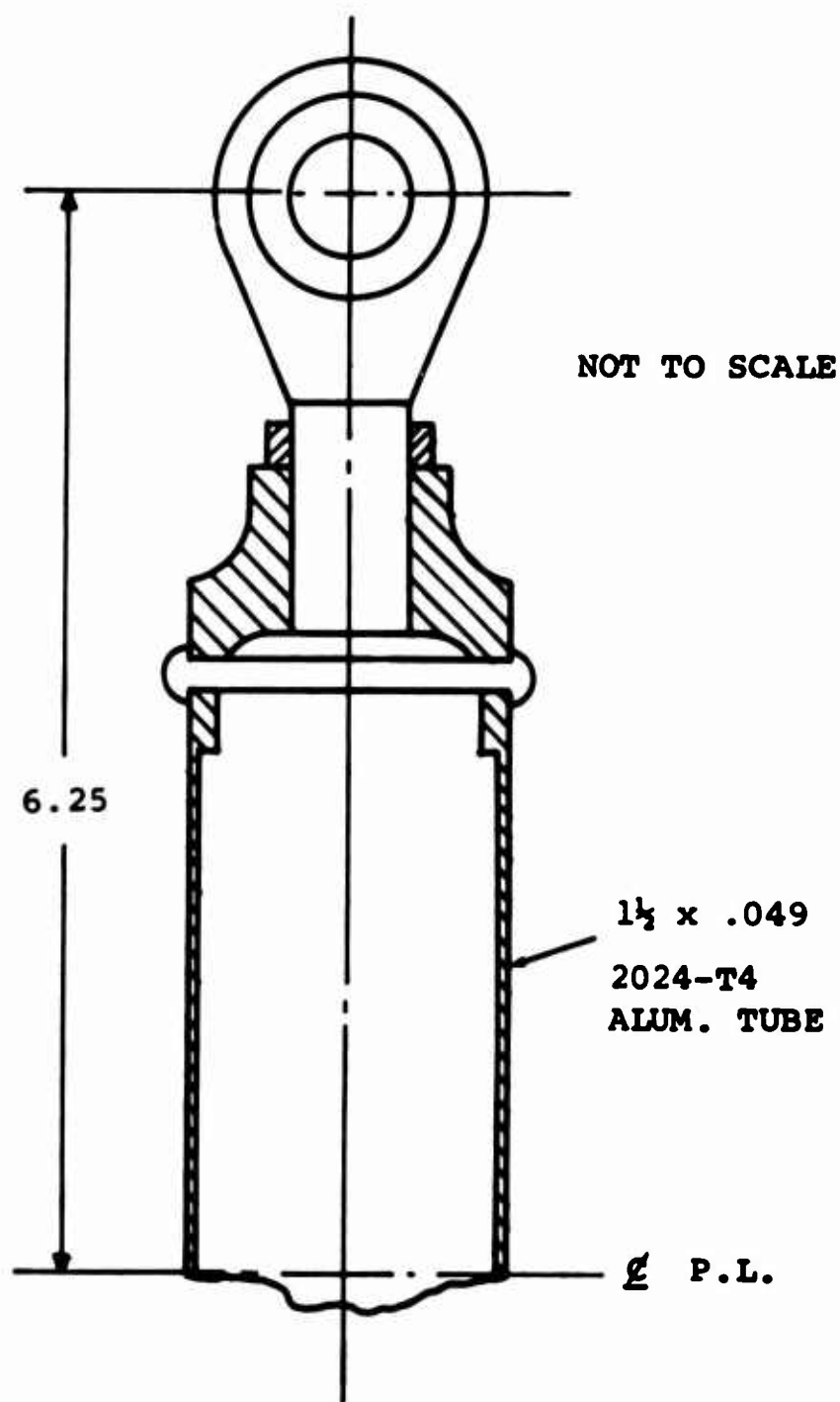
FIGURE 4. MODIFIED VZ-2 PITCH LINK.
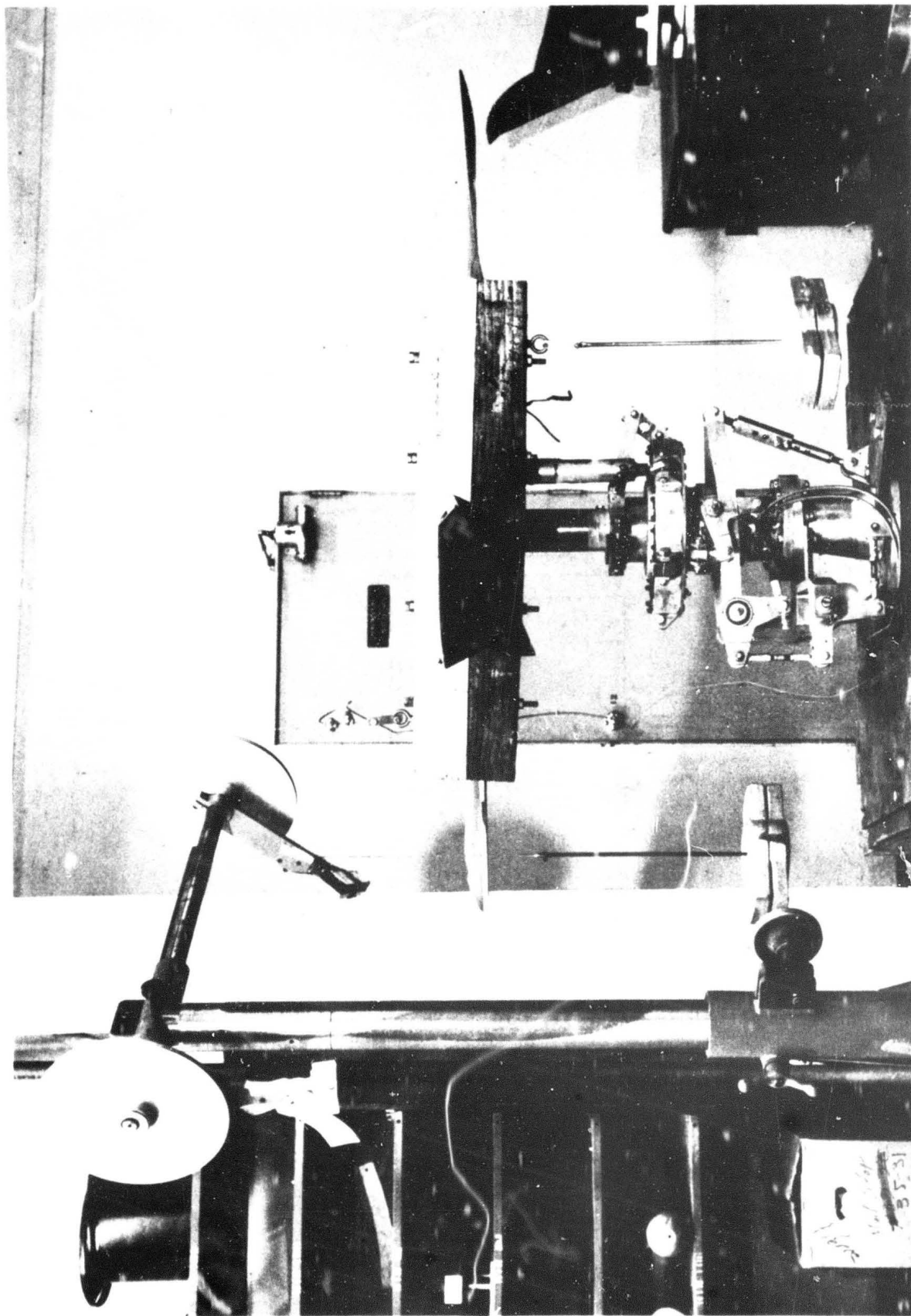
FIGURE 5. MONOCYCLIC TEST PROPELLER WITH SINGLE RIGID CYCLIC LINK AND MODIFIED VZ-2 PITCH LINKS.

26
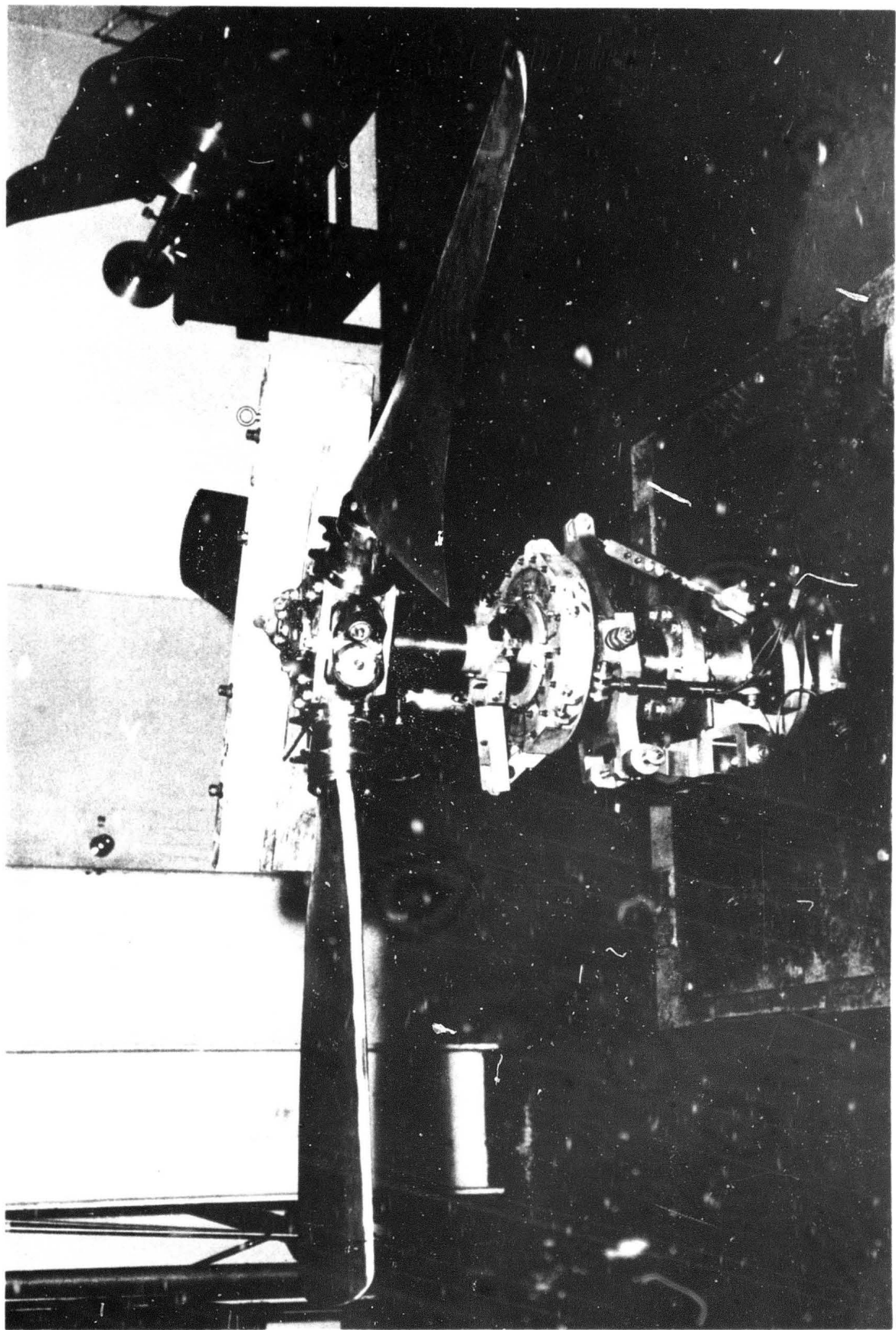
FIGURE 6. MONOCYCLIC TEST PROPELLER WITH MULTI-LINK-BELL-CRANK CYCLIC CONTROL AND MODIFIED VZ-2 PITCH LINKS.

27

6.1

3/4 x .049
2024-T3
ALUM. TUBE

₵ P.L.
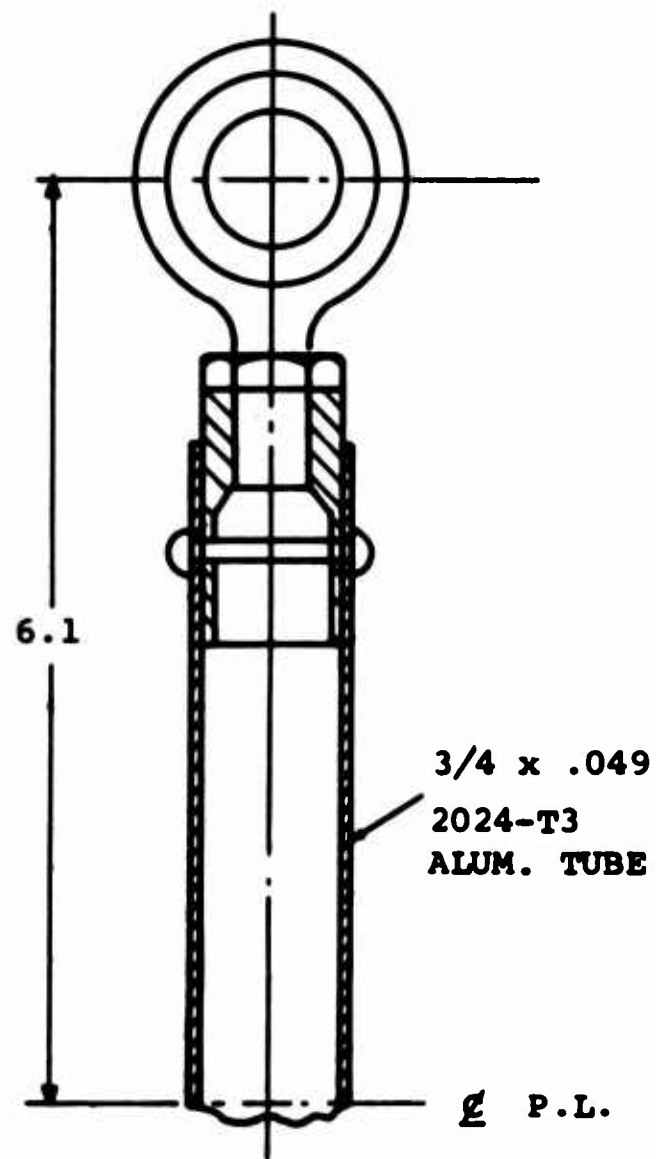
NOT TO SCALE

FIGURE 7. VZ-2 PITCH LINK,
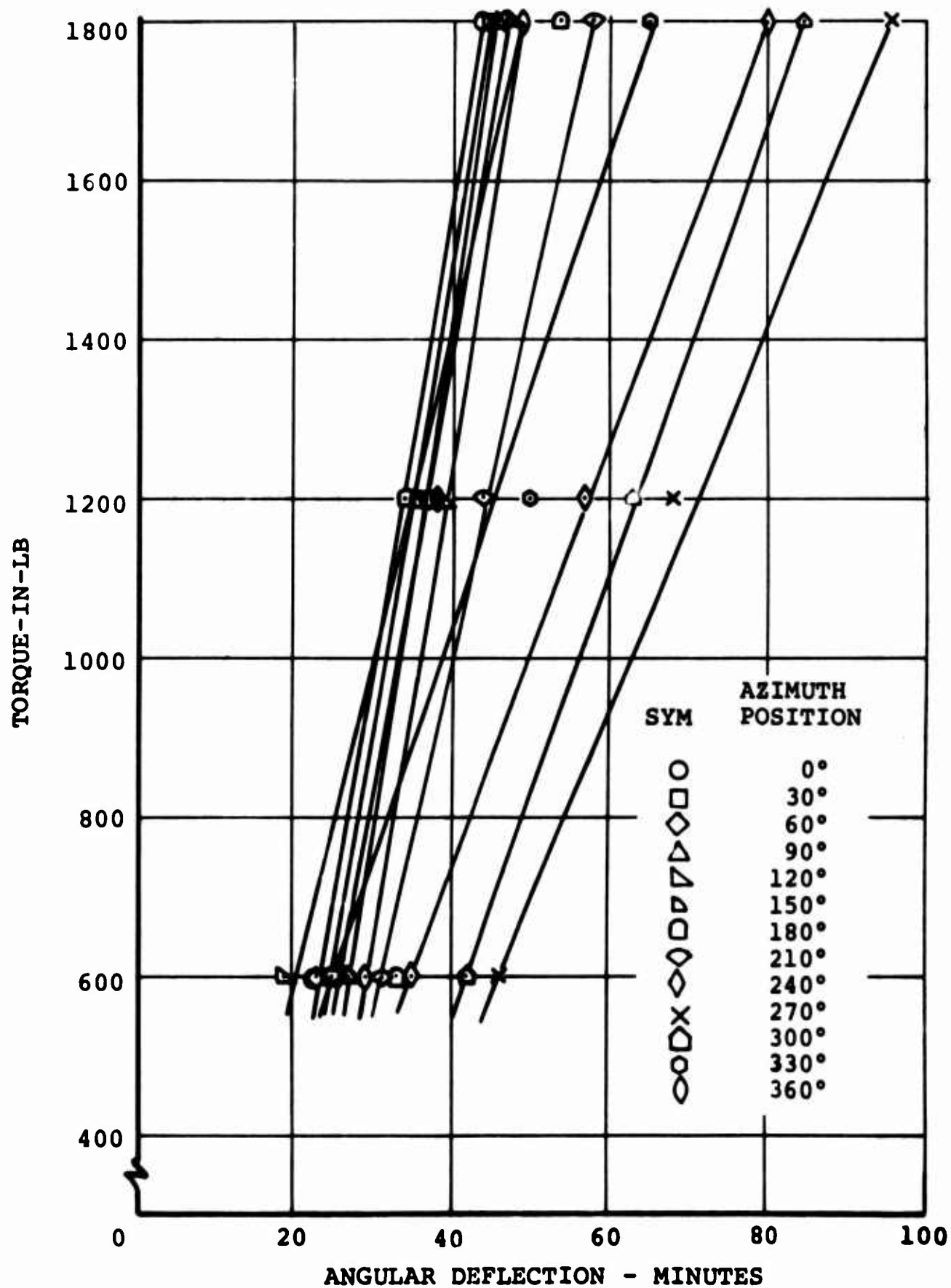
FIGURE 8a. CONTROL SYSTEM STIFFNESS AS A FUNCTION OF AZI-
MUTH ANGLE, CONFIGURATION A (β = 8°, γ = 0°).
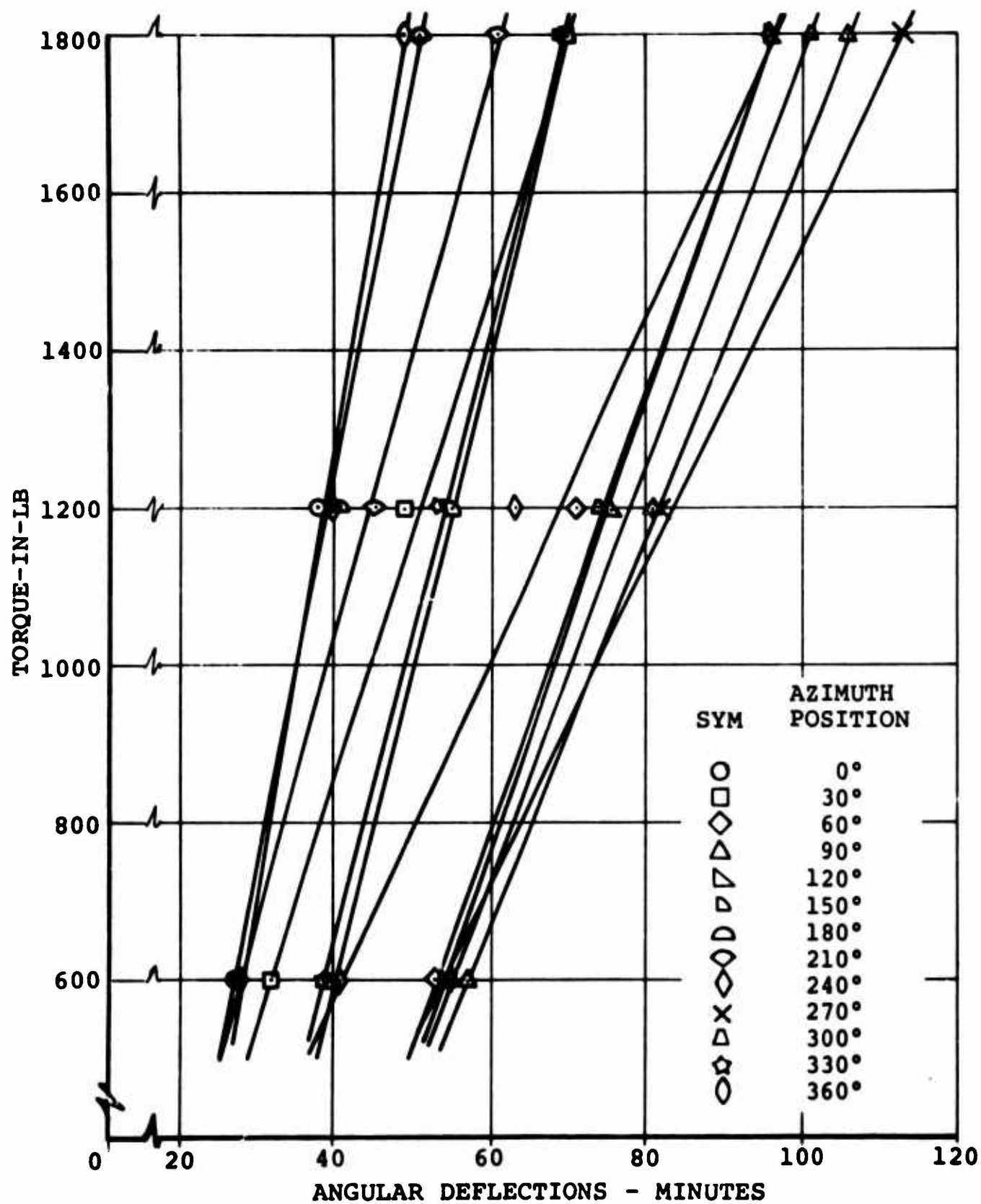
FIGURE 8b. CONTROL SYSTEM STIFFNESS AS A FUNCTION OF
AZIMUTH ANGLE, CONFIGURATIONS B AND C
$(\beta = 8°, \gamma = 0°)$.

30
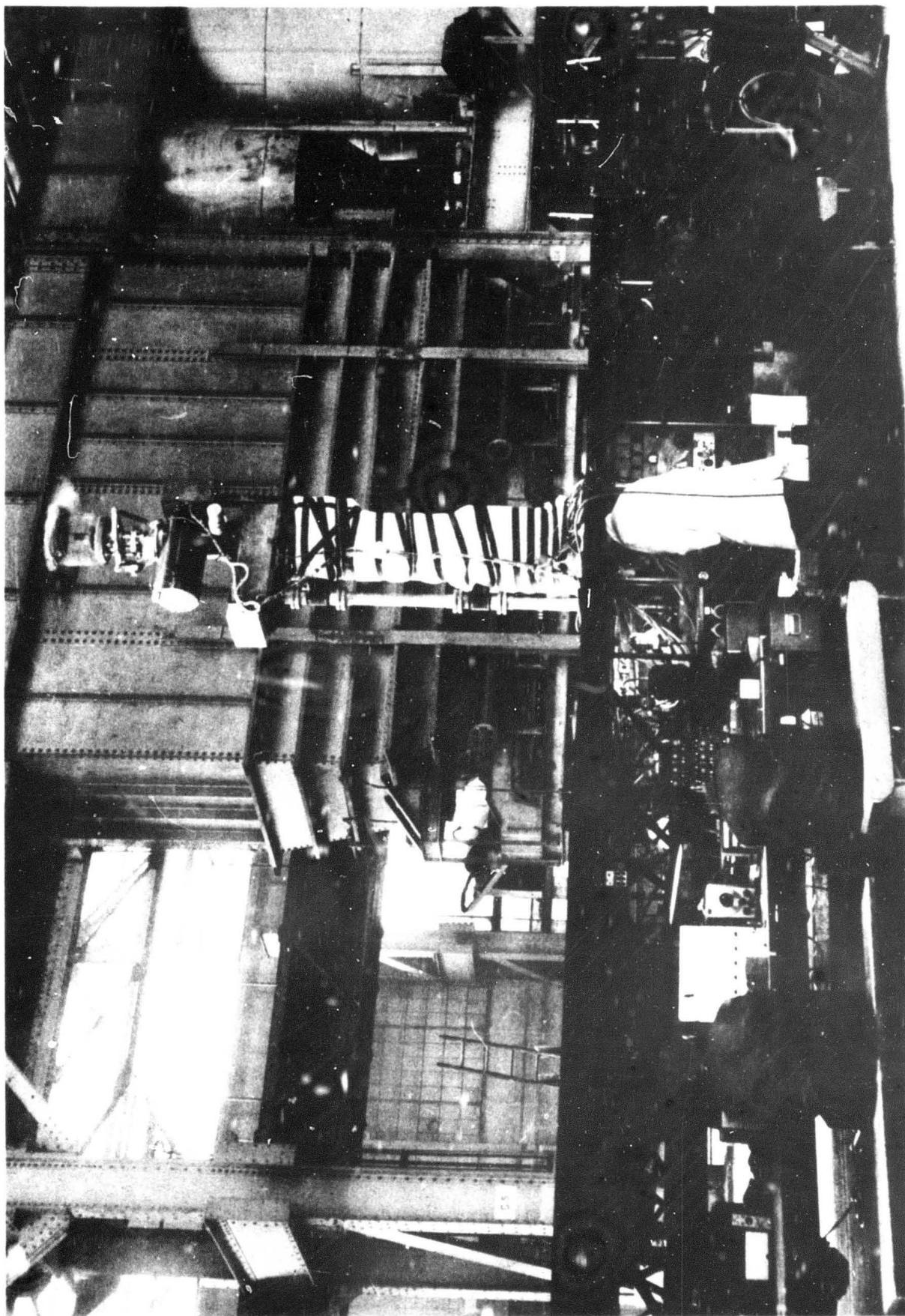
FIGURE 9. GENERAL VIEW OF CART TEST FACILITY WITH SIX-FOOT MONOCYCLIC TEST PROPELLER.

31
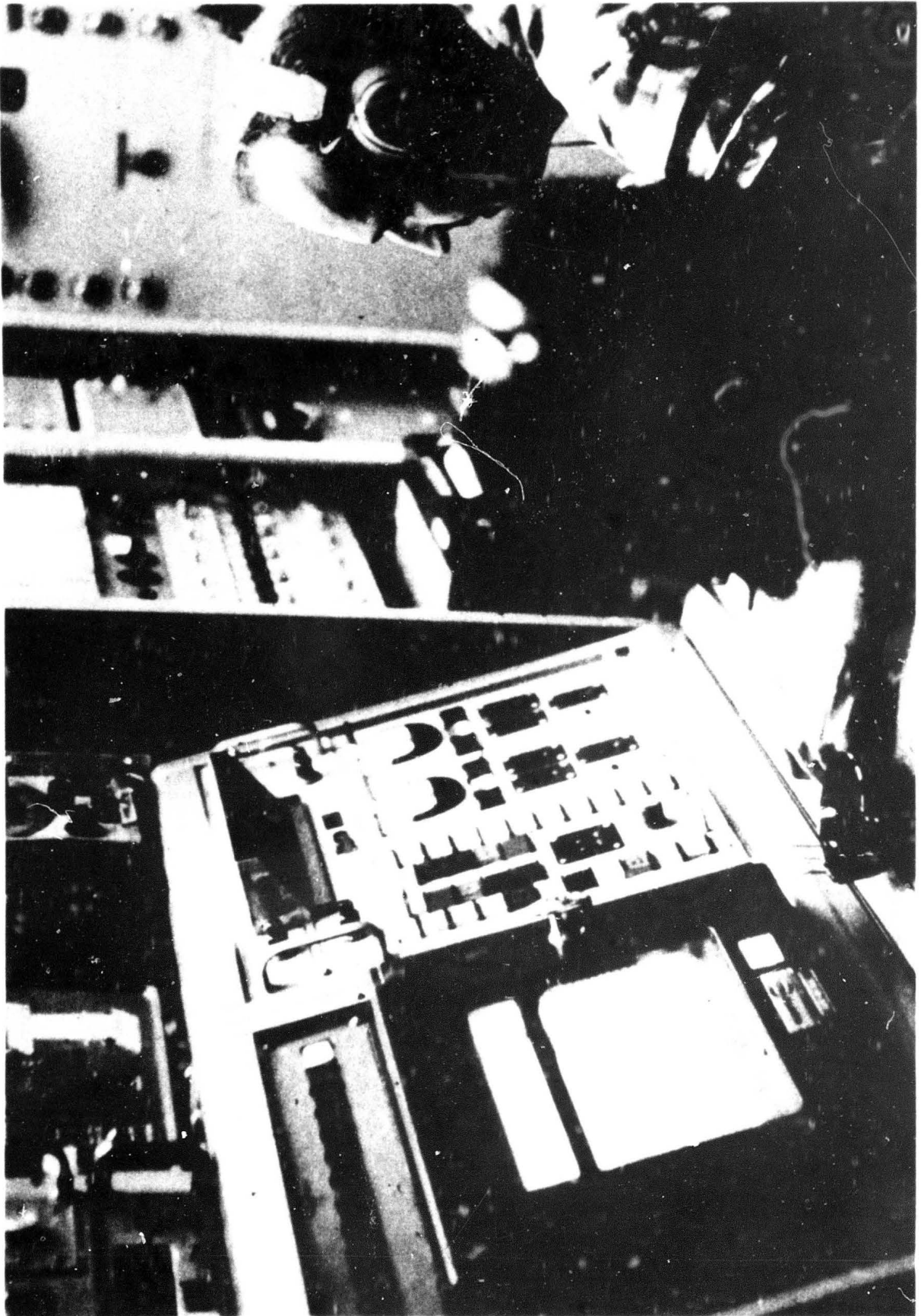
FIGURE 10. CONTROL CONSOLE OF DATA SYSTEM.

32
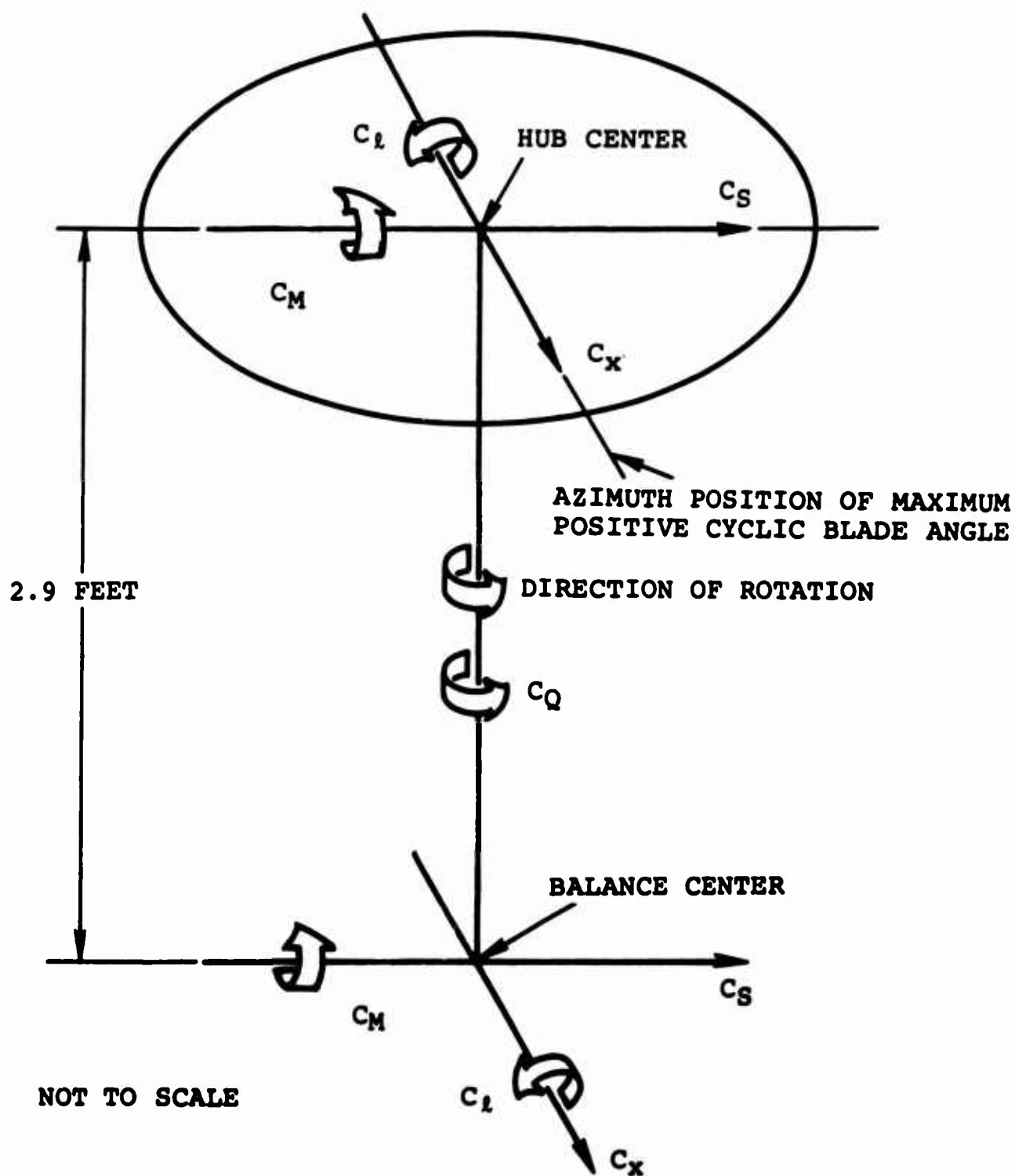
FIGURE 11. SIX-COMPONENT STRAIN GAUGE BALANCE AXES GEOMETRY.

33
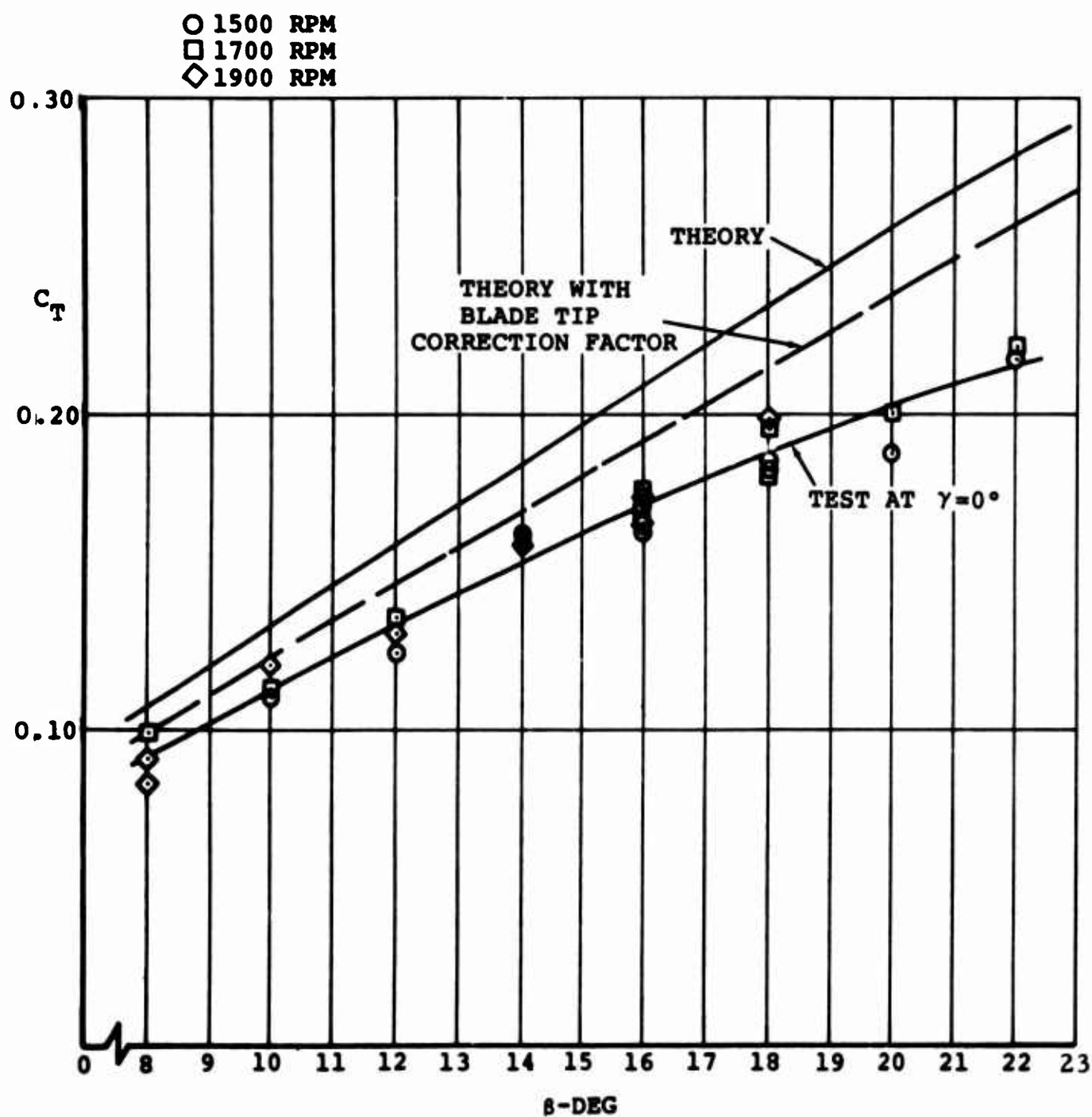
FIGURE 12.   PROPELLER THRUST CHARACTERISTICS.
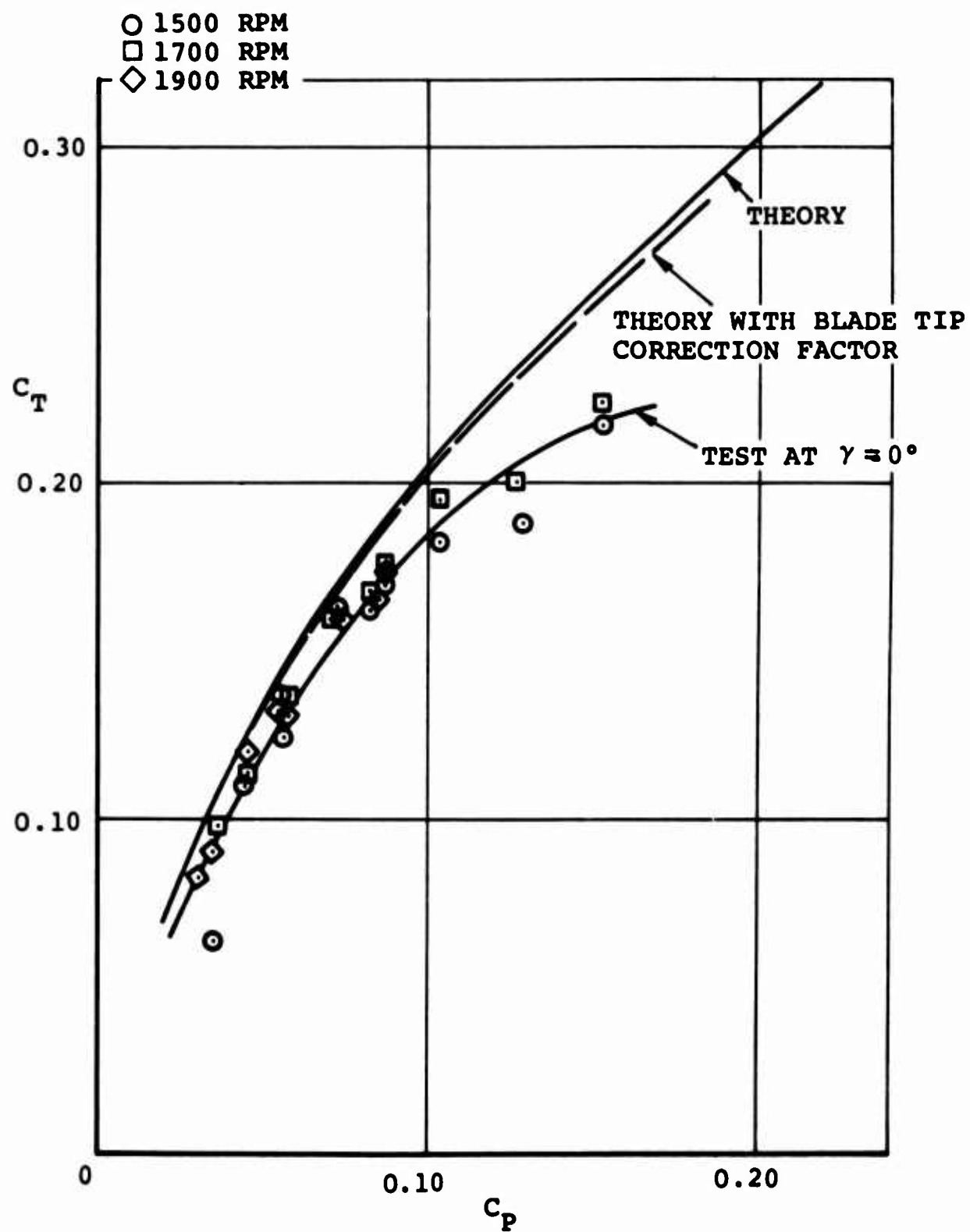
FIGURE 13. PROPELLER CHARACTERISTICS.
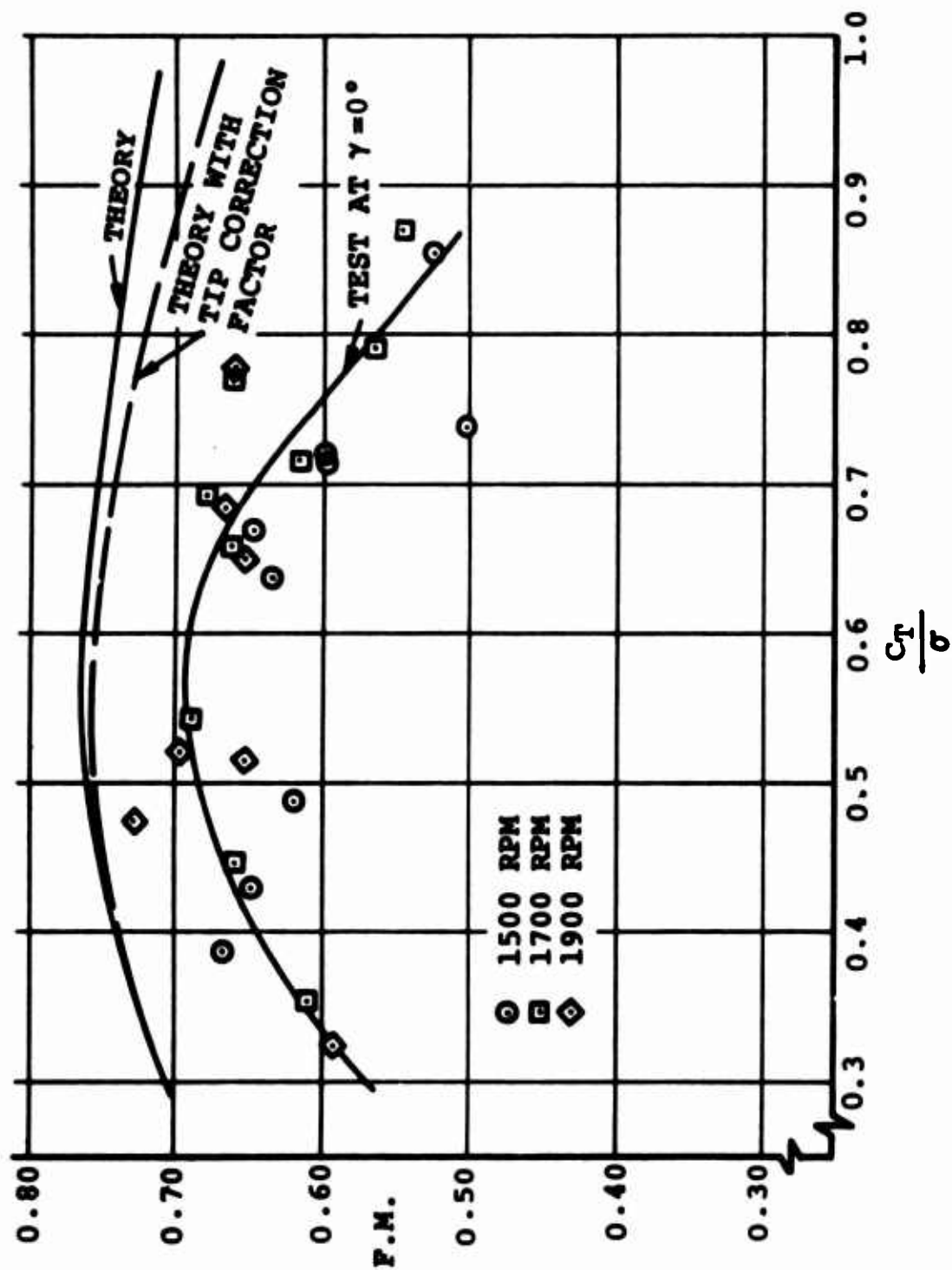
FIGURE 14. PROPELLER FIGURE OF MERIT.
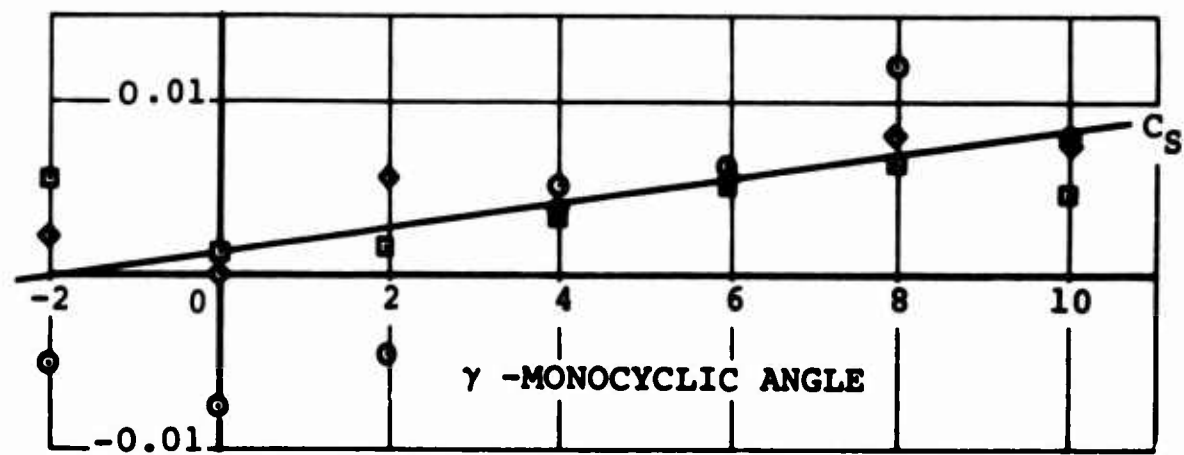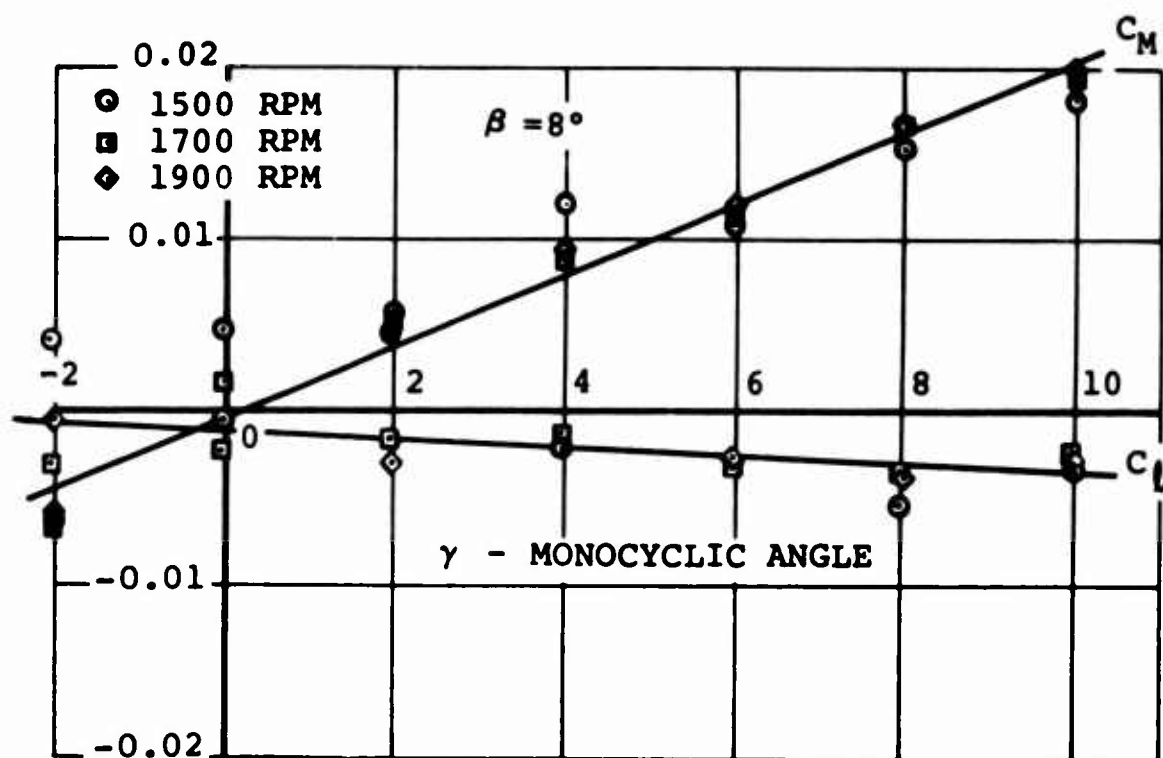
FIGURE 15a.   FORCE AND MOMENT COEFFICIENTS ABOUT HUB
               CENTER, β = 8°.
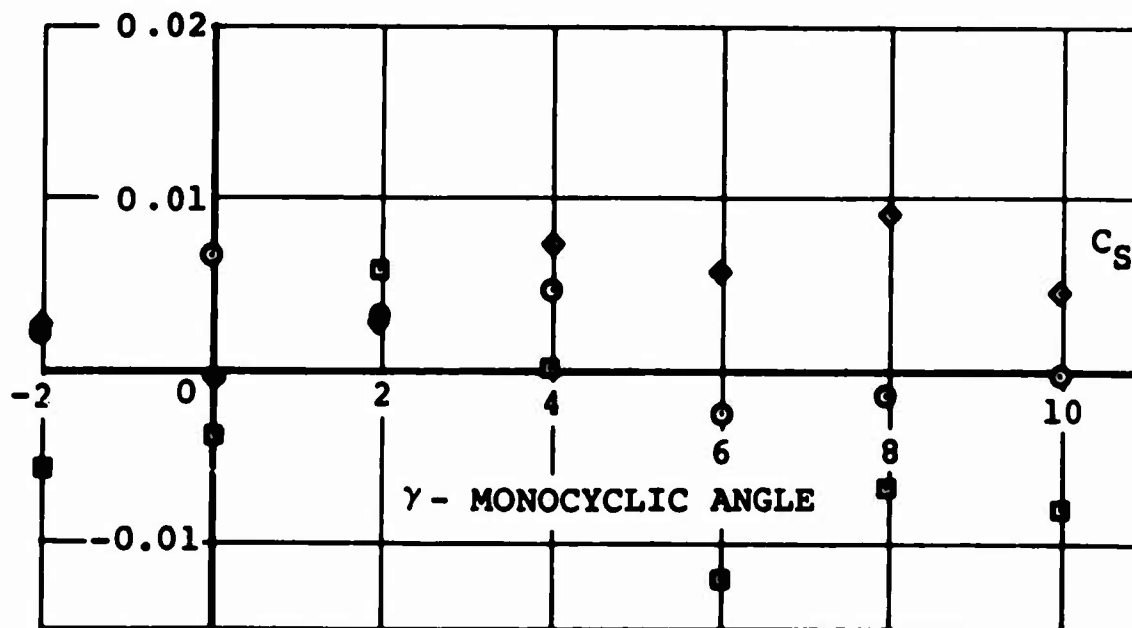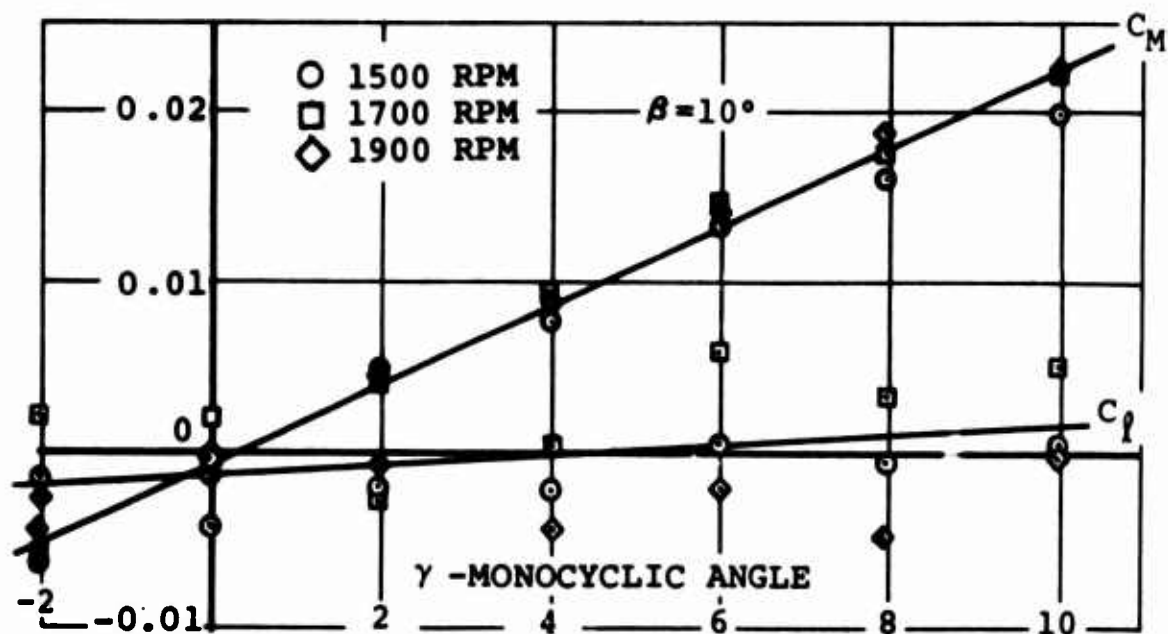
FIGURE 15b.   FORCE AND MOMENT COEFFICIENTS ABOUT HUB
              CENTER, $\beta = 10°$,
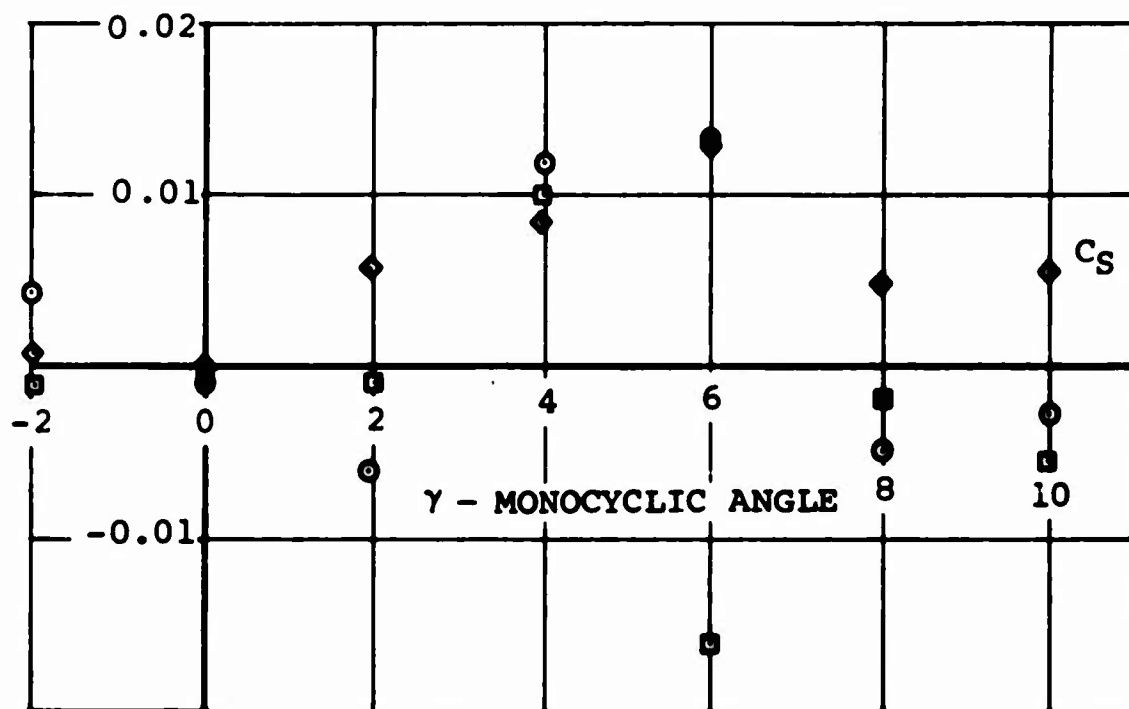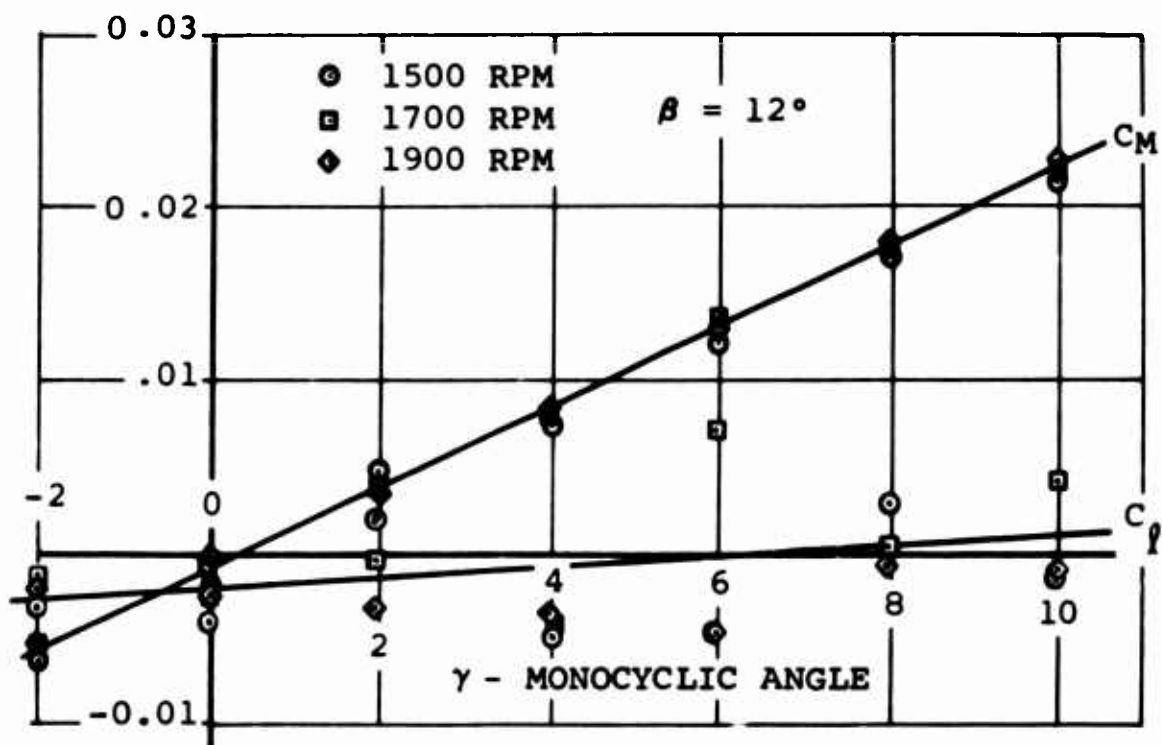
FIGURE 15c.   FORCE AND MOMENT COEFFICIENTS ABOUT HUB
               CENTER, β = 12°.
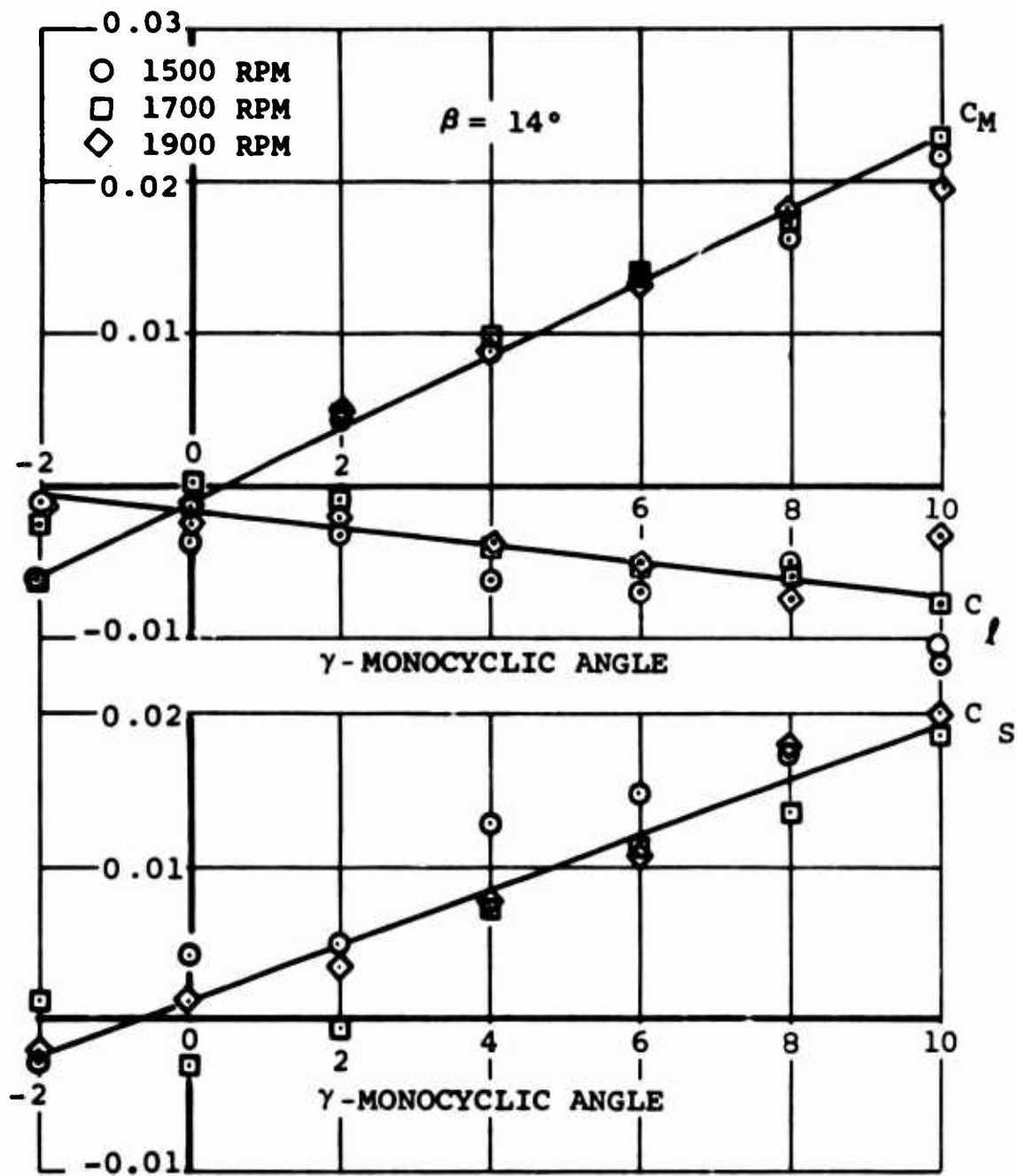
FIGURE 15d.   FORCE AND MOMENT COEFFICIENTS ABOUT HUB
              CENTER, $\beta = 14°$,
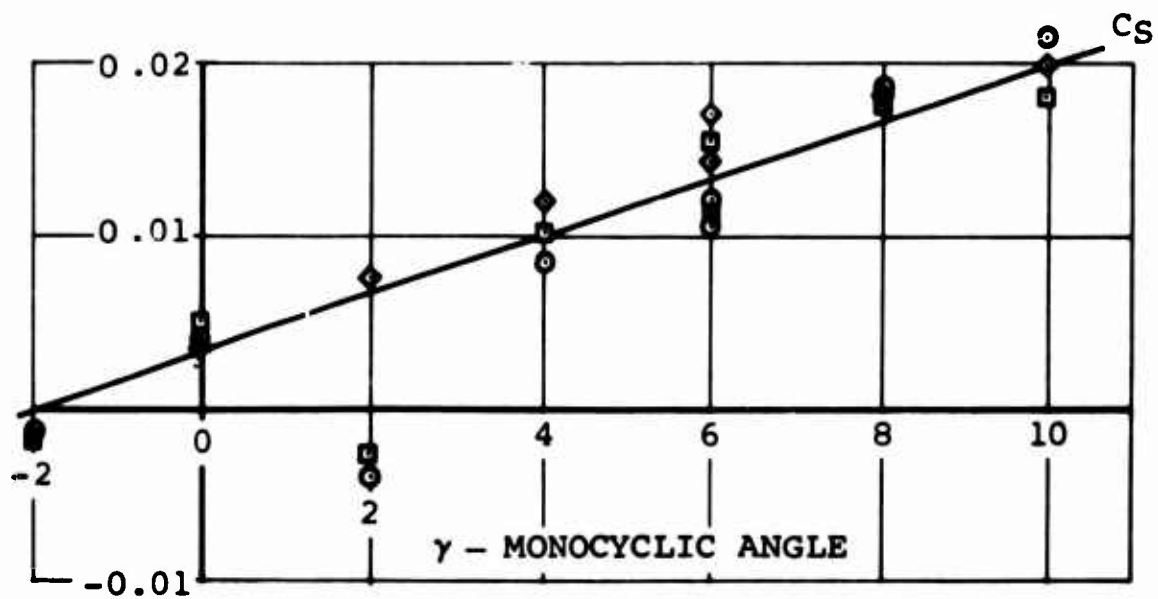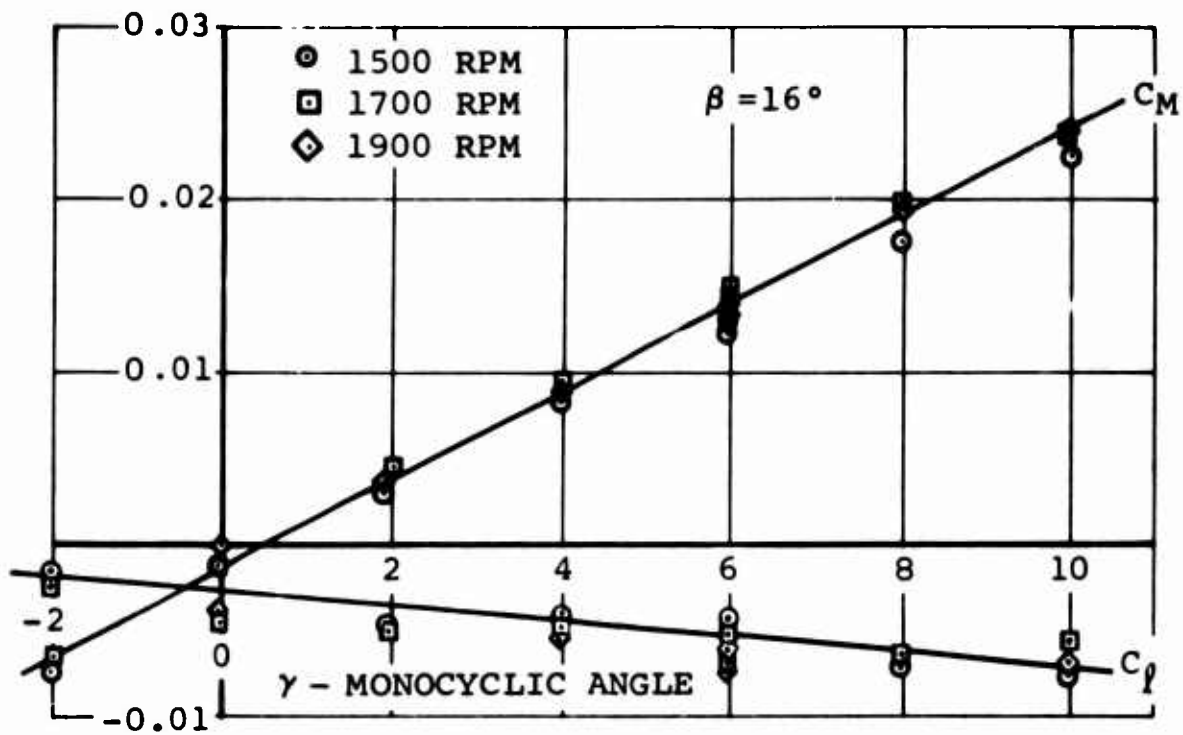
FIGURE 15e.   FORCE AND MOMENT COEFFICIENTS ABOUT HUB
CENTER, β = 16°.

41
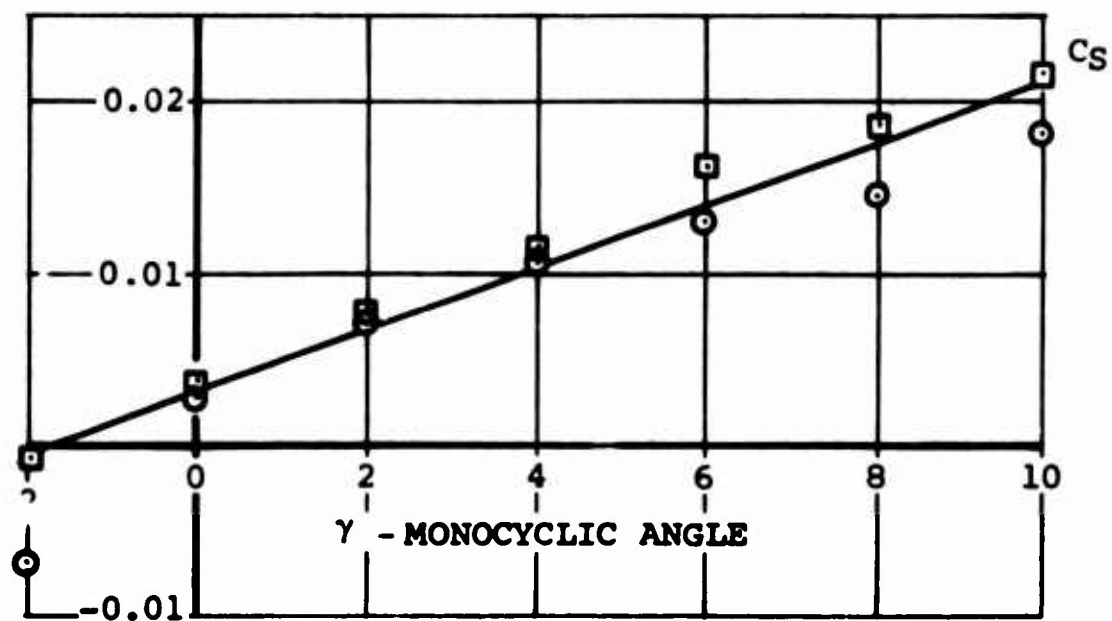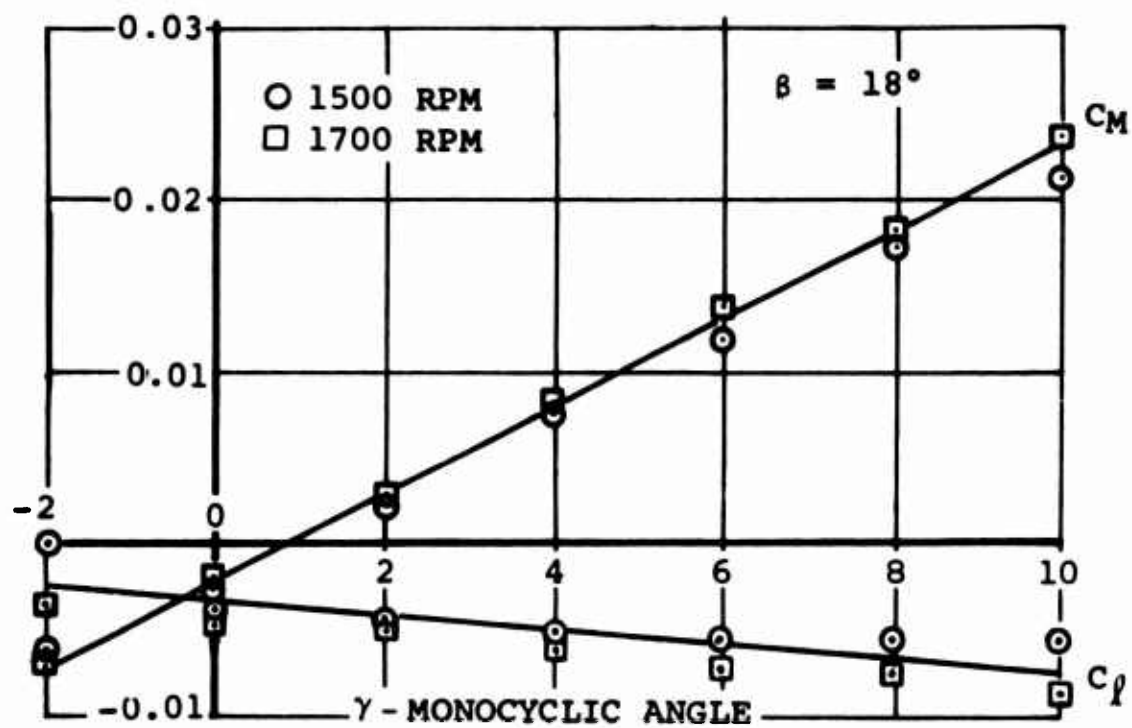
FIGURE 15f. FORCE AND MOMENT COEFFICIENTS ABOUT HUB
CENTER, β = 18°.

42
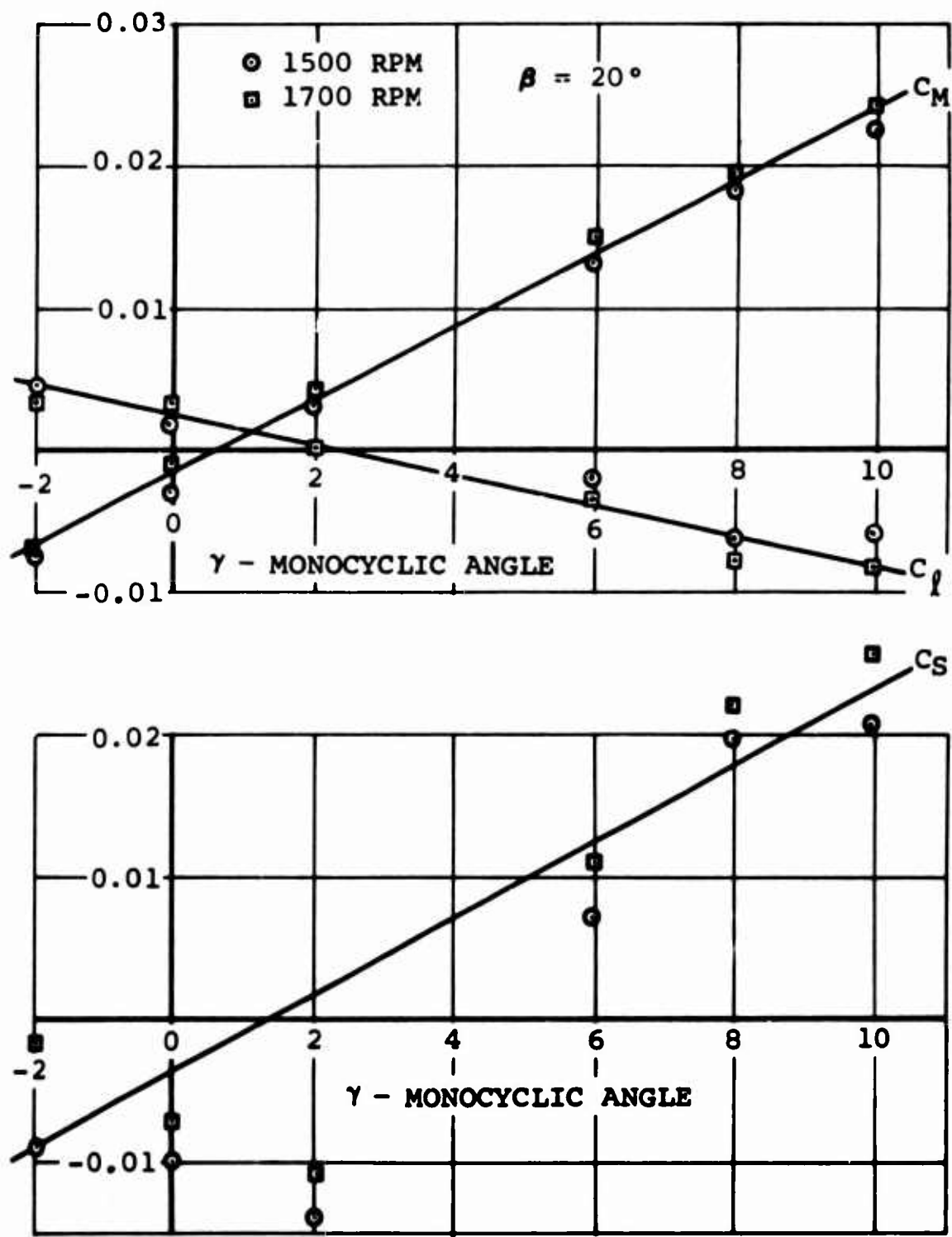
FIGURE 15g.   FORCE AND MOMENT COEFFICIENTS ABOUT HUB
CENTER, $\beta = 20°$.
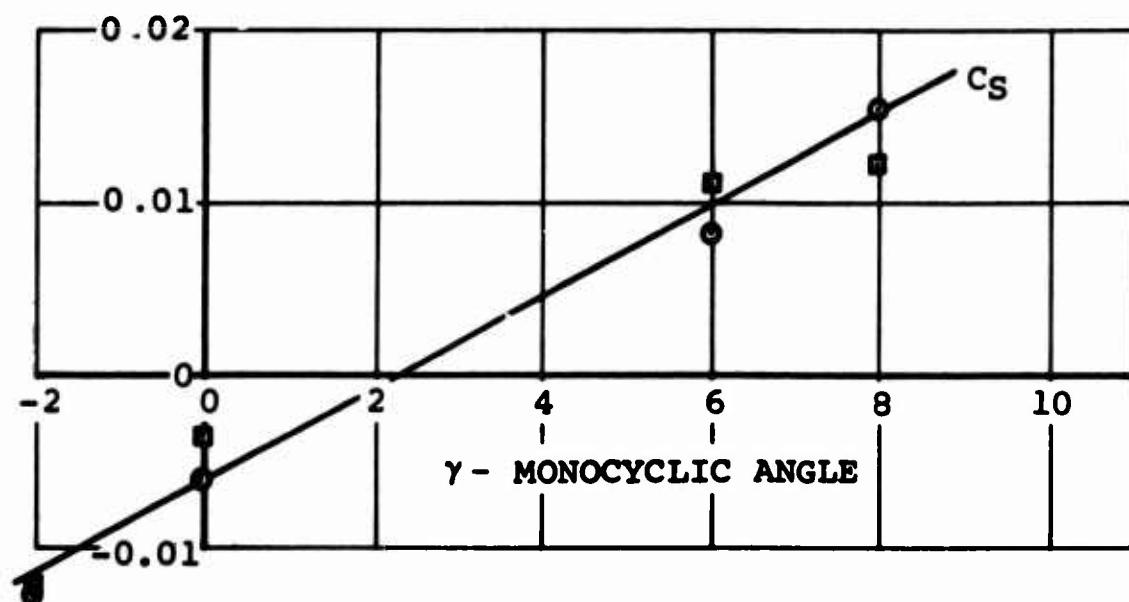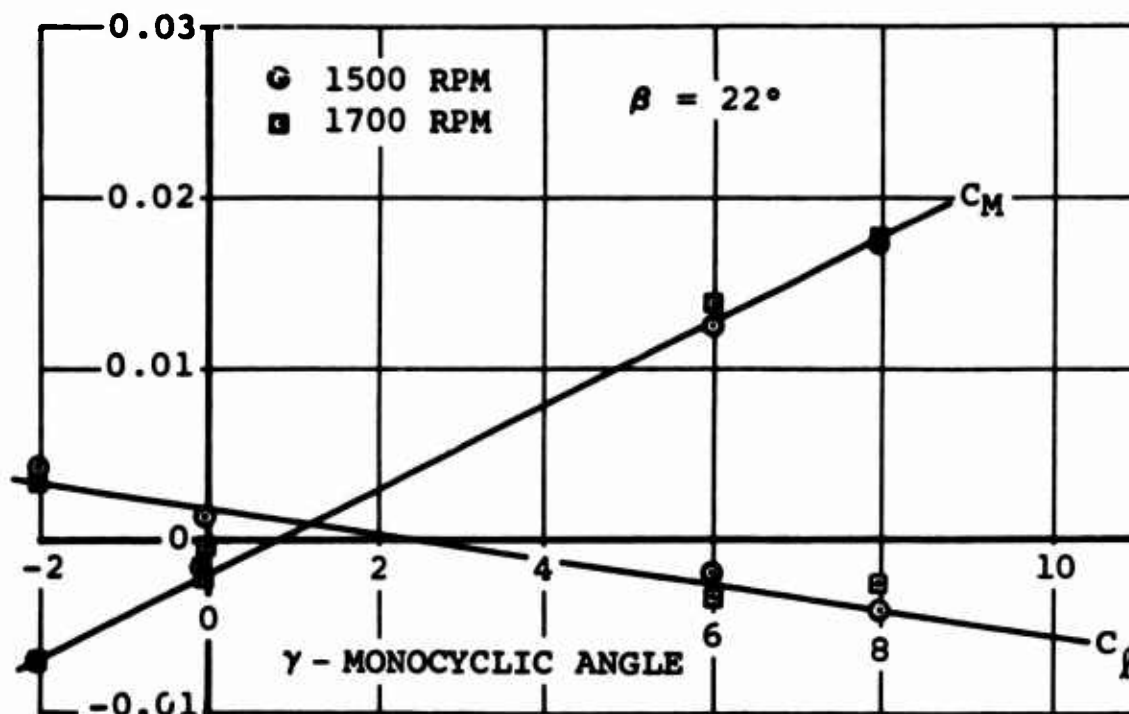
FIGURE 15h.   FORCE AND MOMENT COEFFICIENTS ABOUT HUB
CENTER, β = 22°

44
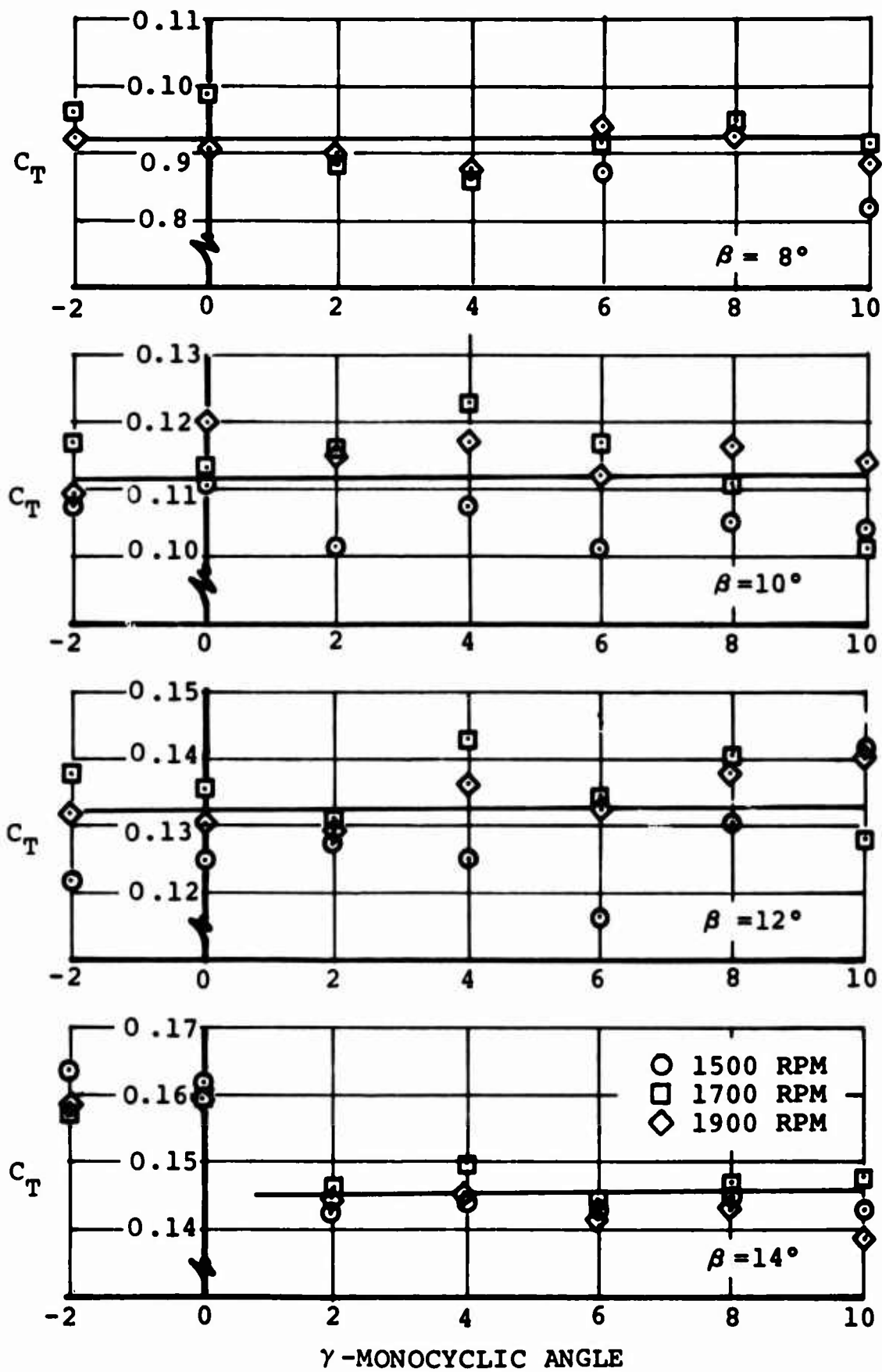
FIGURE 16a. EFFECT OF MONOCYCLIC CONTROL ON THRUST
β = 8°, 10°, 12°, and 14°.

45
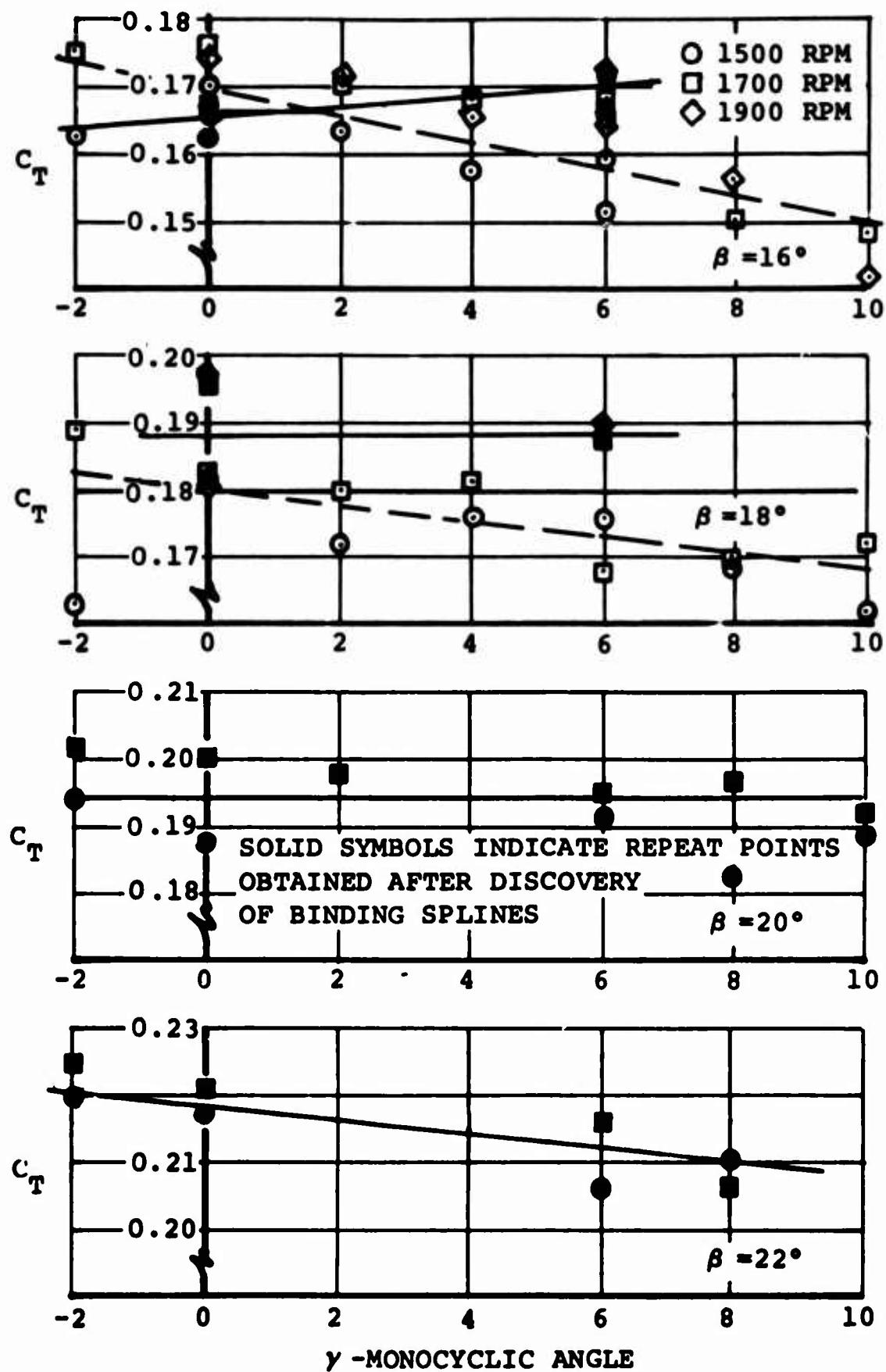
FIGURE 16b. EFFECT OF MONOCYCLIC CONTROL ON THRUST
β = 16°, 18°, 20°, and 22°.

46
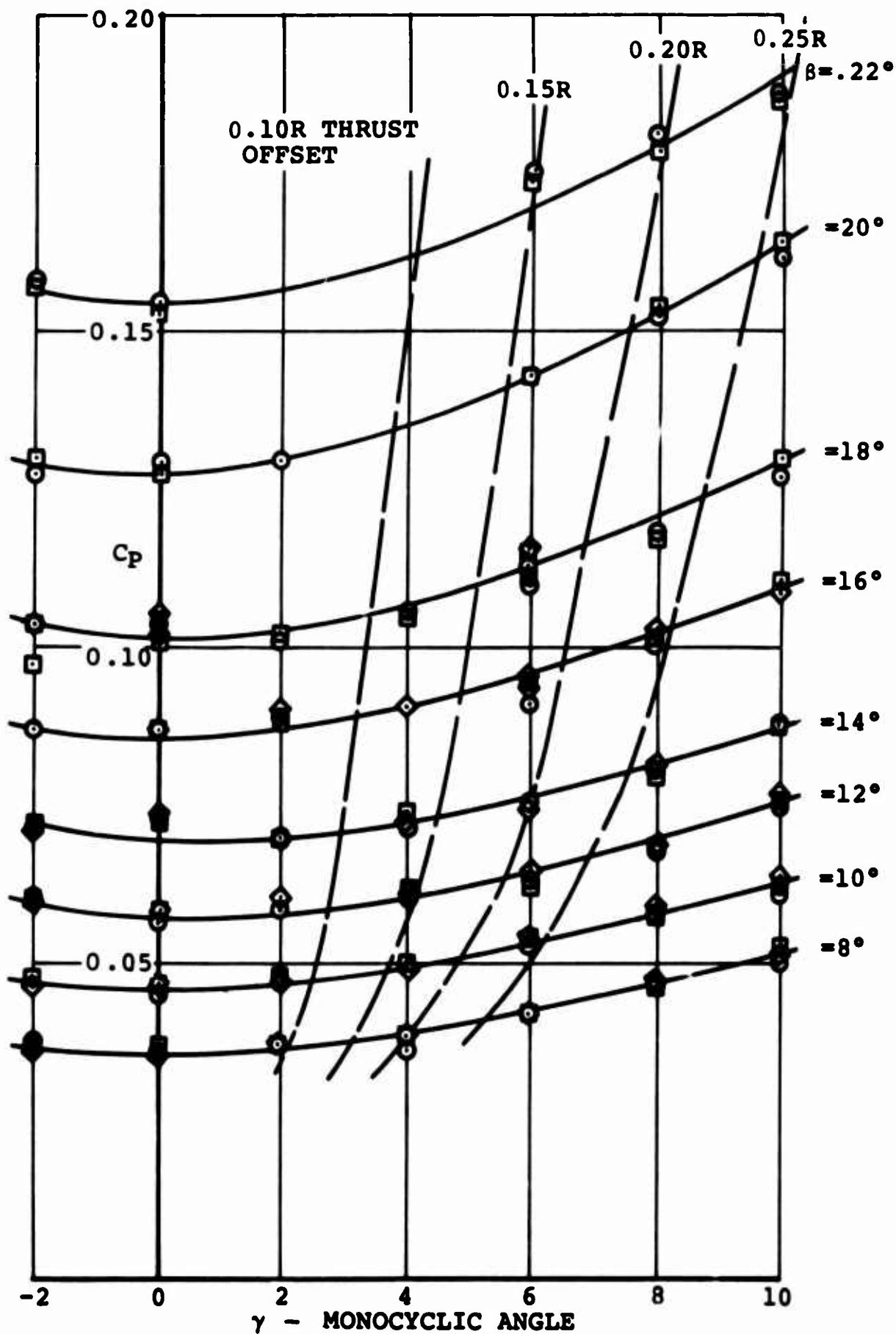
FIGURE 17.   EFFECT OF MONOCYCLIC CONTROL ON POWER
REQUIRED.

47
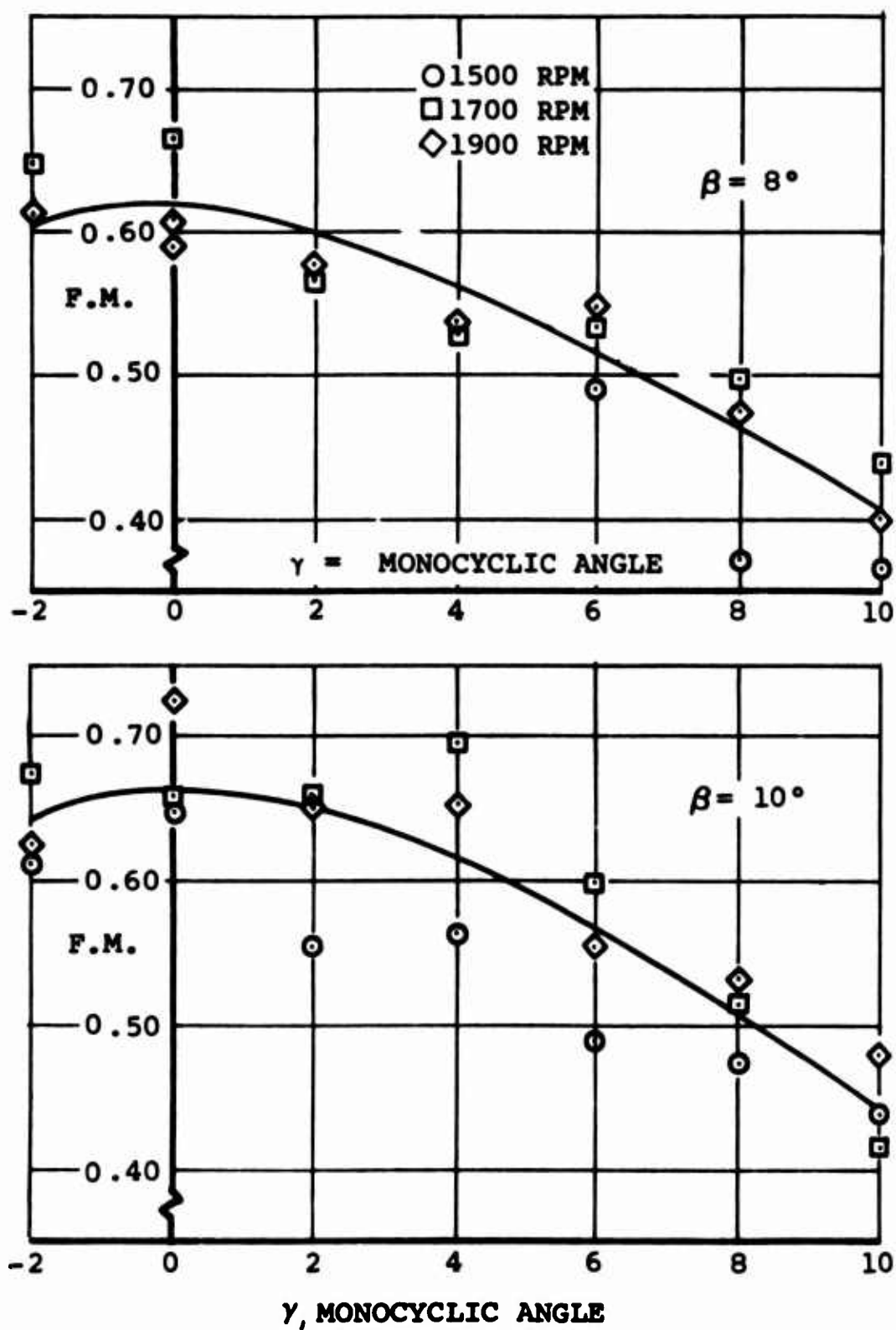
FIGURE 18a. EFFECT OF MONOCYCLIC CONTROL ON FIGURE OF MERIT, $\beta = 8°$ and $10°$.
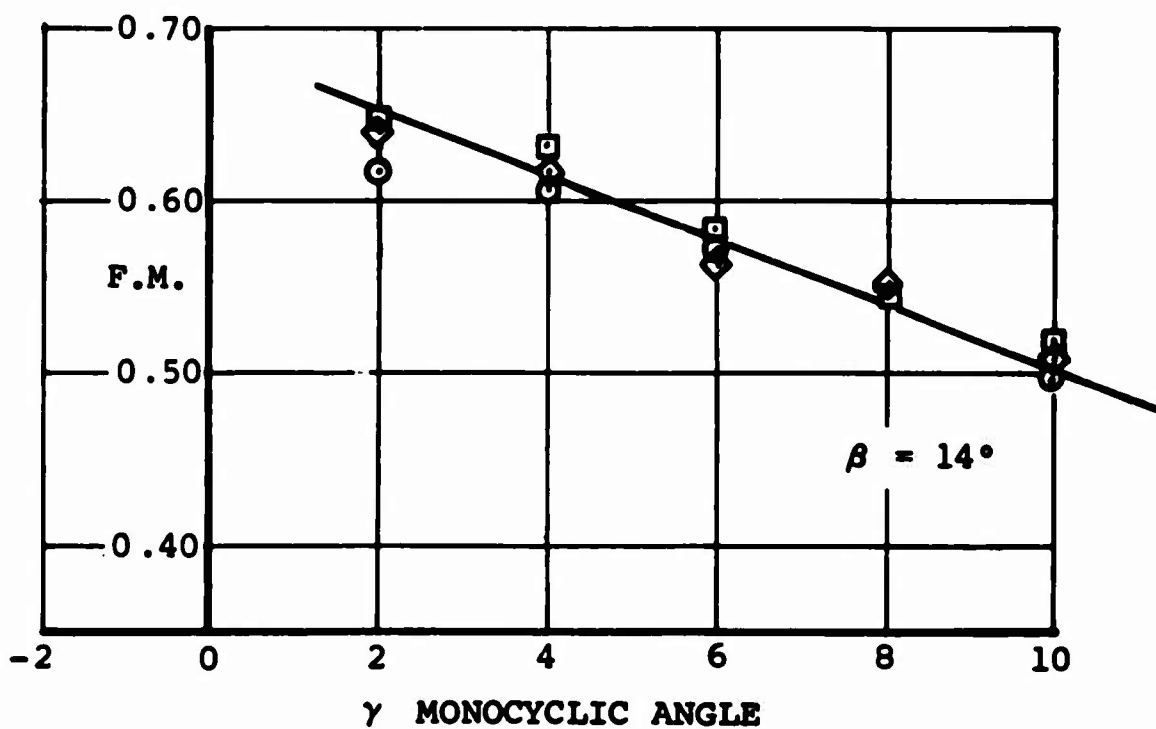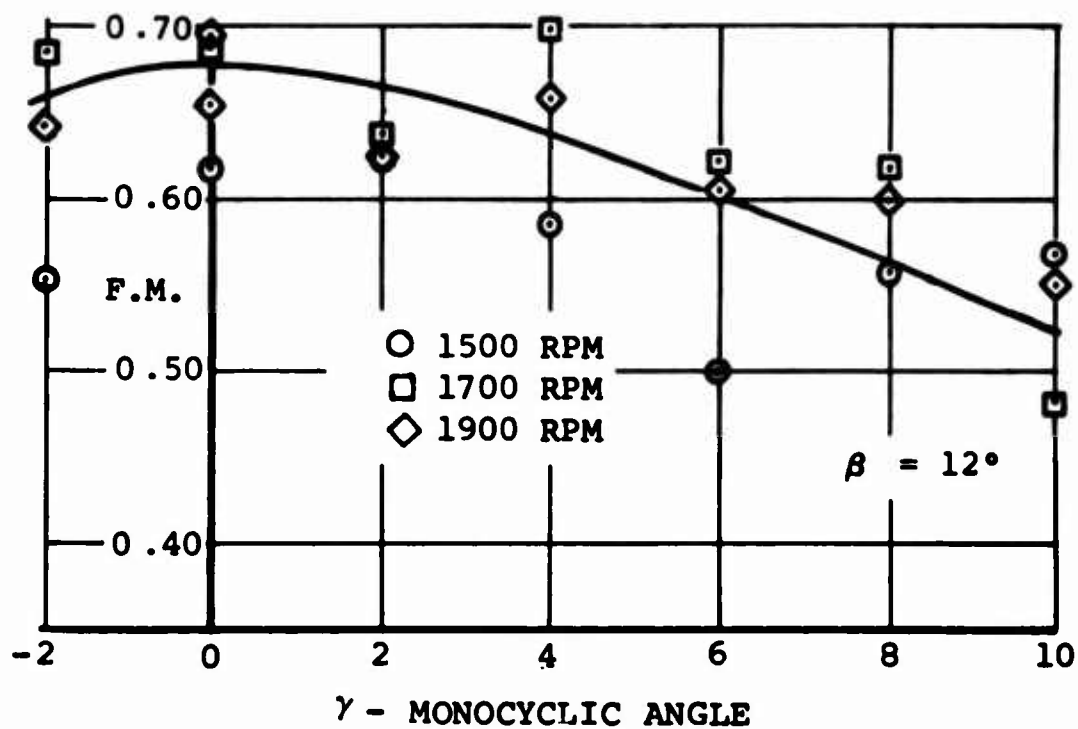
FIGURE 18b.   EFFECT OF MONOCYCLIC CONTROL ON FIGURE
OF MERIT, β = 12° and 14°.

49
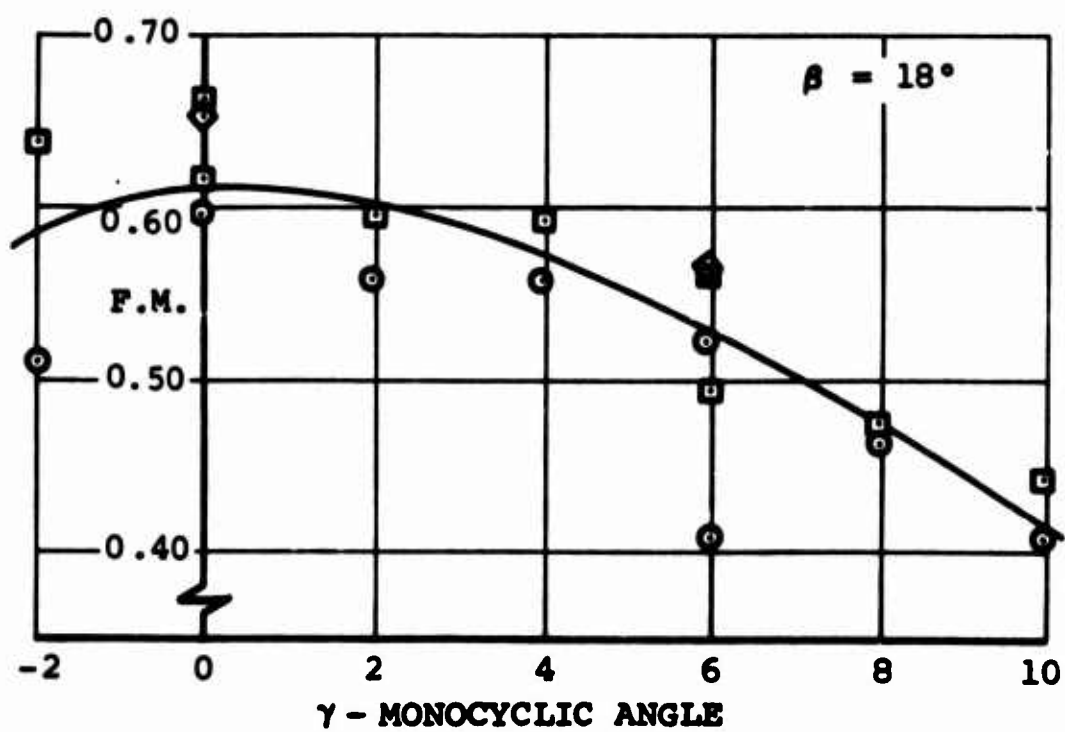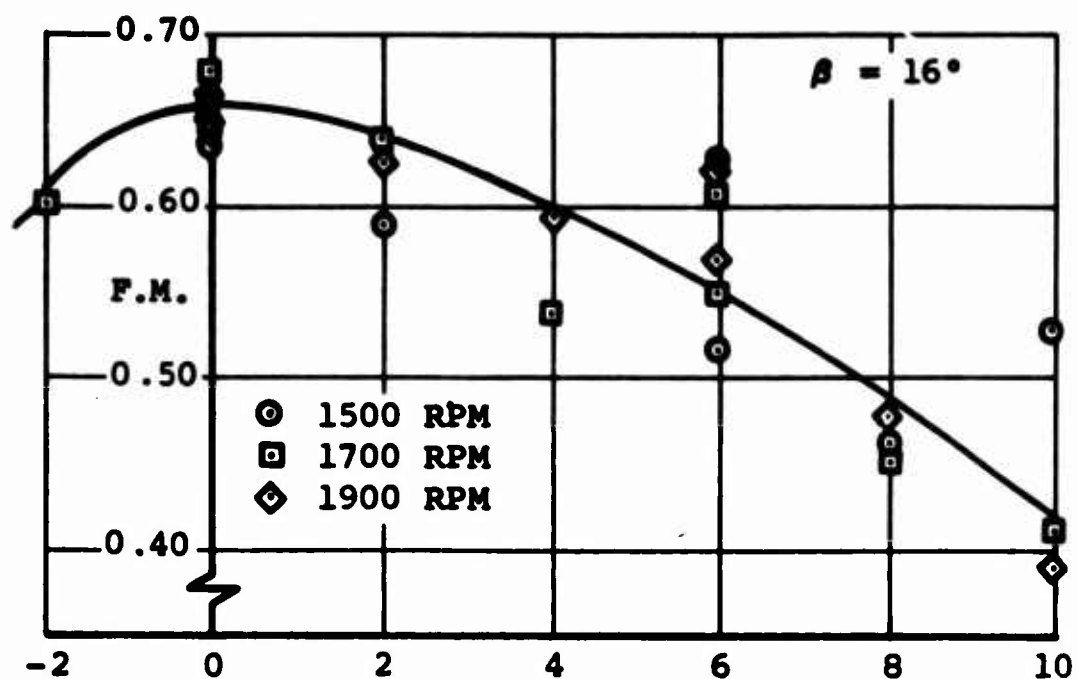
FIGURE 18c. EFFECT OF MONOCYCLIC CONTROL ON FIGURE OF MERIT, β = 16° and 18°.
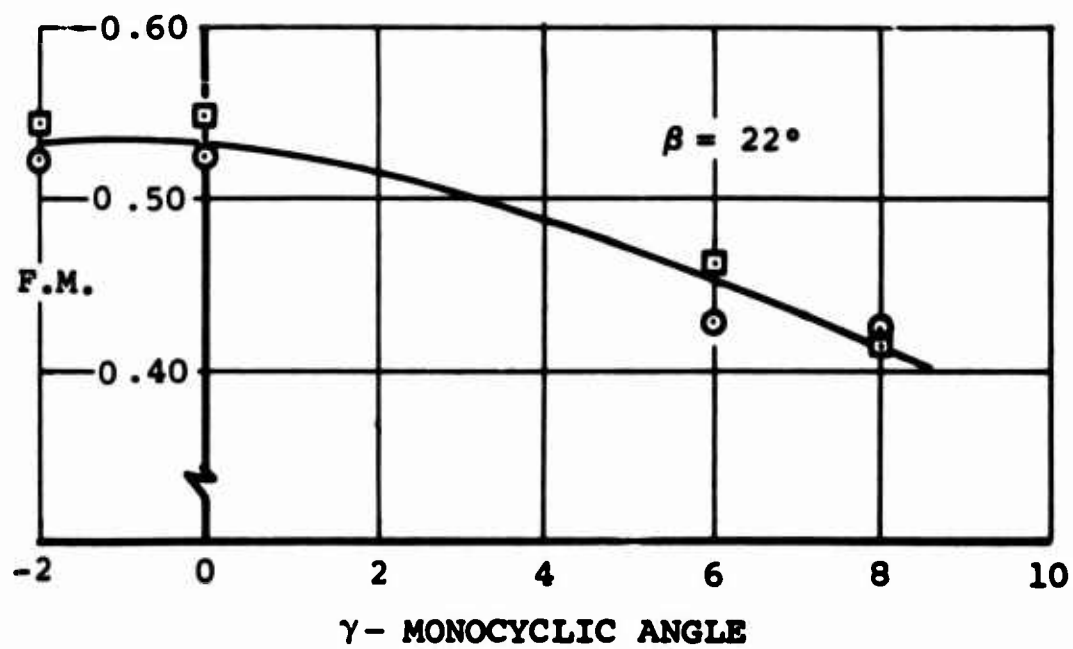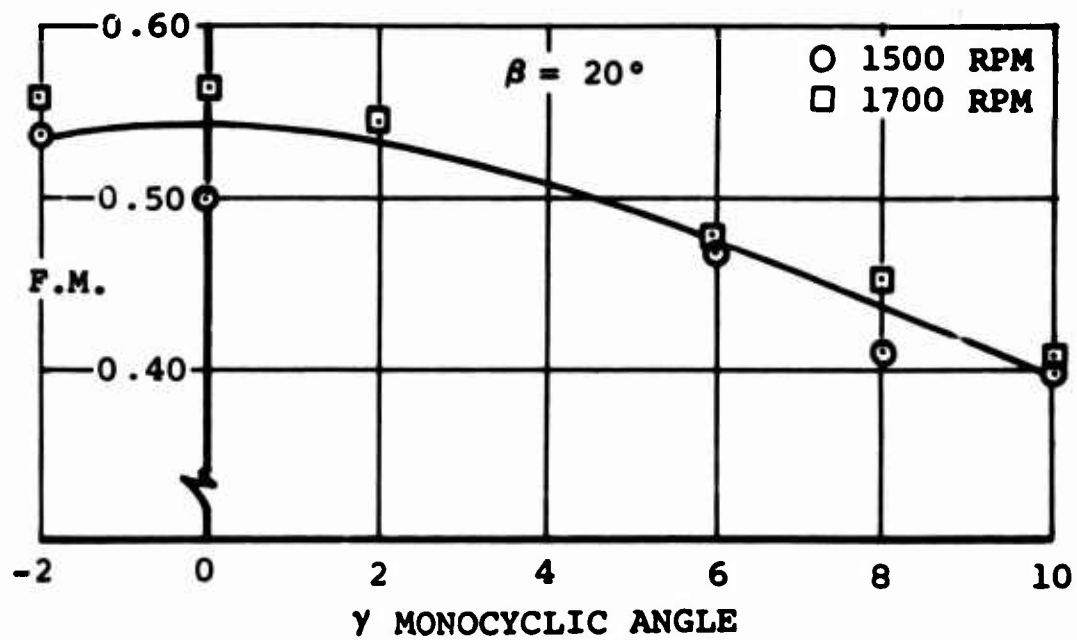
FIGURE 18d.   EFFECT OF MONOCYCLIC CONTROL ON FIGURE OF MERIT, β = 20° and 22°.

51
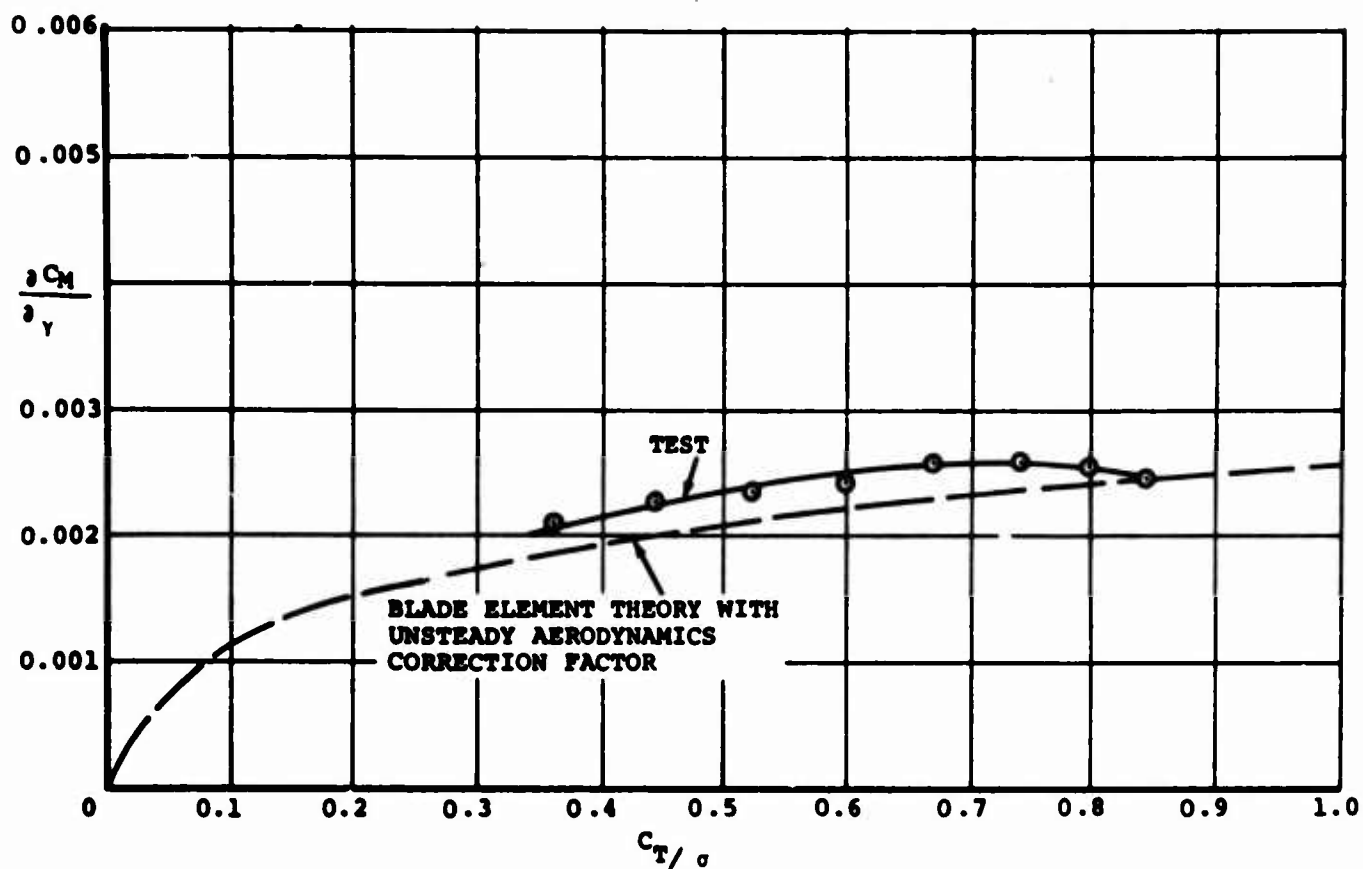
FIGURE 19. MONOCYCLIC CONTROL POWER FROM THEORY AND TEST.

NOTE: MODIFIED VZ-2 PROP DATA WAS OBTAINED
FROM REF (3)
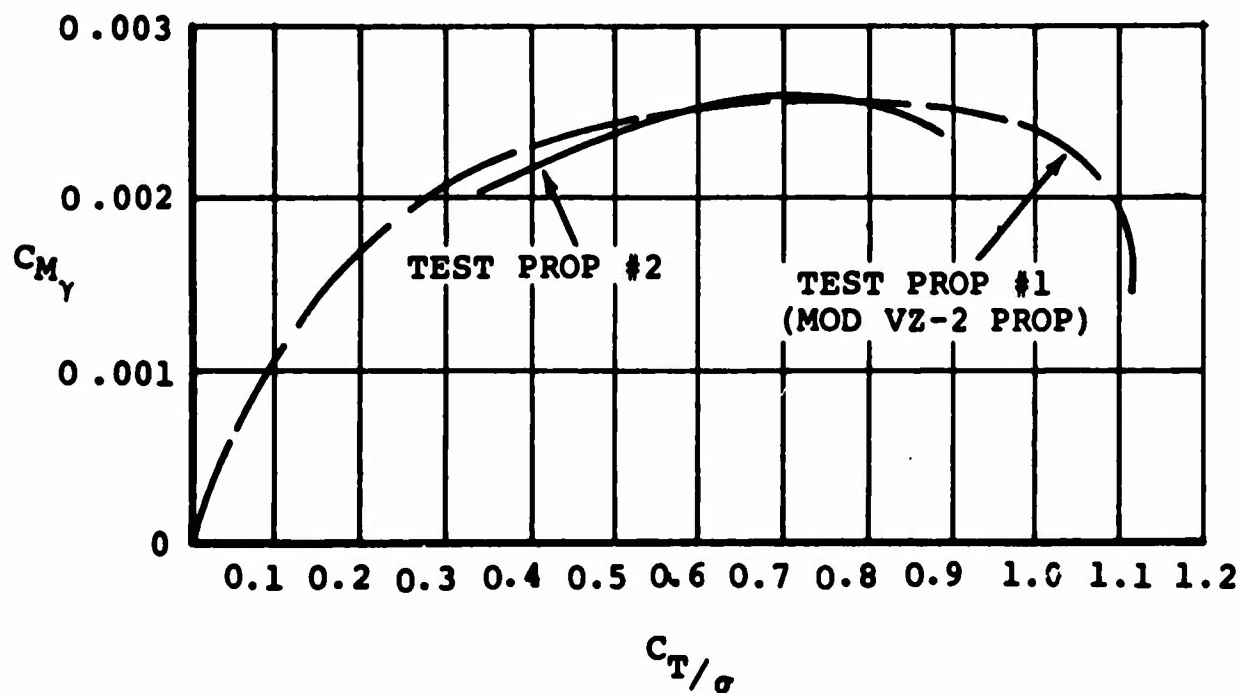
FIGURE 20. MONOCYCLIC CONTROL POWER COMPARISON.
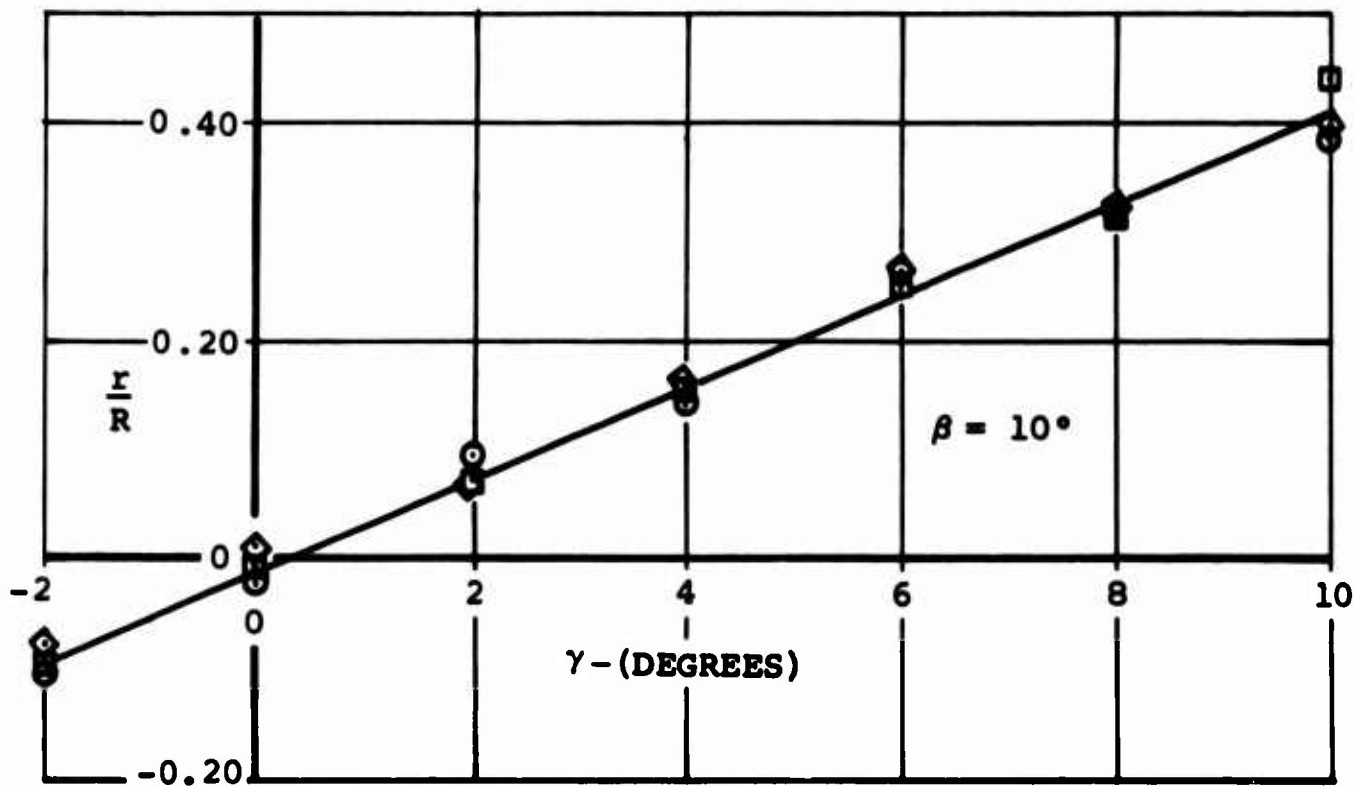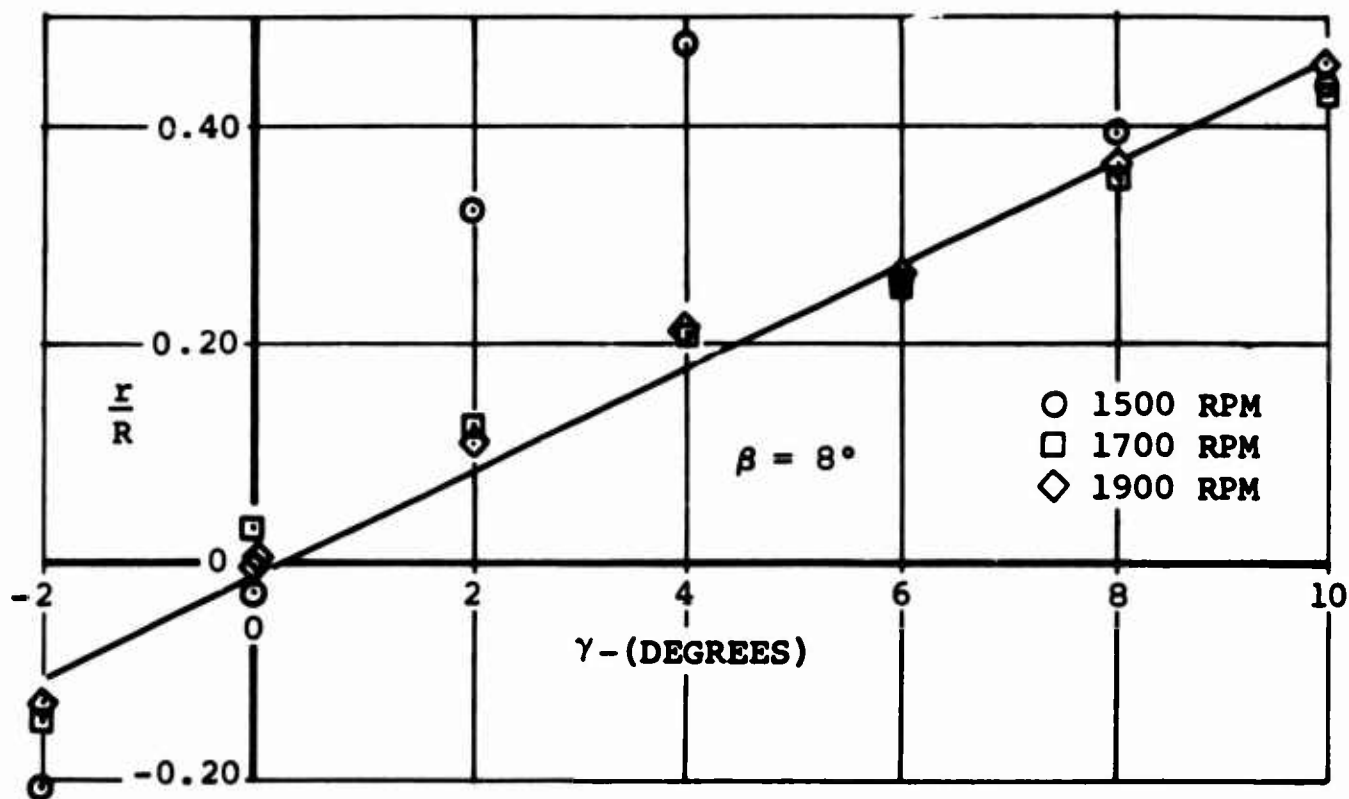
FIGURE 21a.   CYCLIC CONTROL POWER, IN PERCENT RADIUS
THRUST OFFSET, β= 8° and 10°.

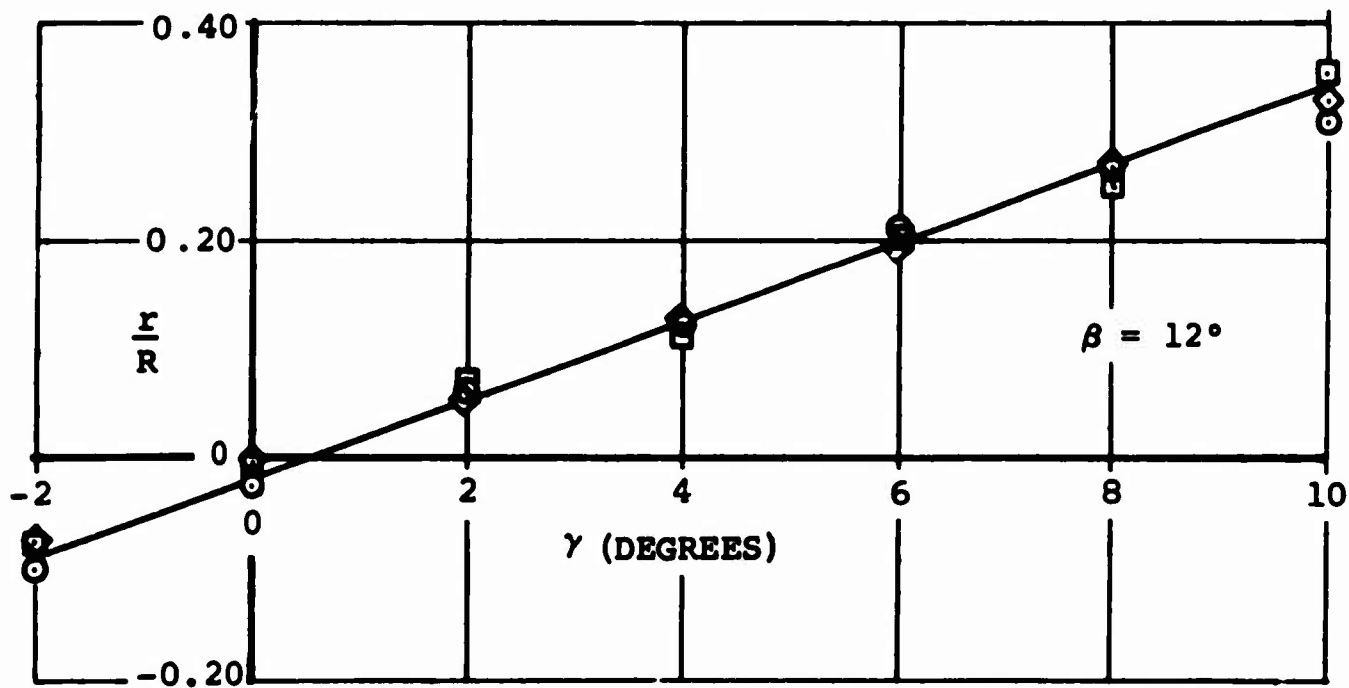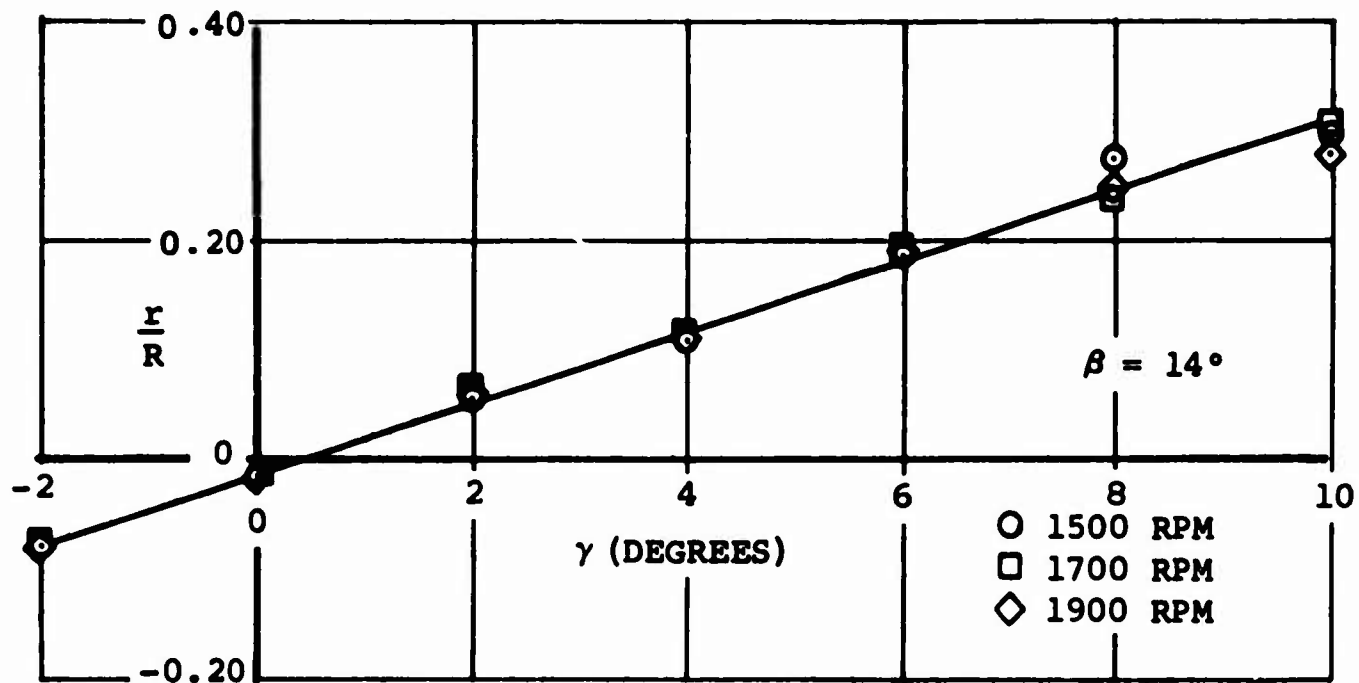FIGURE 21b.   CYCLIC CONTROL POWER, IN PERCENT RADIUS
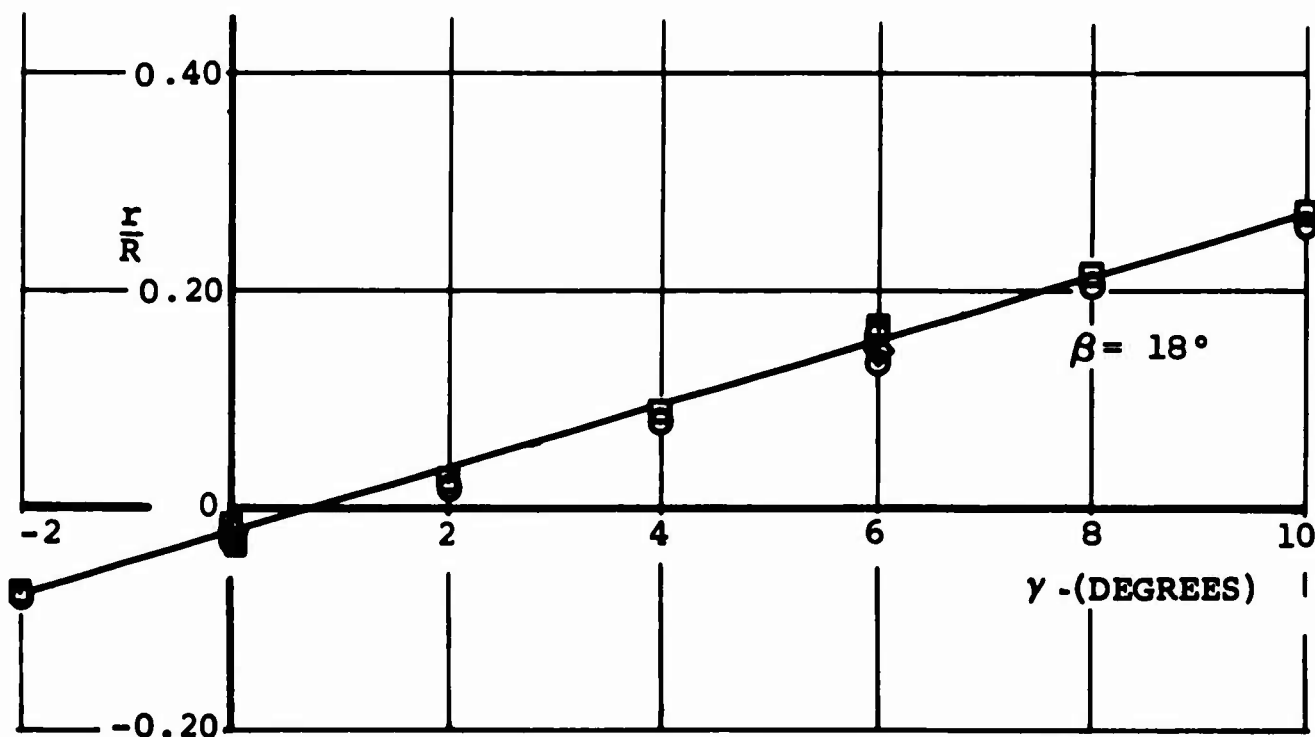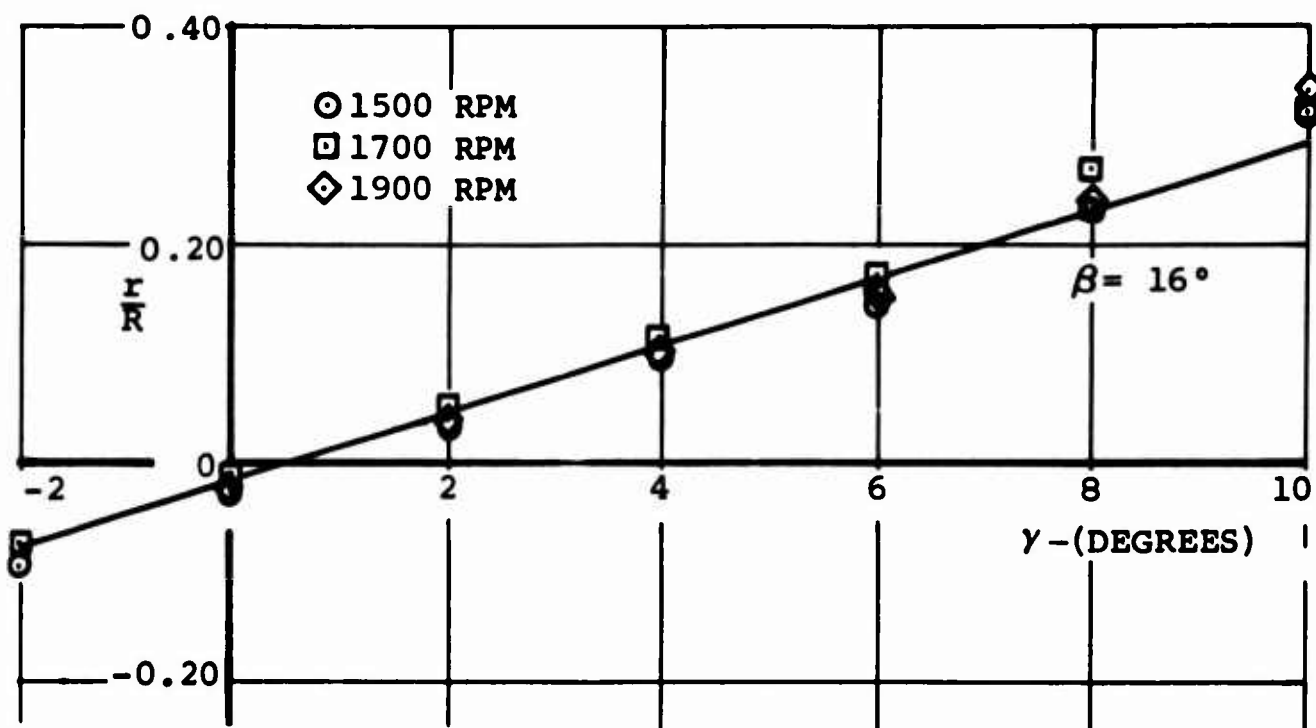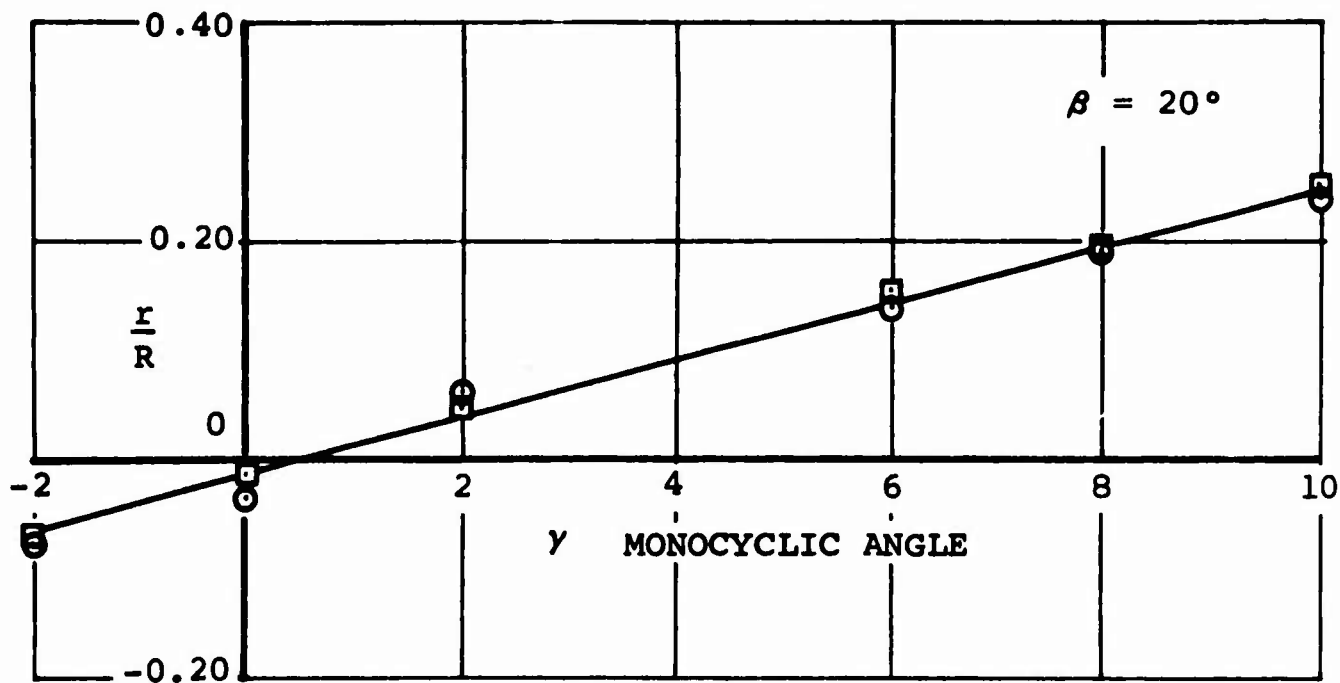THRUST OFFSET, β = 12° and 14°.

FIGURE 21c.   CYCLIC CONTROL POWER, IN PERCENT RADIUS
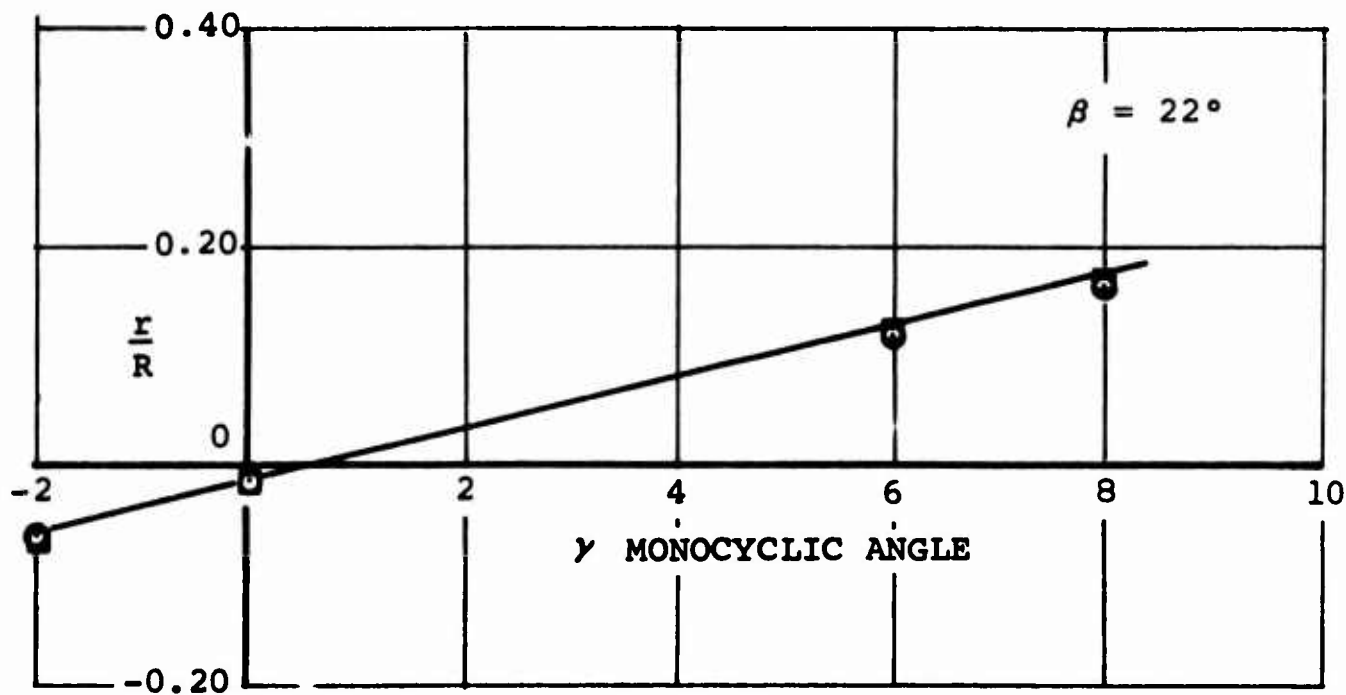THRUST OFFSET, β= 16° and 18°.

FIGURE 21d.   CYCLIC CONTROL POWER, IN PERCENT RADIUS
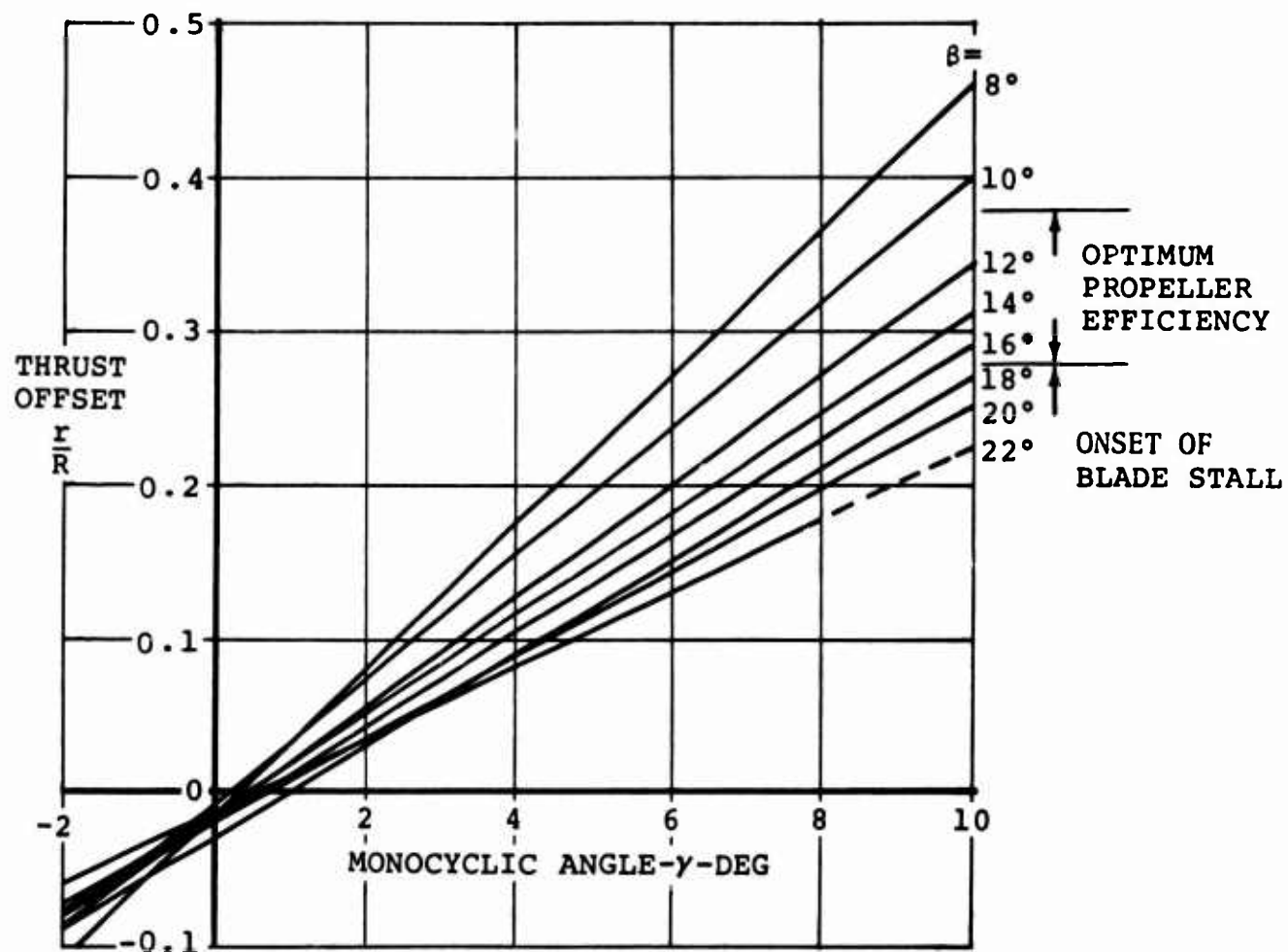THRUST OFFSET, β = 20° and 22°.

56

FIGURE 22.   SUMMARY OF CYCLIC CONTROL POWER, IN PERCENT
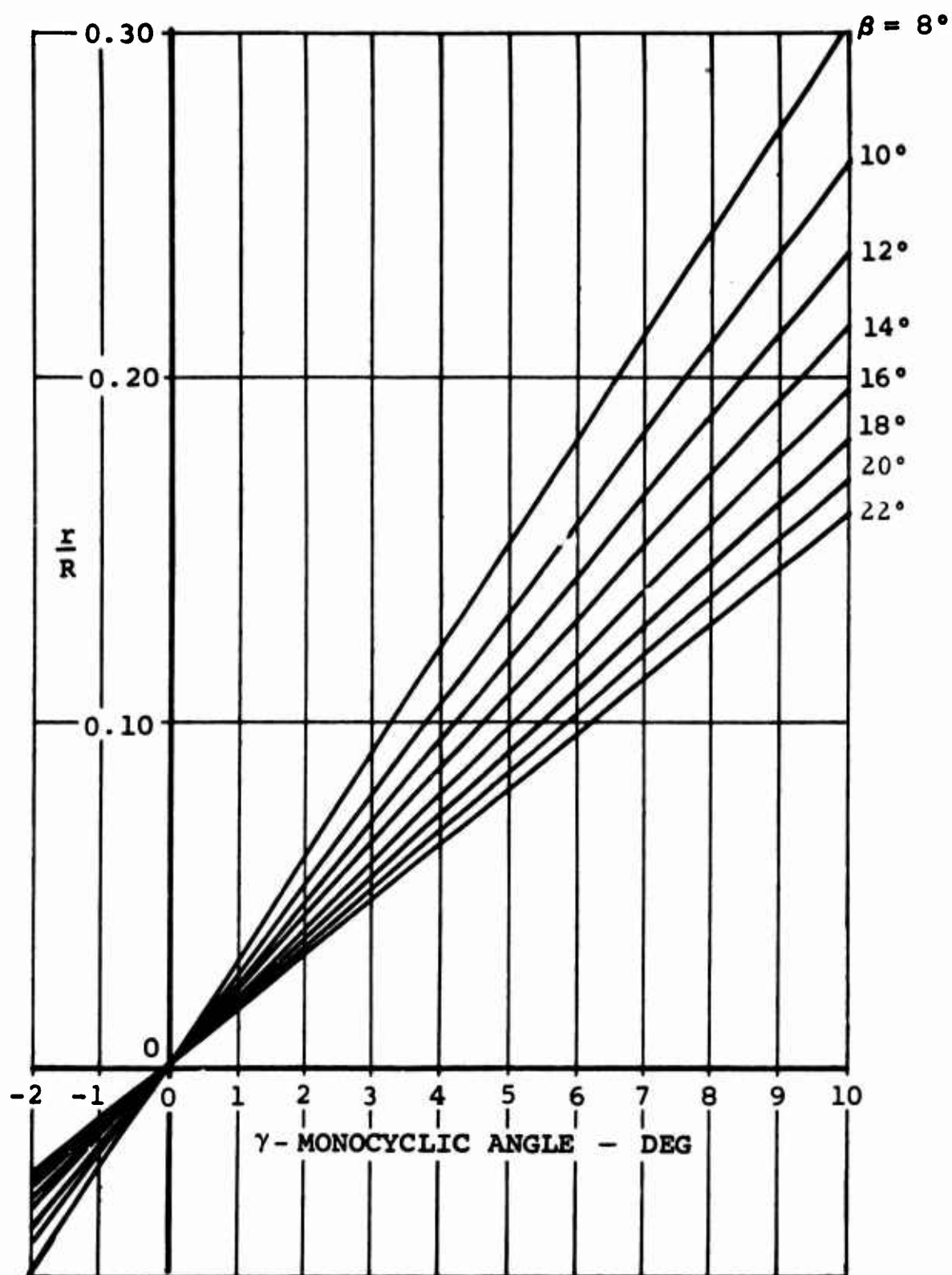RADIUS THRUST OFFSET.

FIGURE 23.   THEORETICAL CYCLIC CONTROL POWER, IN PERCENT
RADIUS THRUST OFFSET.

58
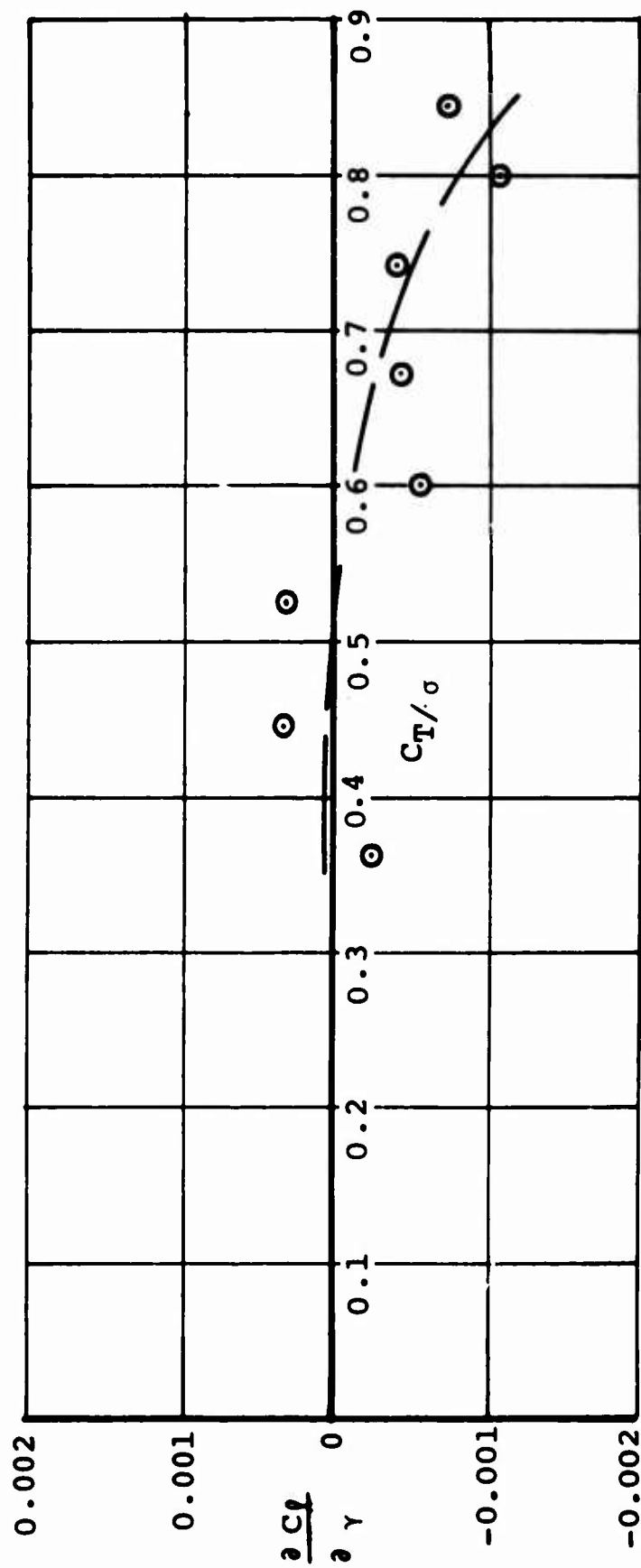
FIGURE 24. EFFECT OF MONOCYCLIC CONTROL ON ROLLING MOMENT.

59
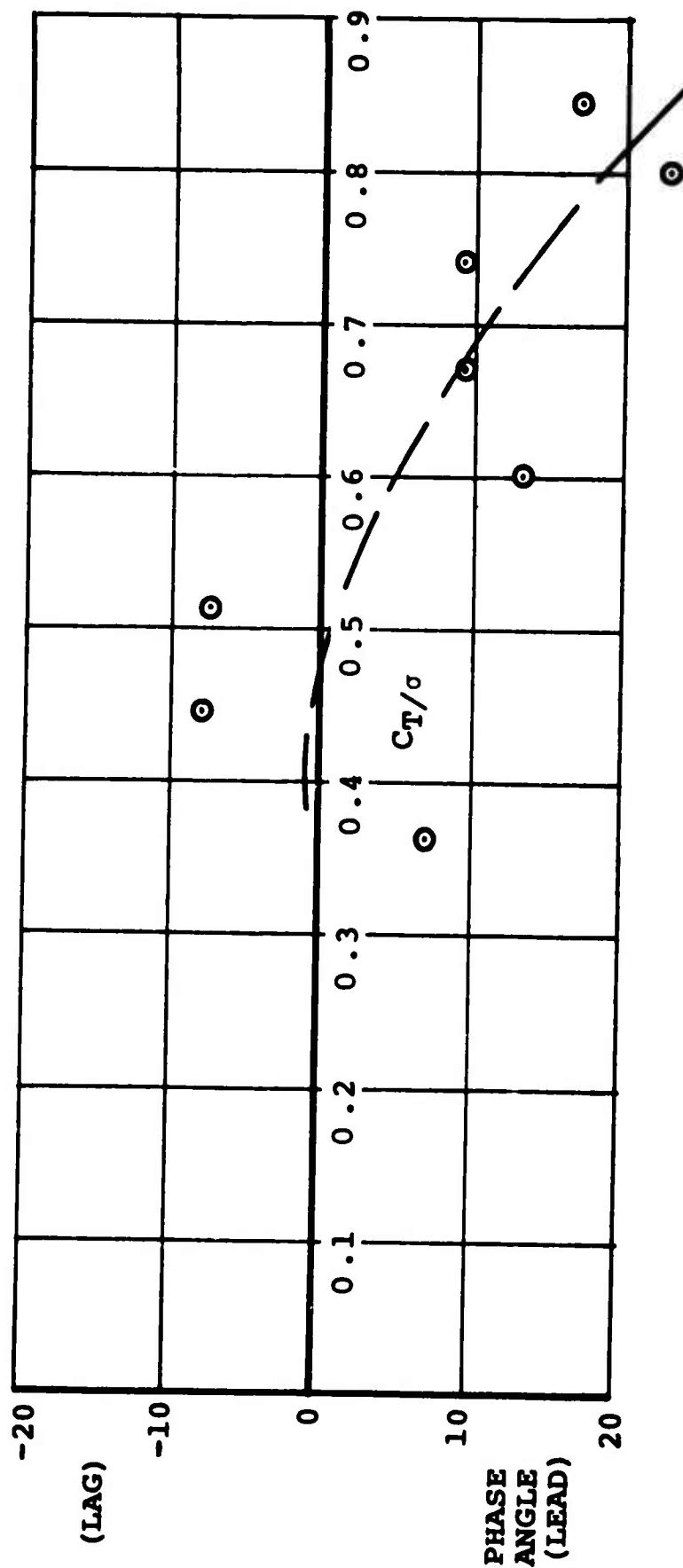
FIGURE 25. PHASE ANGLE OF RESULTANT MOMENT DUE TO MONOCYCLIC INPUT.

60
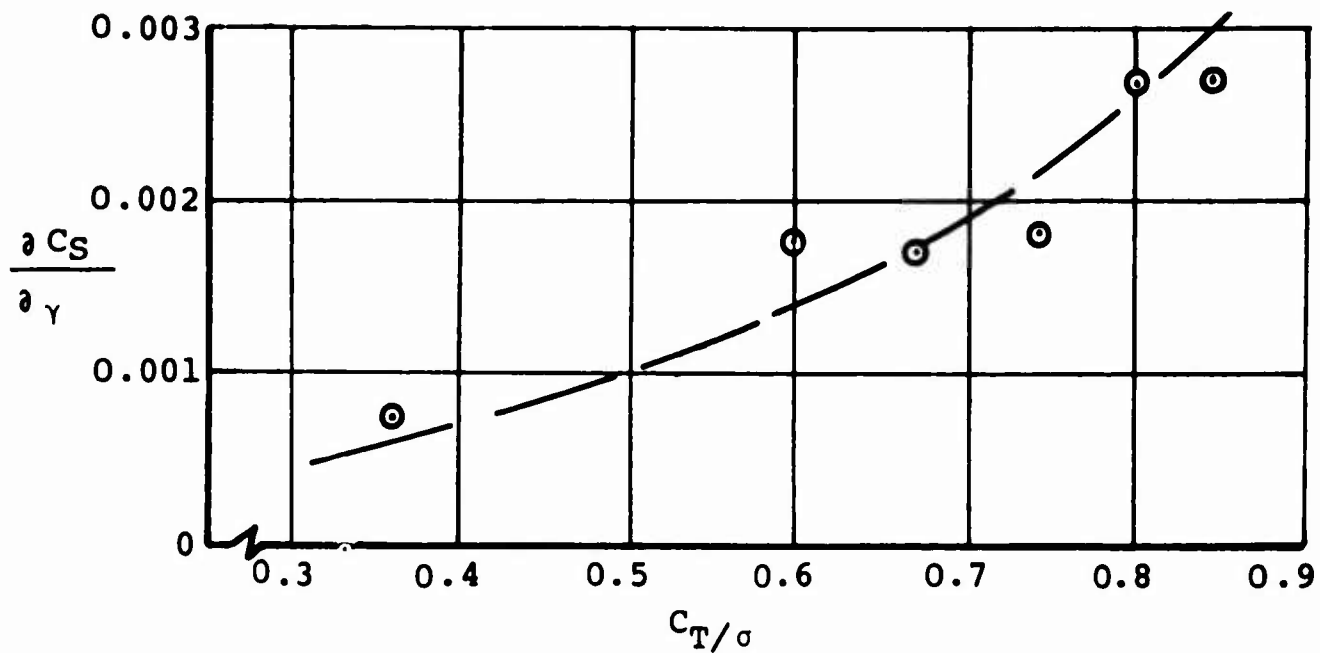
FIGURE 26.   EFFECT OF MONOCYCLIC CONTROL ON SIDE FORCE.
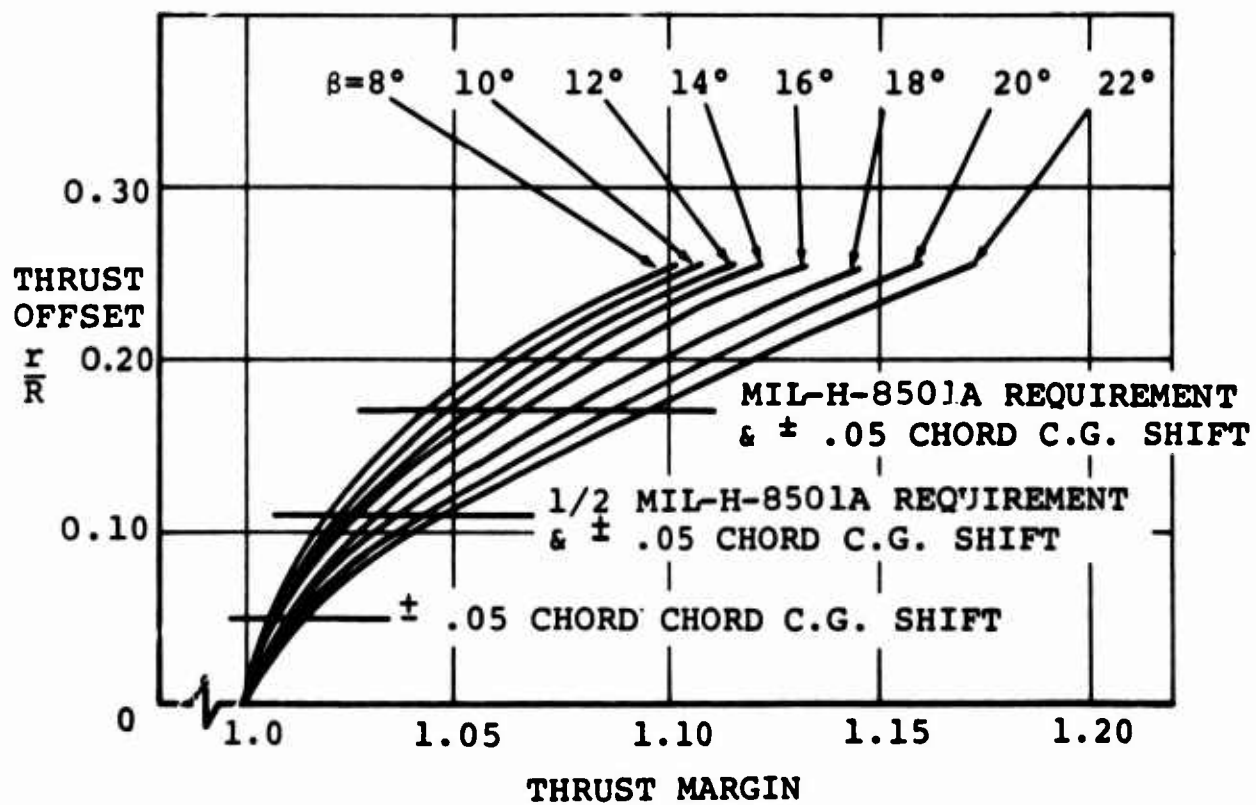
FIGURE 27.   THRUST MARGIN REQUIRED TO HOVER AT CONSTANT
ALTITUDE.

61
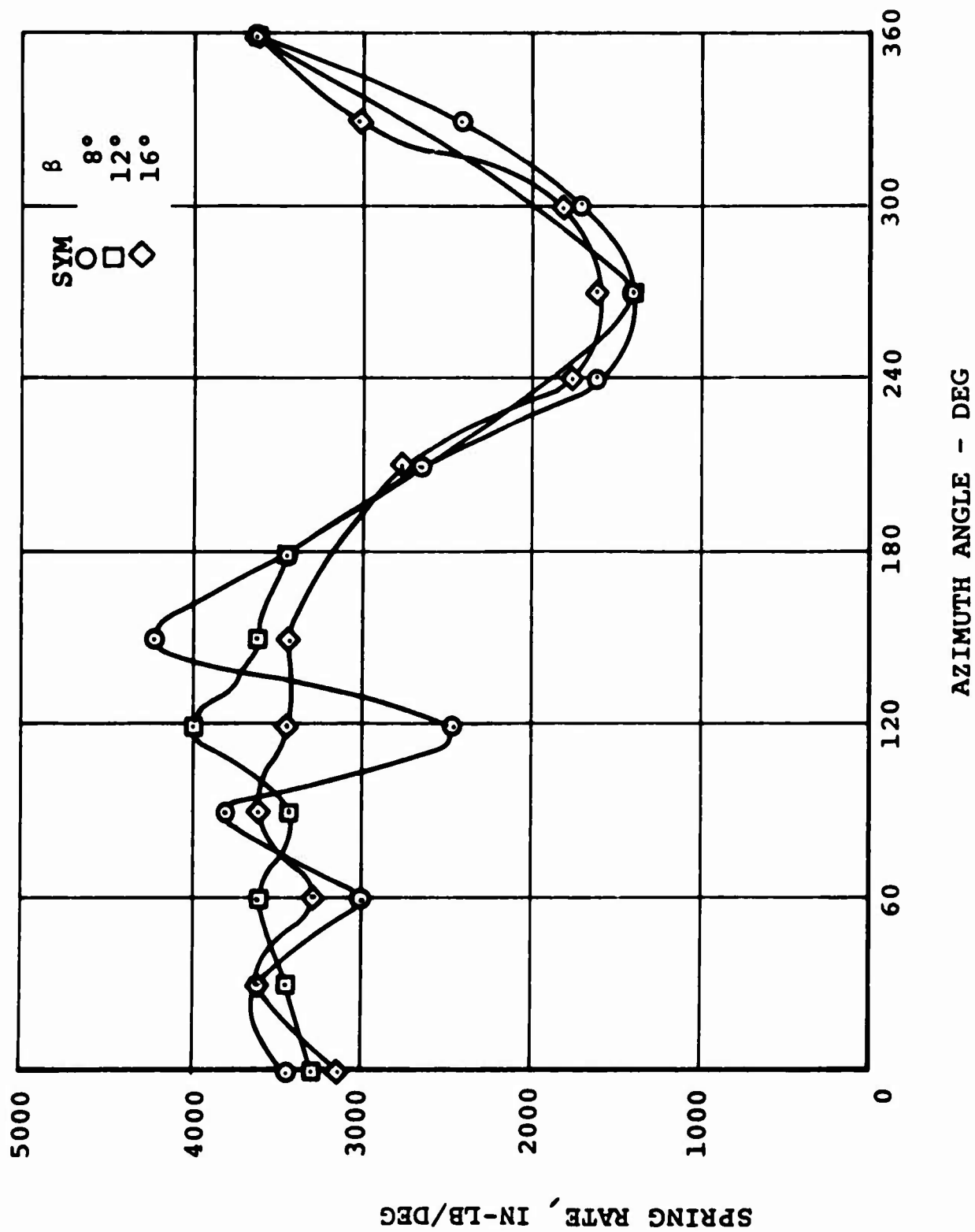
FIGURE 28a. SPRING RATE VARIATION WITH AZIMUTH POSITION, AT CONSTANT CYCLIC ANGLE, CONFIGURATION A (γ = 0°).
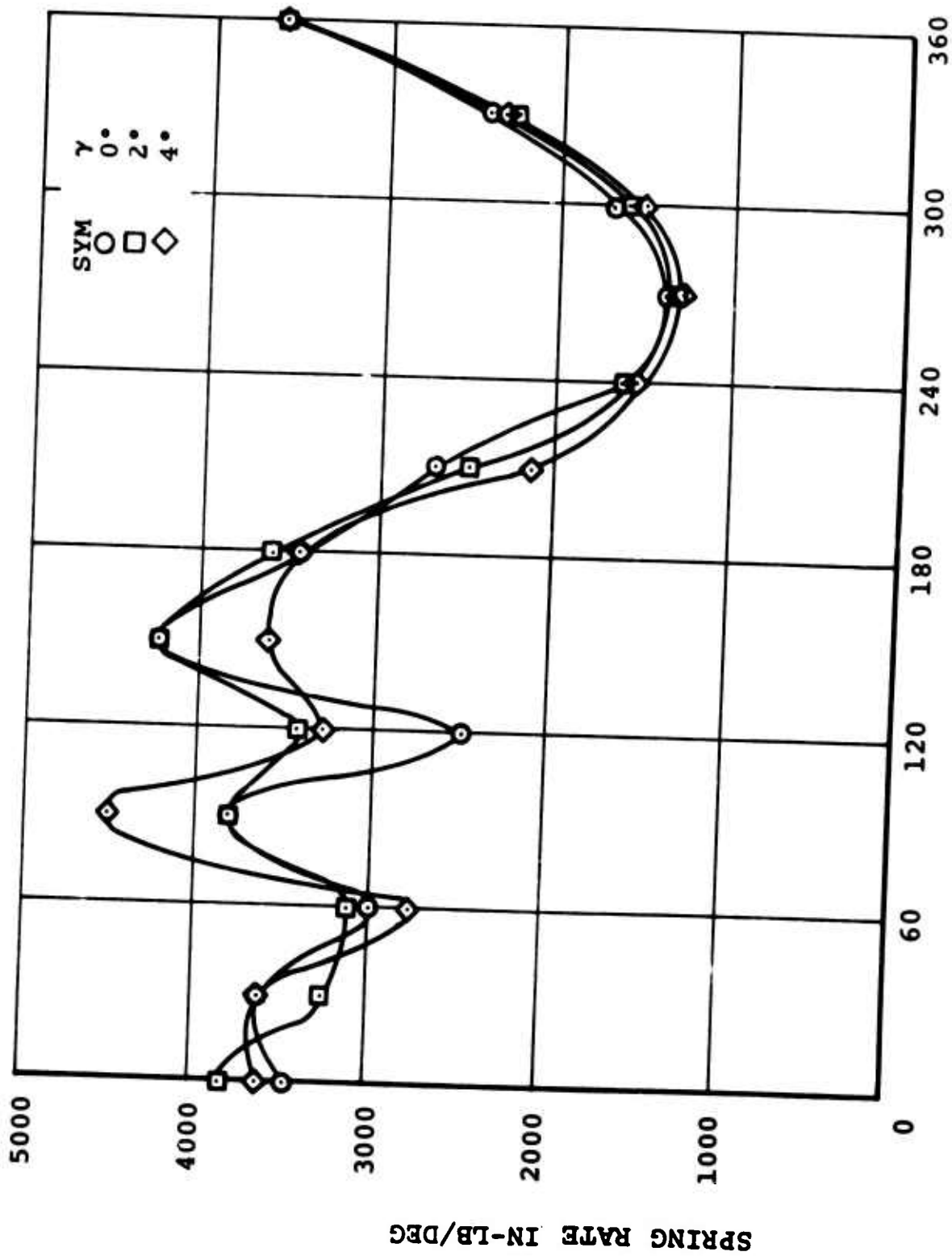
FIGURE 28b. SPRING RATE VARIATION WITH AZIMUTH POSITION, AT CONSTANT COLLECTIVE ANGLE, CONFIGURATION A (β = 8°).
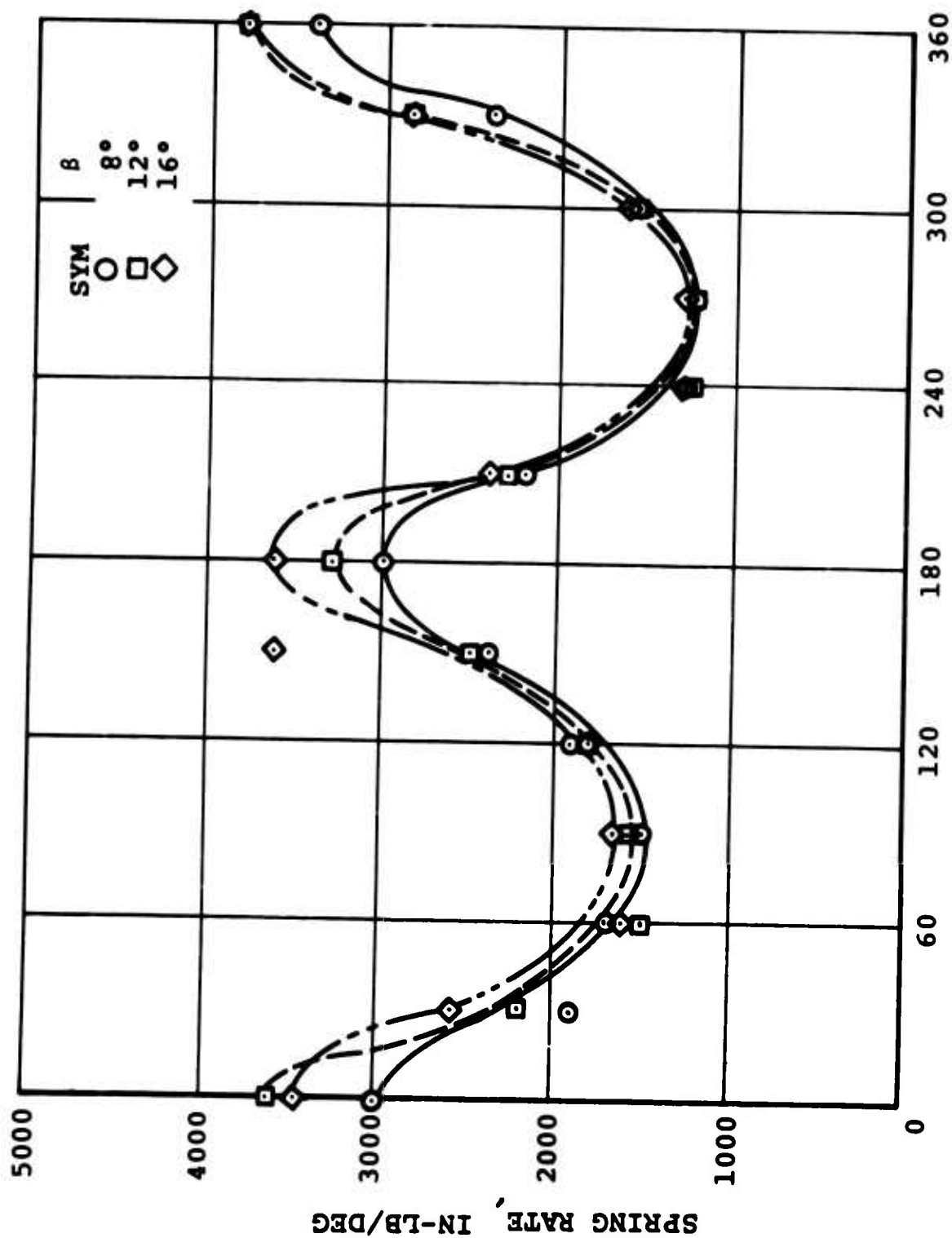
FIGURE 28c. SPRING RATE VARIATION WITH AZIMUTH POSITION, AT CONSTANT CYCLIC ANGLE, CONFIGURATIONS B AND C ($\gamma = 0°$).

64
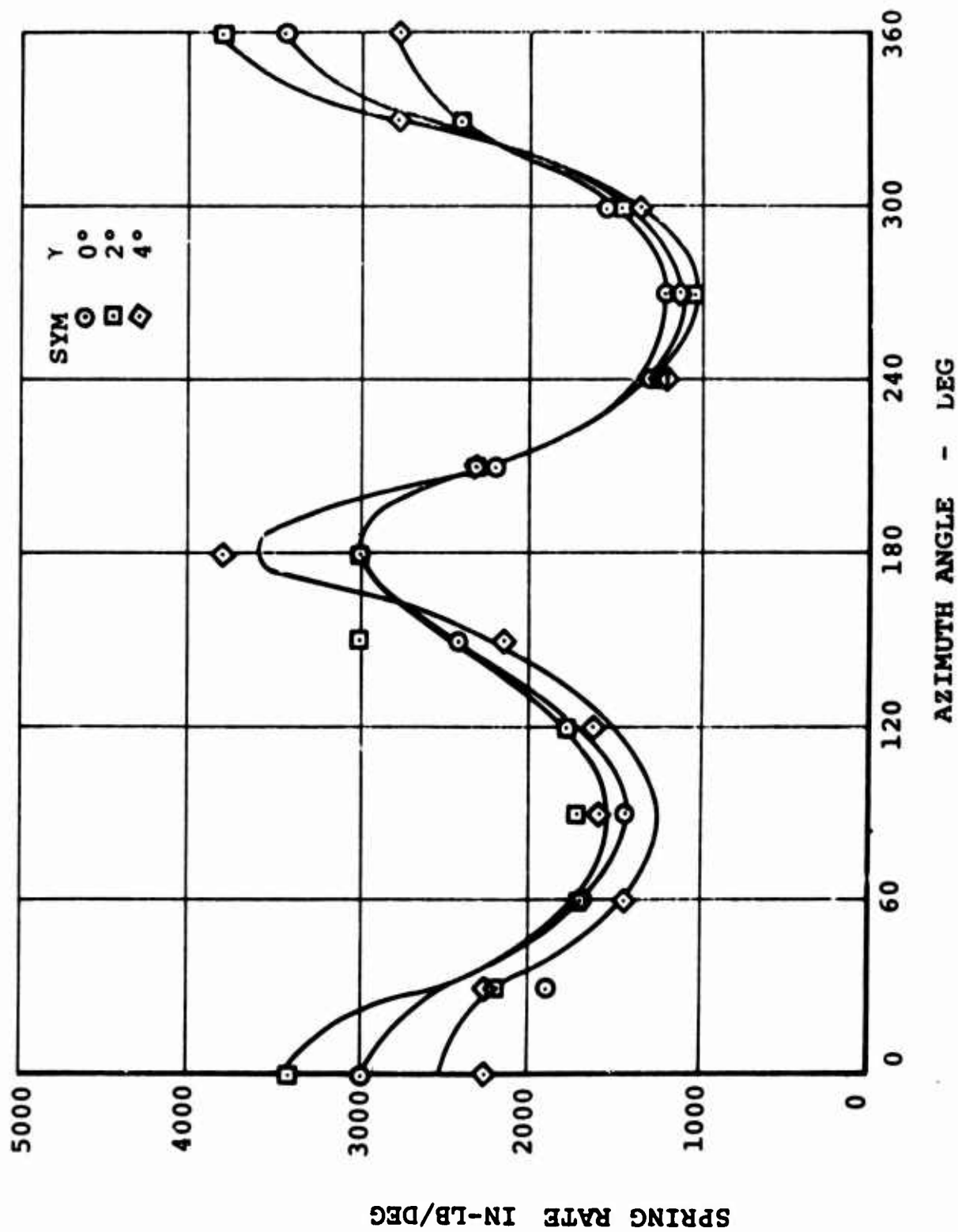
FIGURE 28d. SPRING RATE VARIATION WITH AZIMUTH POSITION, AT CONSTANT COLLECTIVE ANGLE, CONFIGURATIONS B AND C (β = 8°).

65
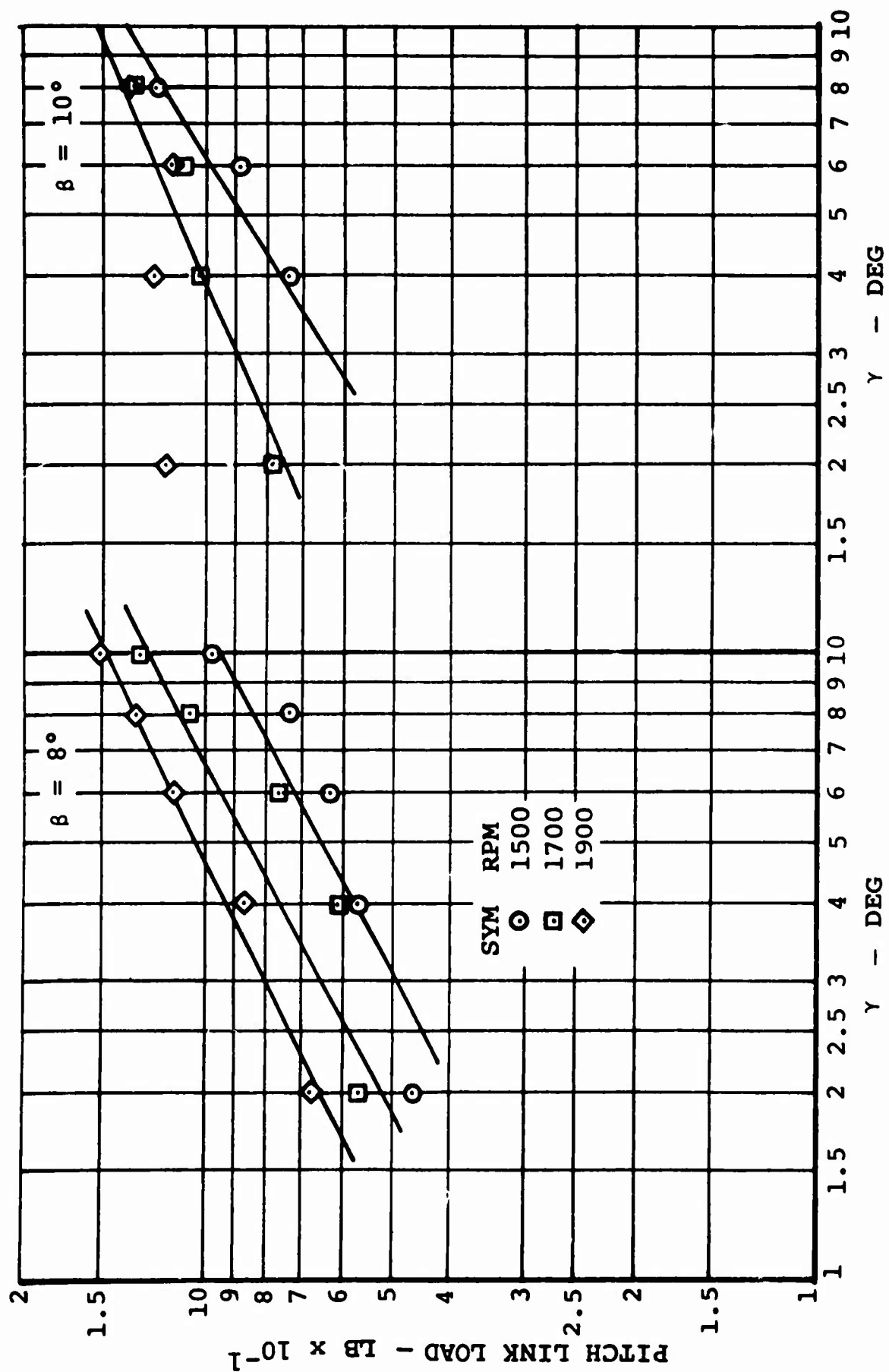
FIGURE 29a. OSCILLATORY PITCH LINK LOAD AS A FUNCTION OF CYCLIC ANGLE, CONFIGURATION A, $\beta = 8°$ AND 10°.

66
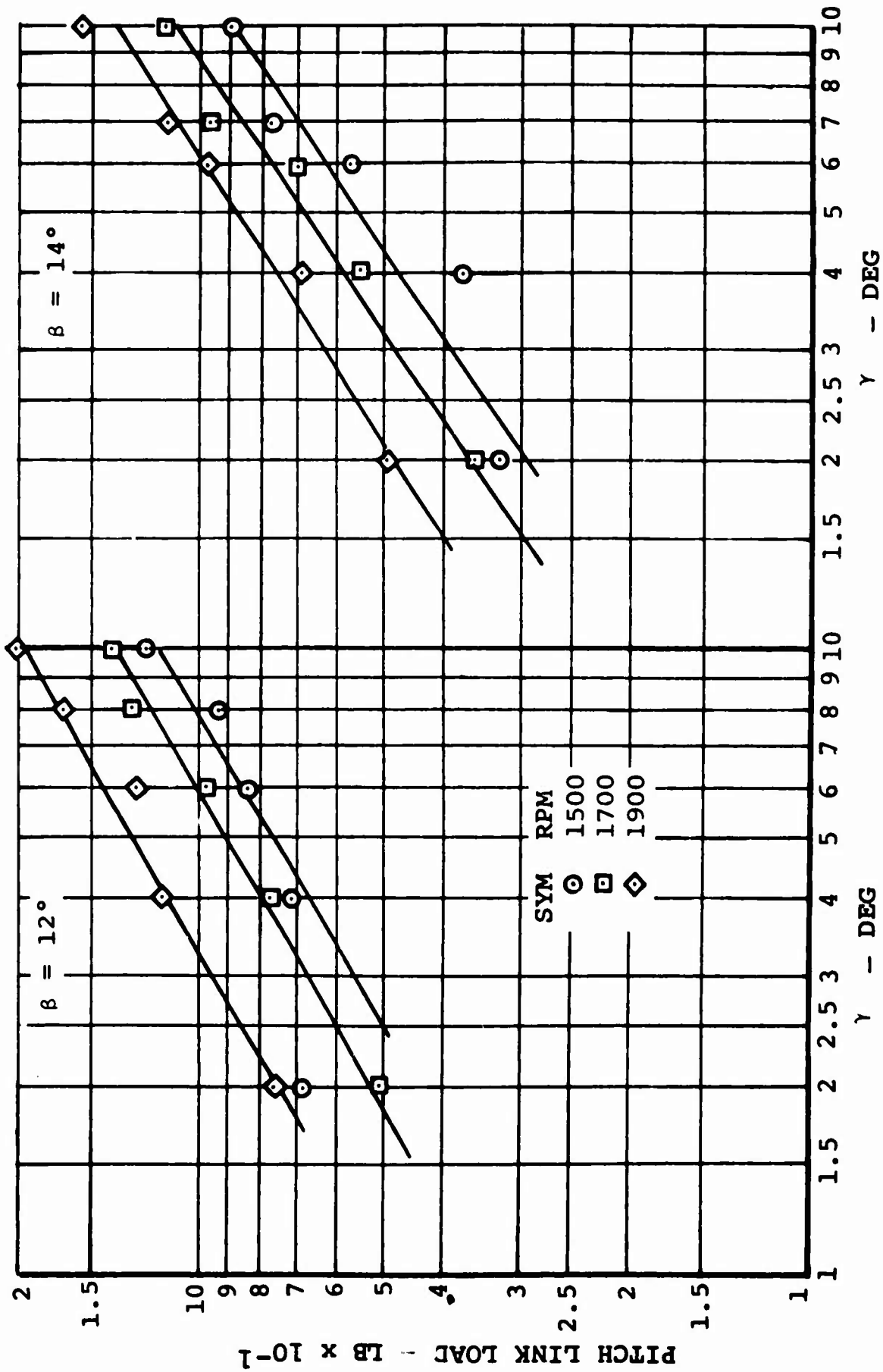
FIGURE 29b. OSCILLATORY PITCH LINK LOAD AS A FUNCTION OF CYCLIC ANGLE, CONFIGURATION A, β = 12° AND 14°.
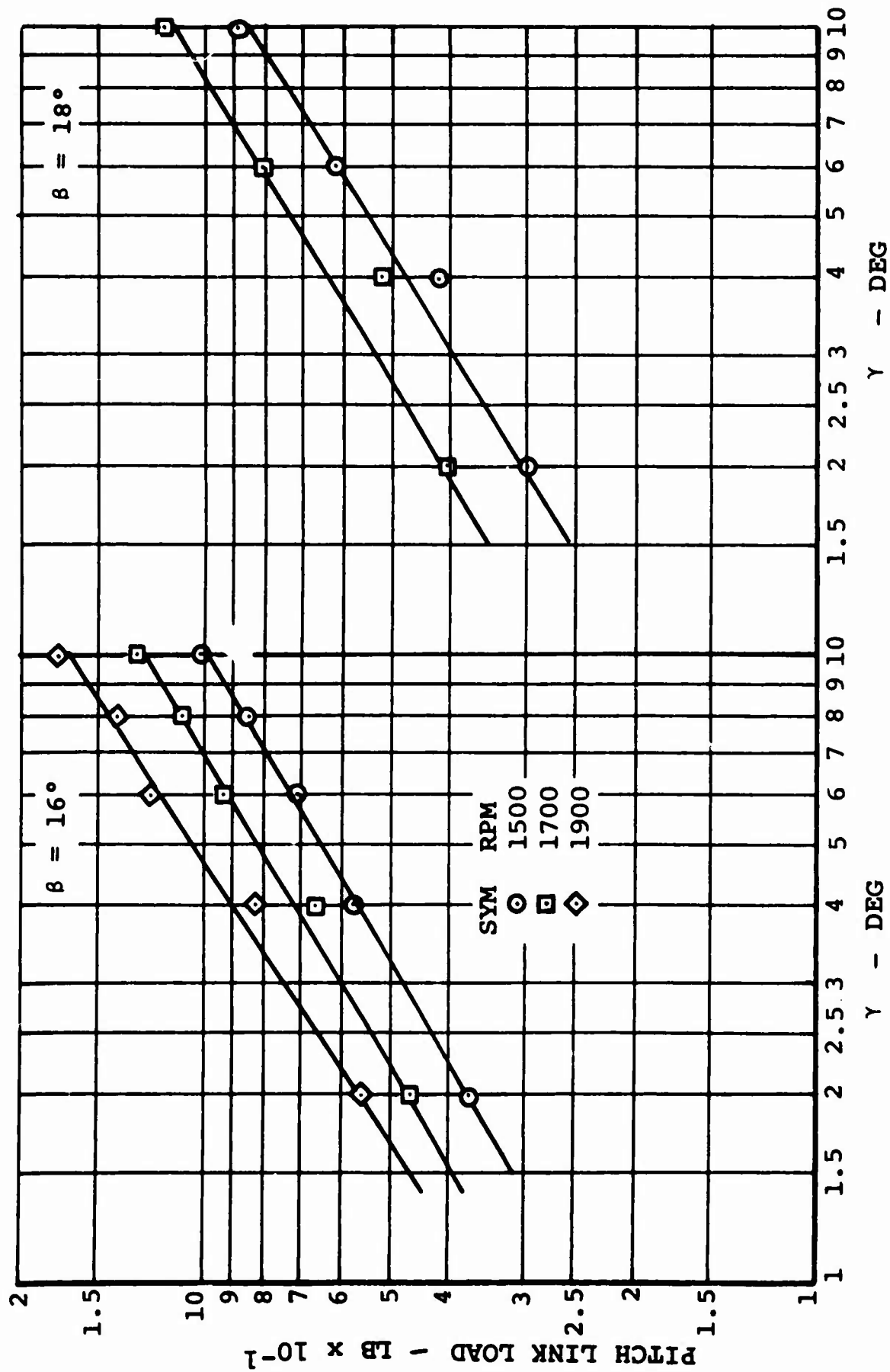
FIGURE 29c. OSCILLATORY PITCH LINK LOAD AS A FUNCTION OF CYCLIC ANGLE, CONFIGURATION A, β = 16° AND 18°.

FIGURE 30d. OSCILLATORY PITCH LINK LOAD AS A FUNCTION OF PROPELLER RPM, CONFIGURATION A, β = 8° AND 10°.

69
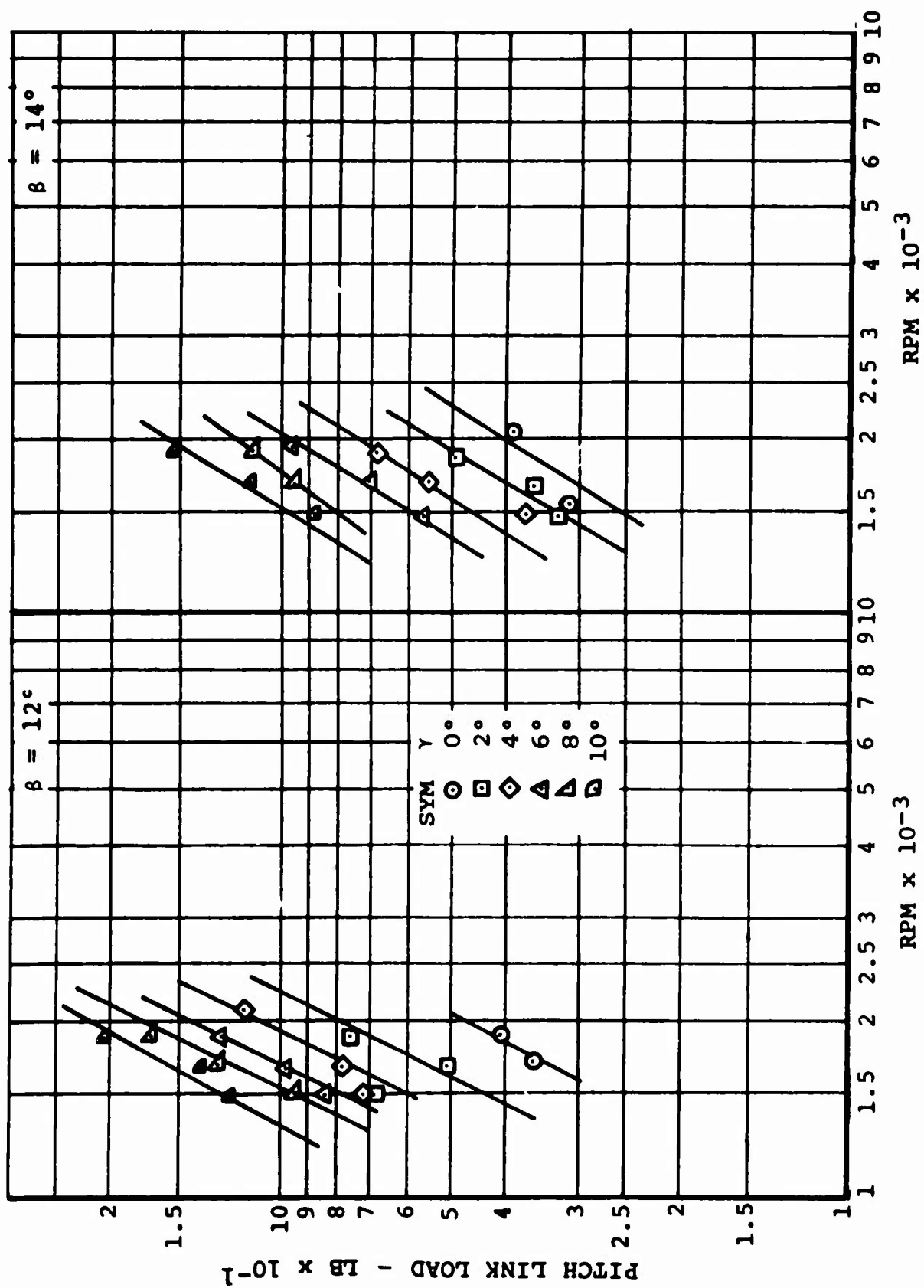
FIGURE 30b. OSCILLATORY PITCH LINK LOAD AS A FUNCTION OF PROPELLER RPM, CONFIGURATION A, β = 12° AND 14°.
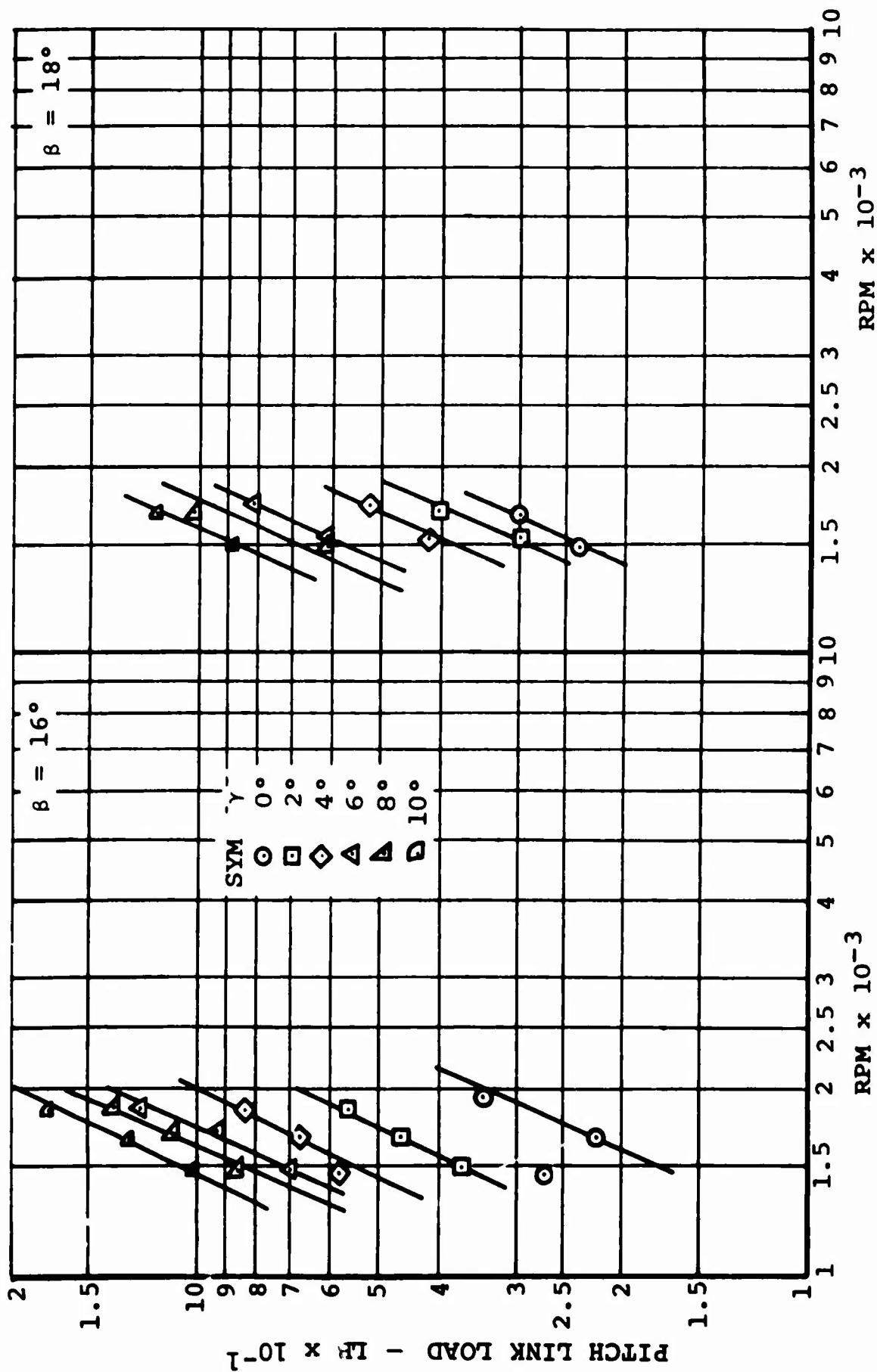
FIGURE 30c. OSCILLATORY PITCH LINK LOAD AS A FUNCTION
OF PROPELLER RPM, CONFIGURATION A,
β = 16° AND 18°.
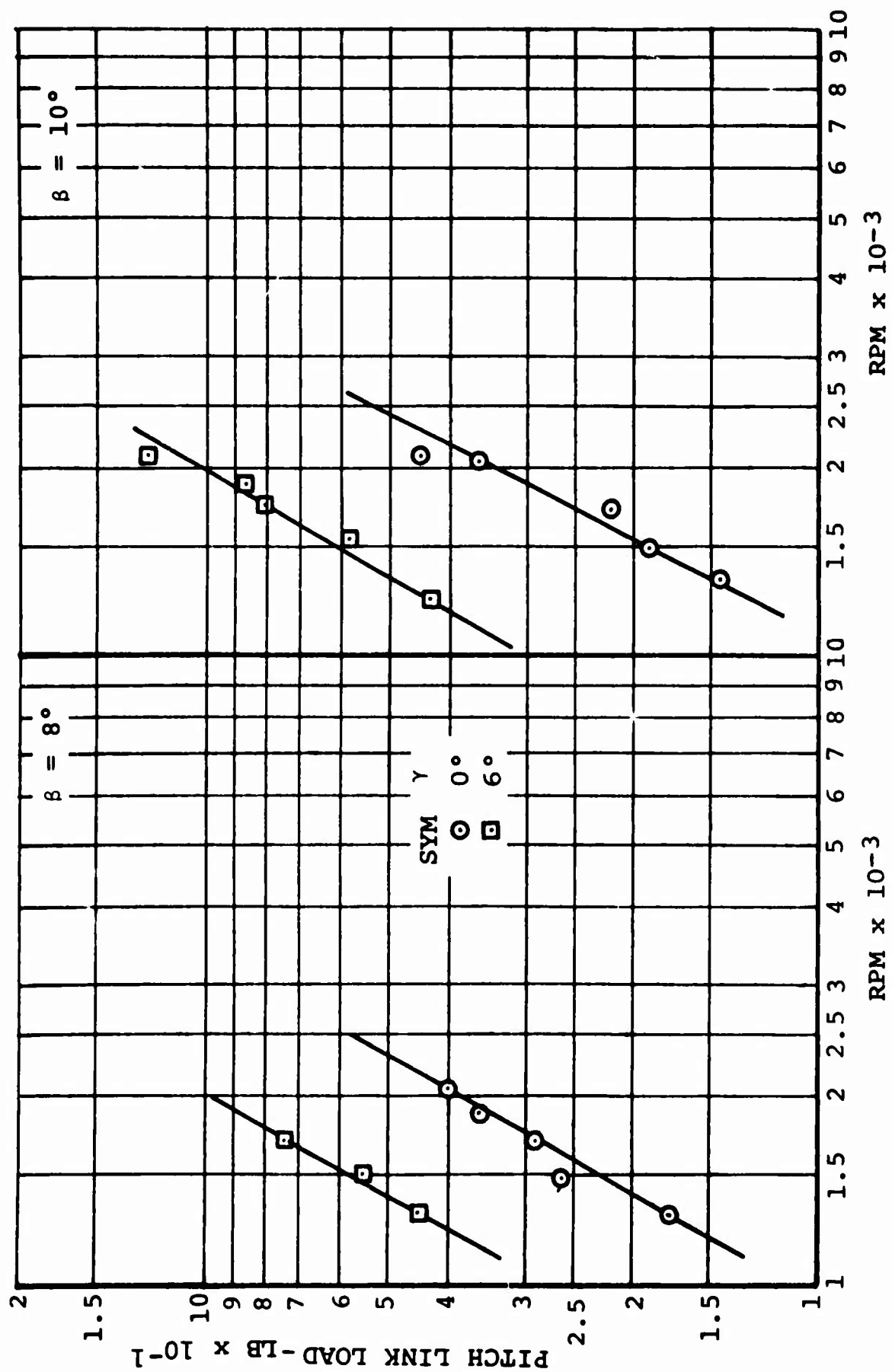
71

FIGURE 30d. OSCILLATORY PITCH LINK LOAD AS A FUNCTION
OF PROPELLER RPM, CONFIGURATION B,
β = 8° AND 10°.
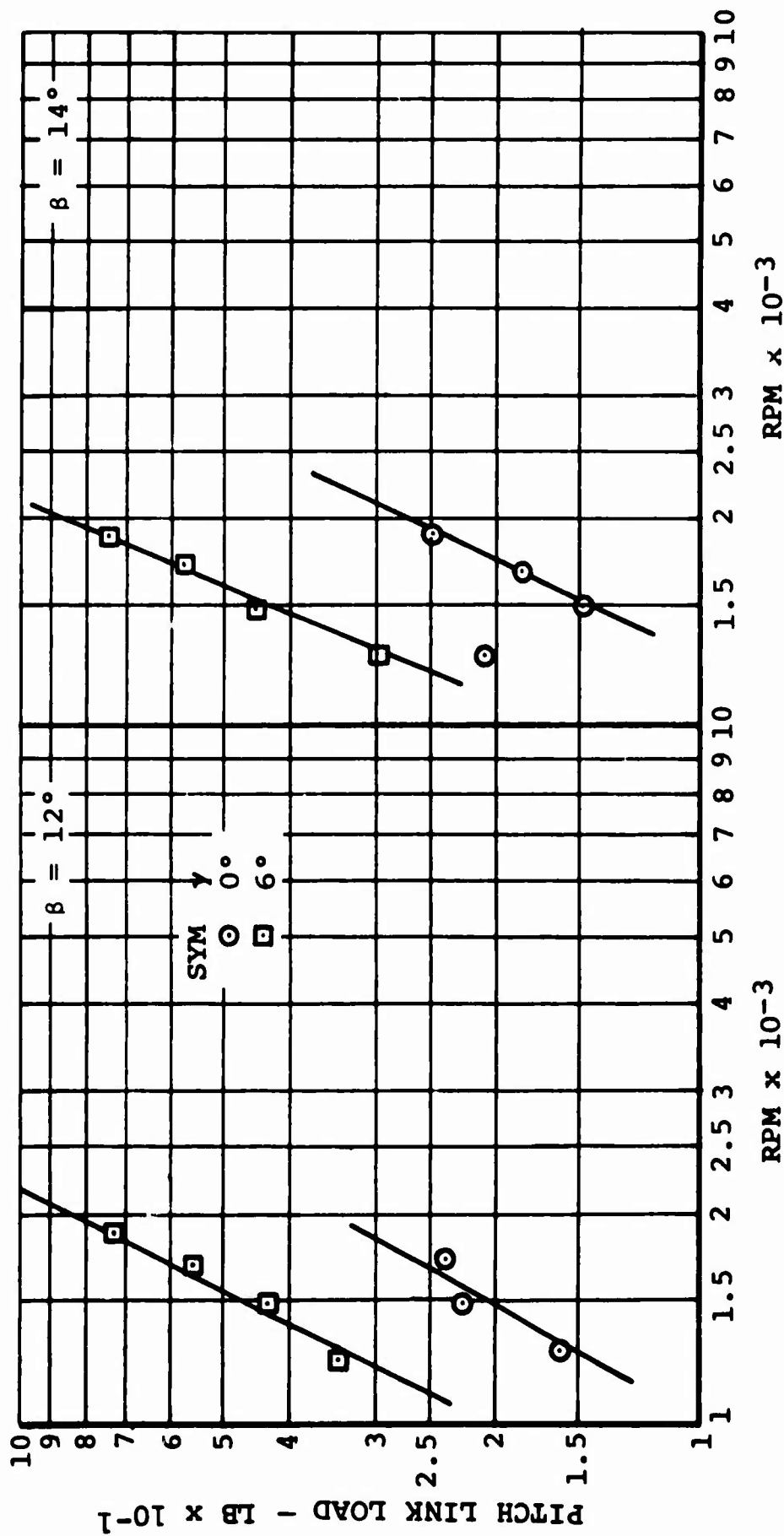
FIGURE 30e. OSCILLATORY PITCH LINK LOAD AS A FUNCTION OF PROPELLER RPM, CONFIGURATION B, β = 12° AND 14°.

73
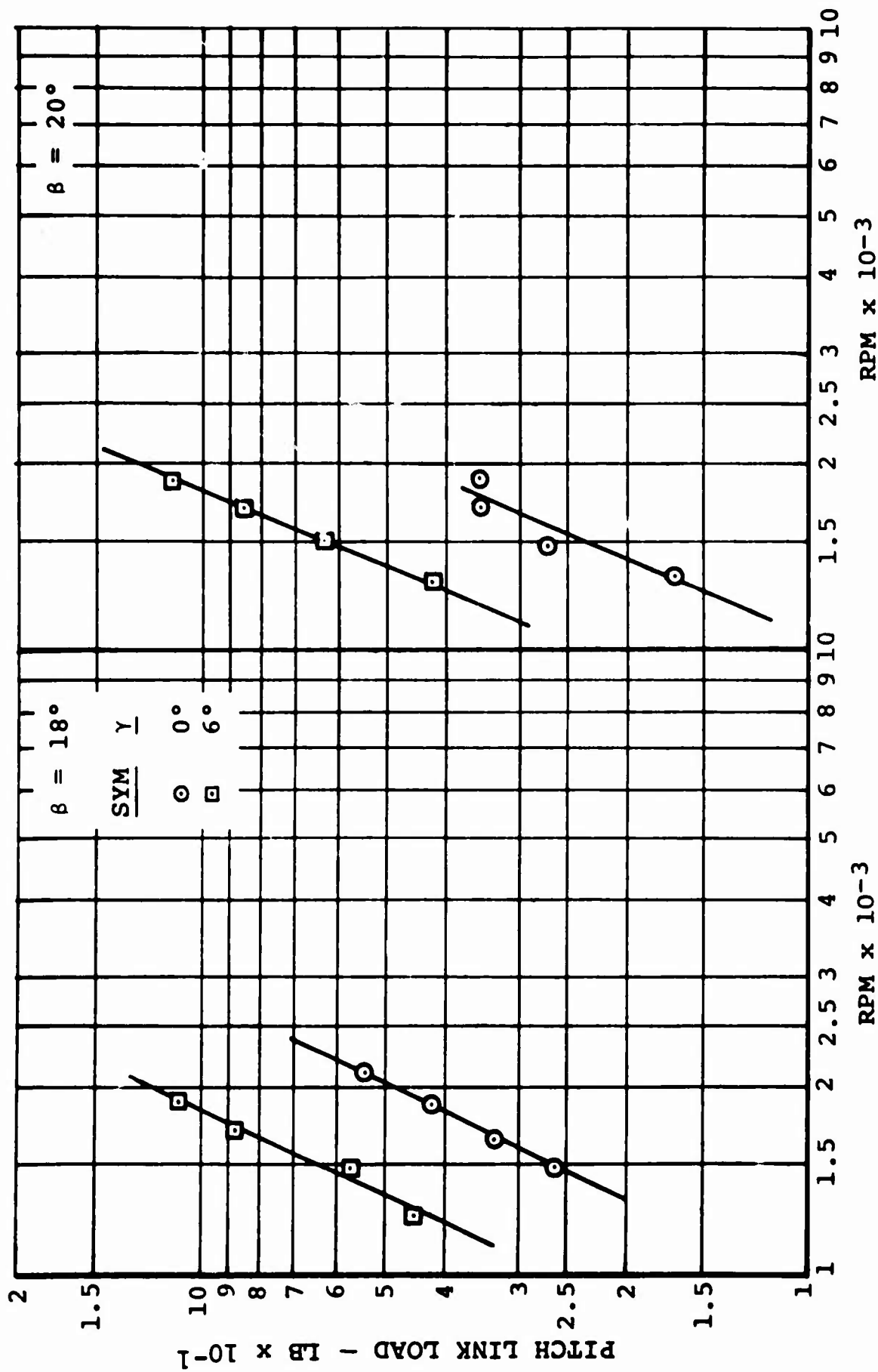
FIGURE 30f. OSCILLATORY PITCH LINK LOAD AS A FUNCTION
OF PROPELLER RPM, CONFIGURATION B,
β = 18° AND 20°.

74
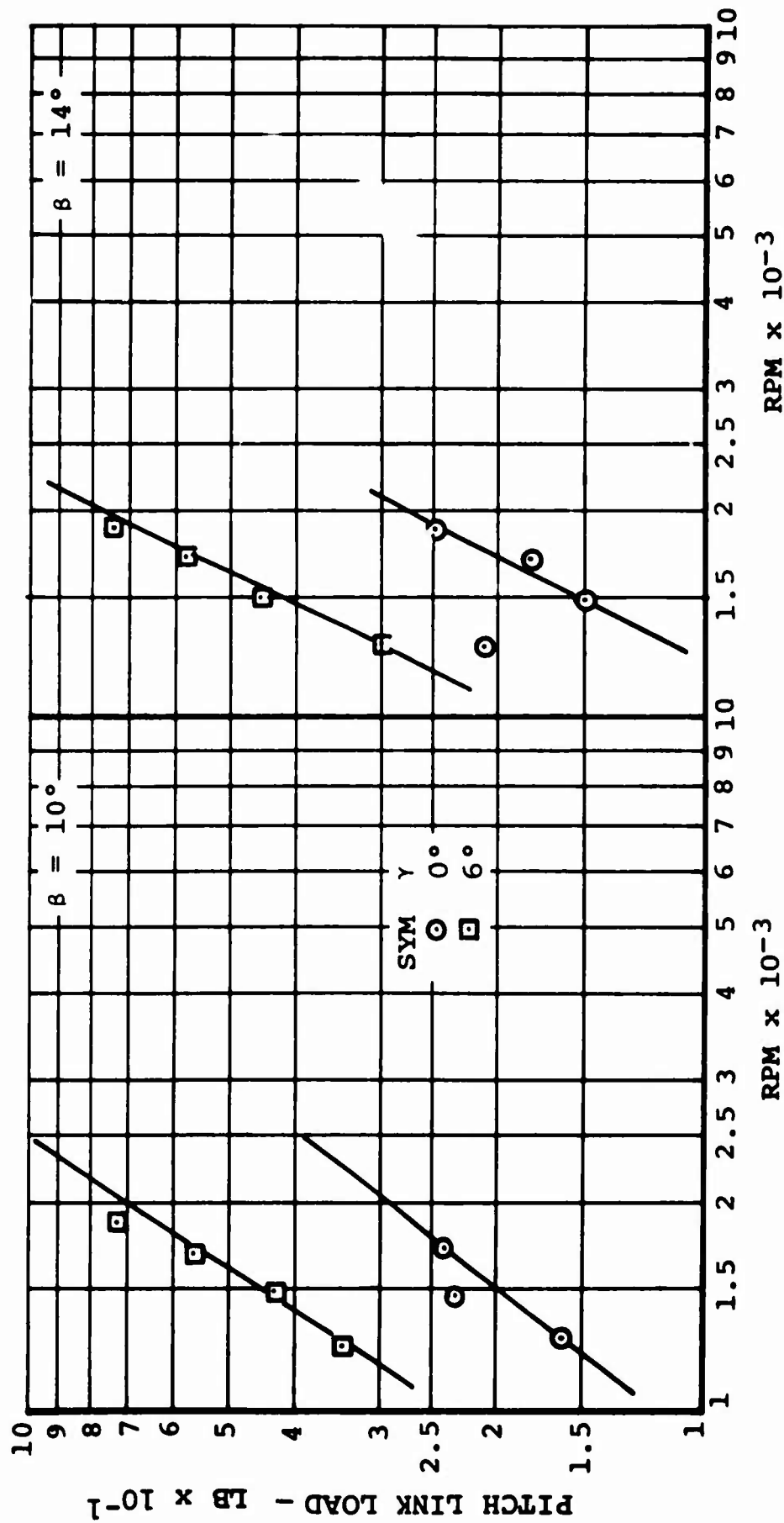
FIGURE 30g. OSCILLATORY PITCH LINK LOAD AS A FUNCTION OF PROPELLER RPM, CONFIGURATION C, β = 10° AND 14°.
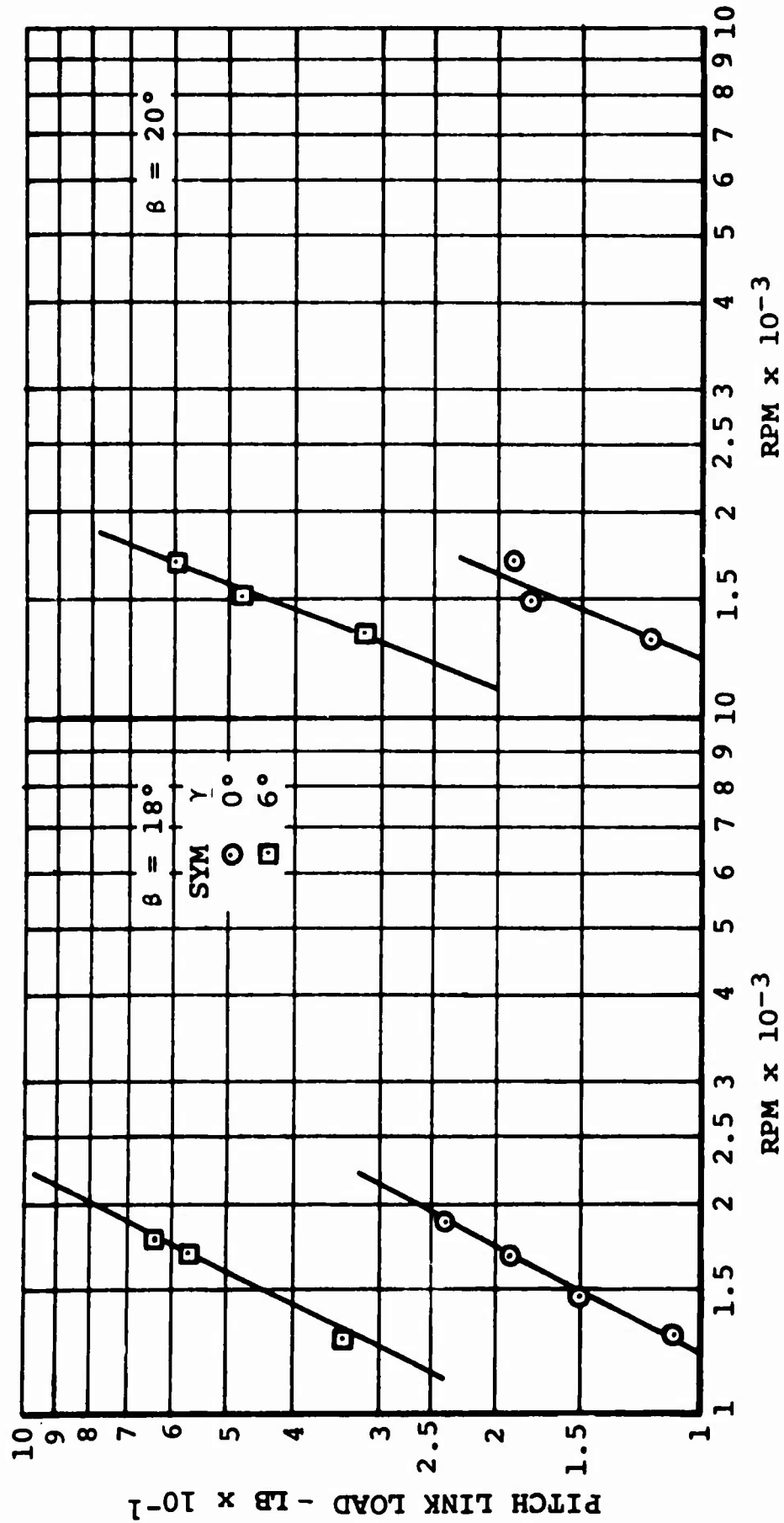
FIGURE 30h. OSCILLATORY PITCH LINK LOAD AS A FUNCTION OF PROPELLER RPM, CONFIGURATION C, β = 18° AND 20°.
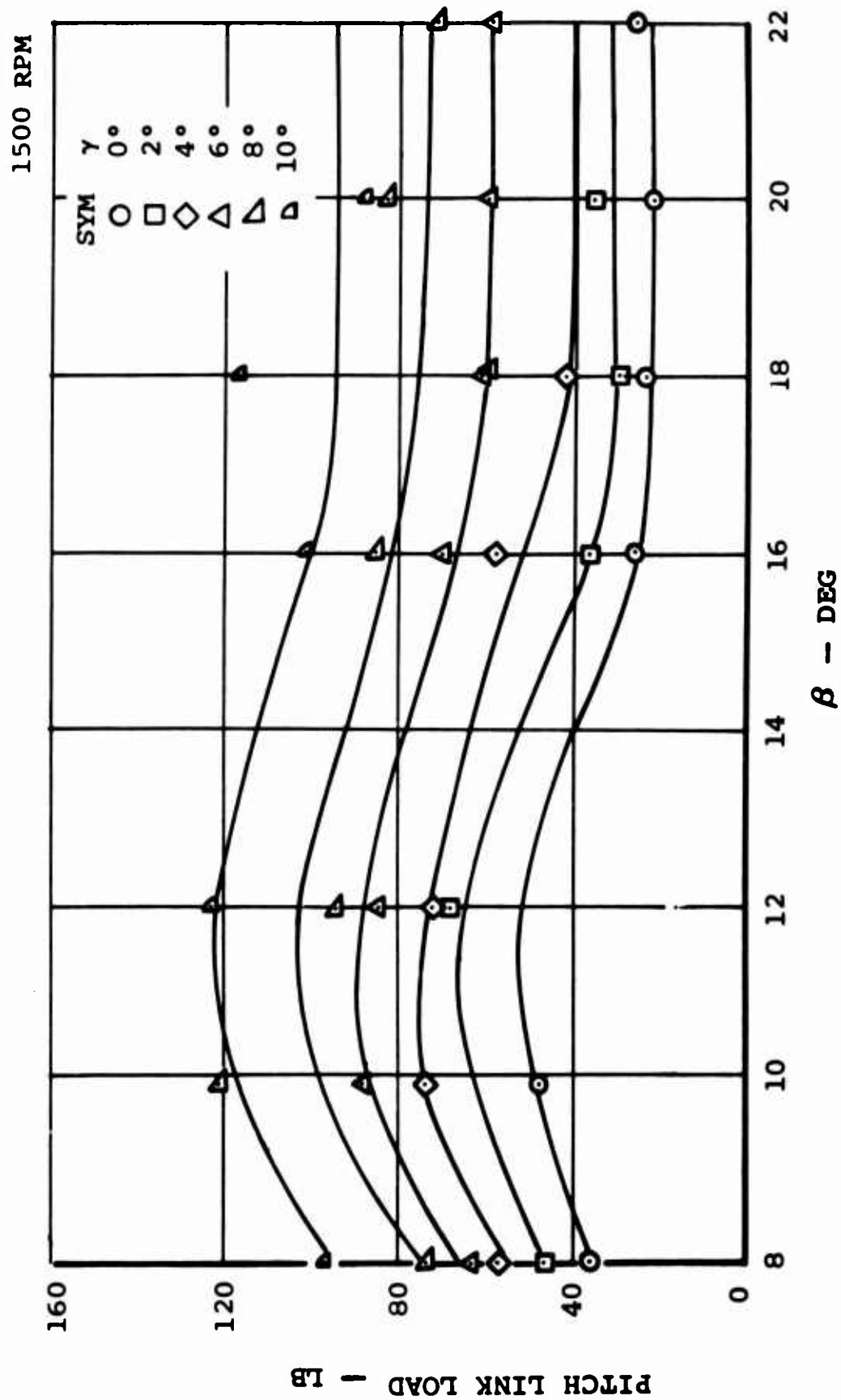
FIGURE 31a. PITCH LINK OSCILLATORY LOAD VARIATION WITH COLLECTIVE ANGLE, CONFIGURATION A, 1500 RPM.

77
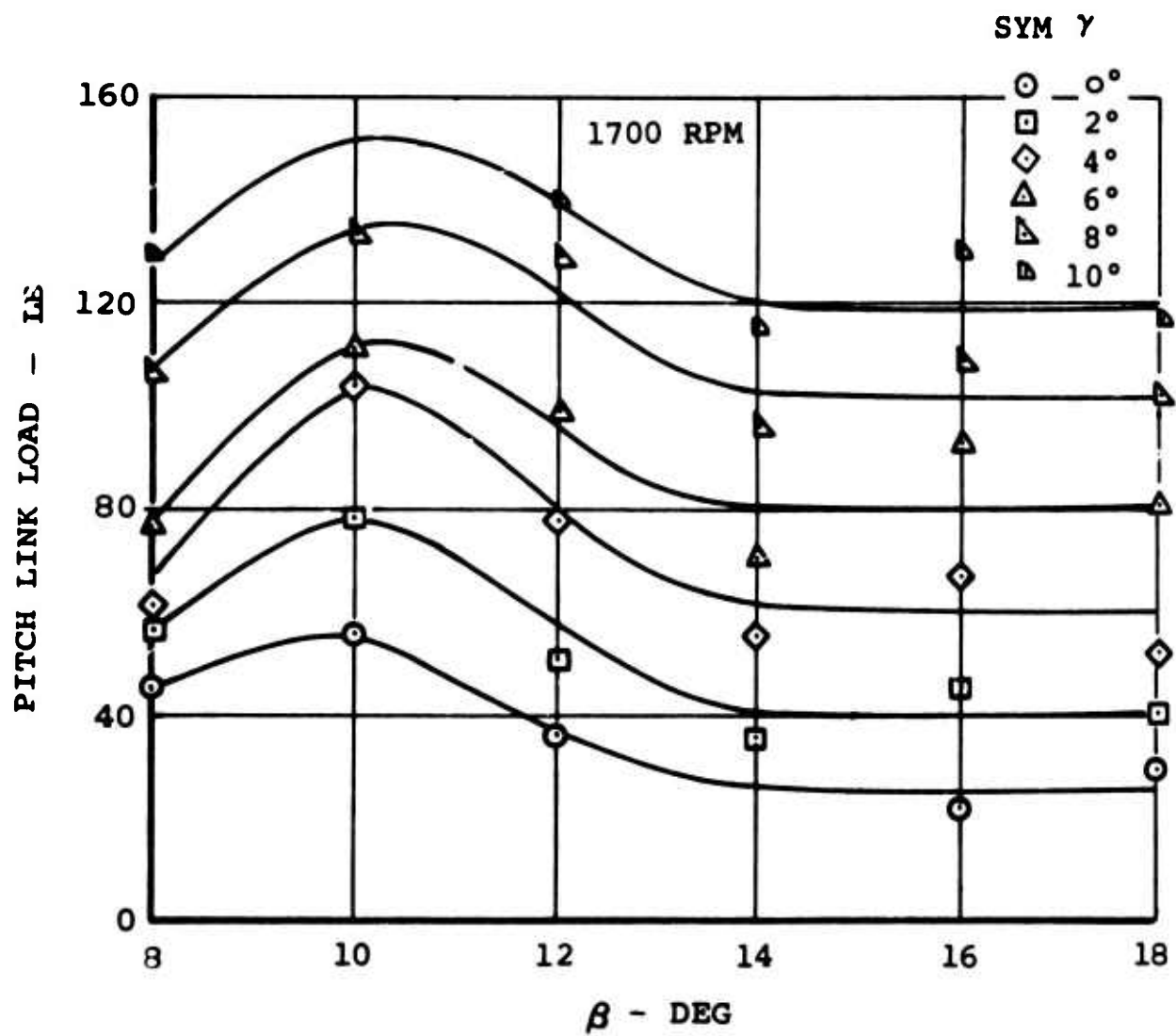
FIGURE 31b. PITCH LINK OSCILLATORY LOAD VARIATION WITH COLLECTIVE ANGLE, CONFIGURATION A, 1700 RPM.
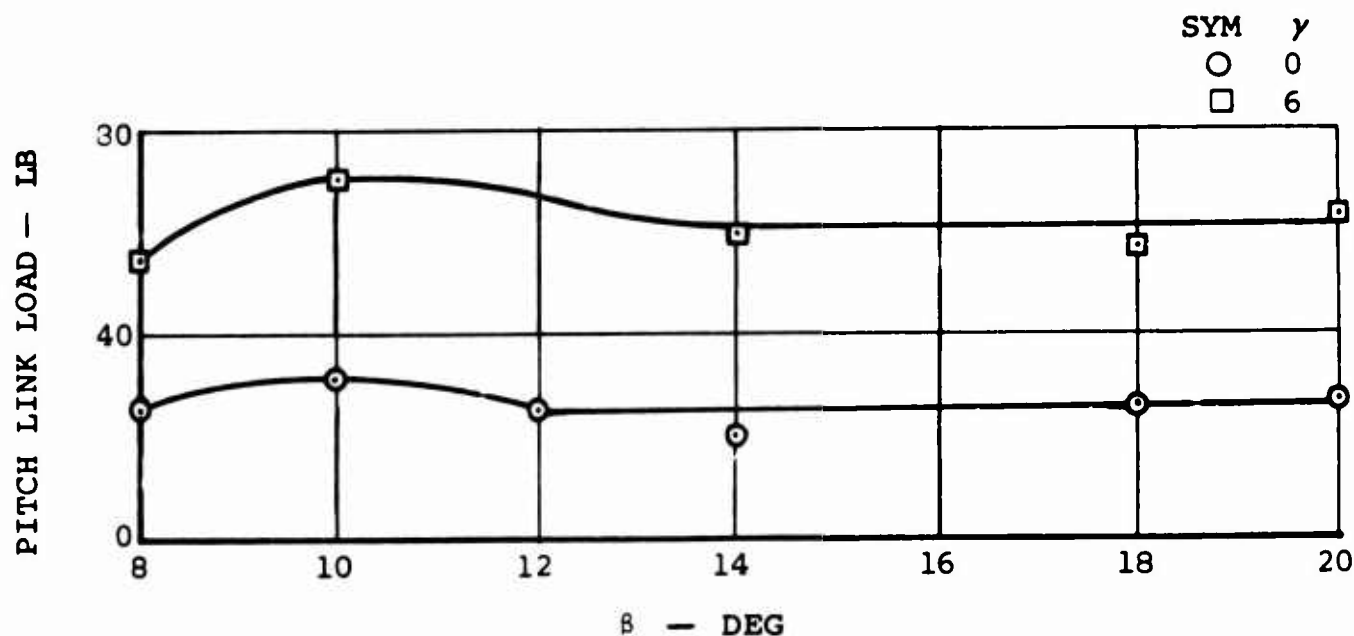
FIGURE 31c.   PITCH LINK OSCILLATORY LOAD VARIATION WITH
COLLECTIVE ANGLE, CONFIGURATION B, 1500 RPM
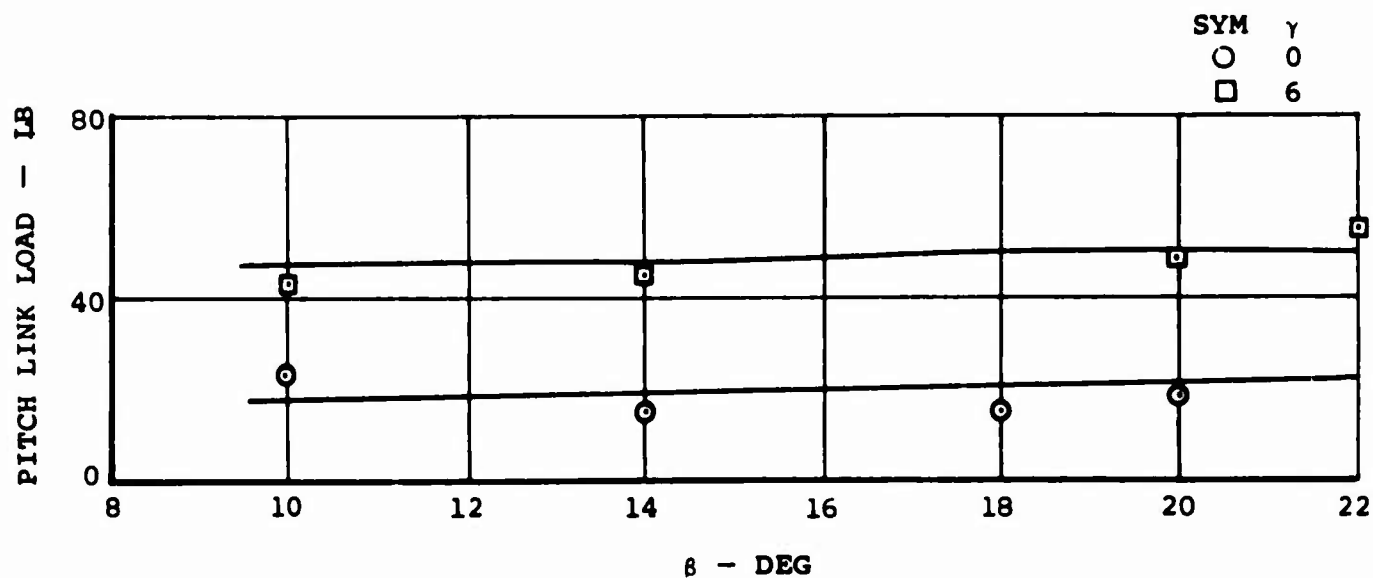
FIGURE 31d.   PITCH LINK OSCILLATORY LOAD VARIATION WITH
COLLECTIVE ANGLE, CONFIGURATION C, 1500 RPM.

79
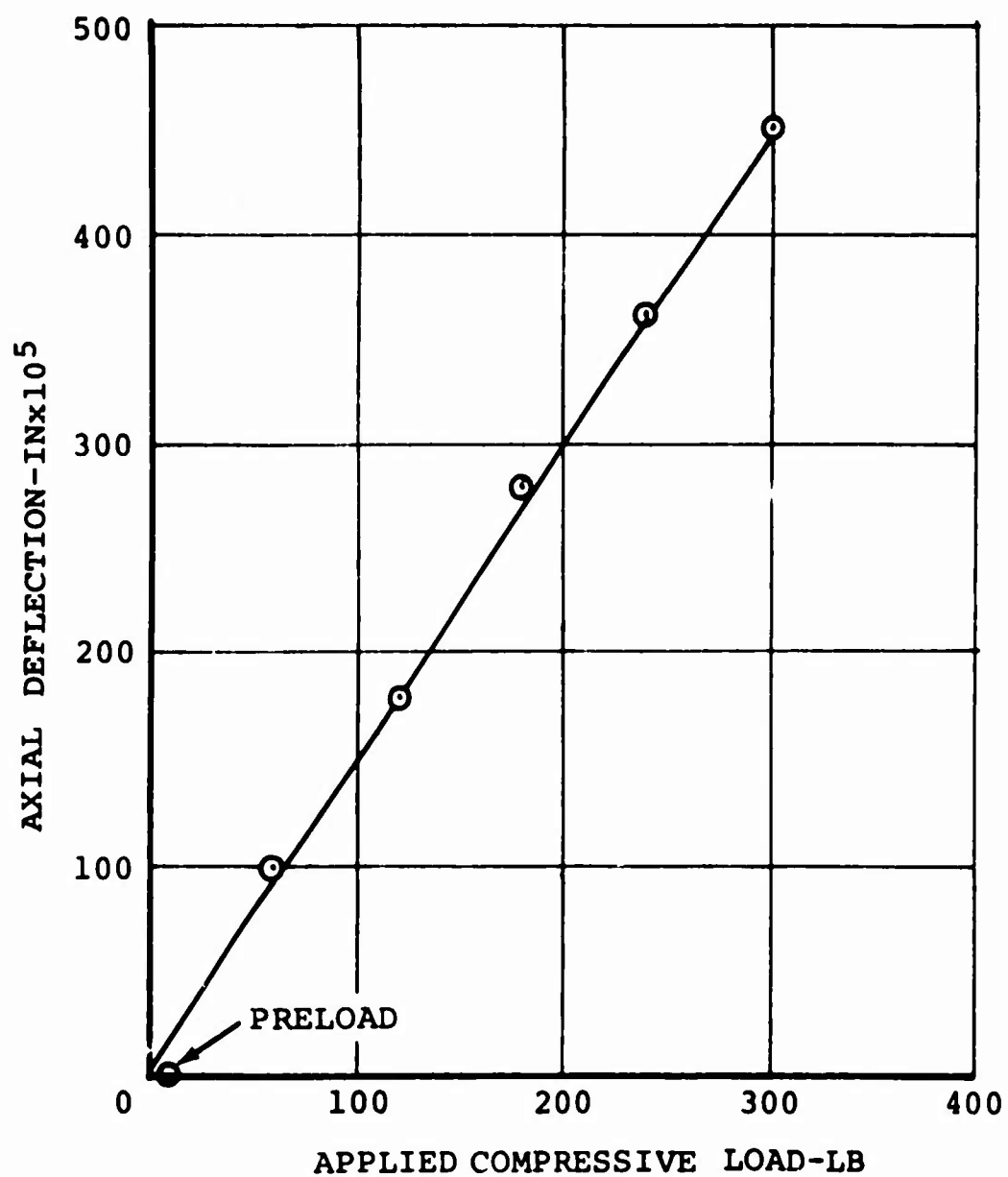
FIGURE 32a.   VZ-2 PITCH LINK AXIAL DEFLECTION IN
COMPRESSION.
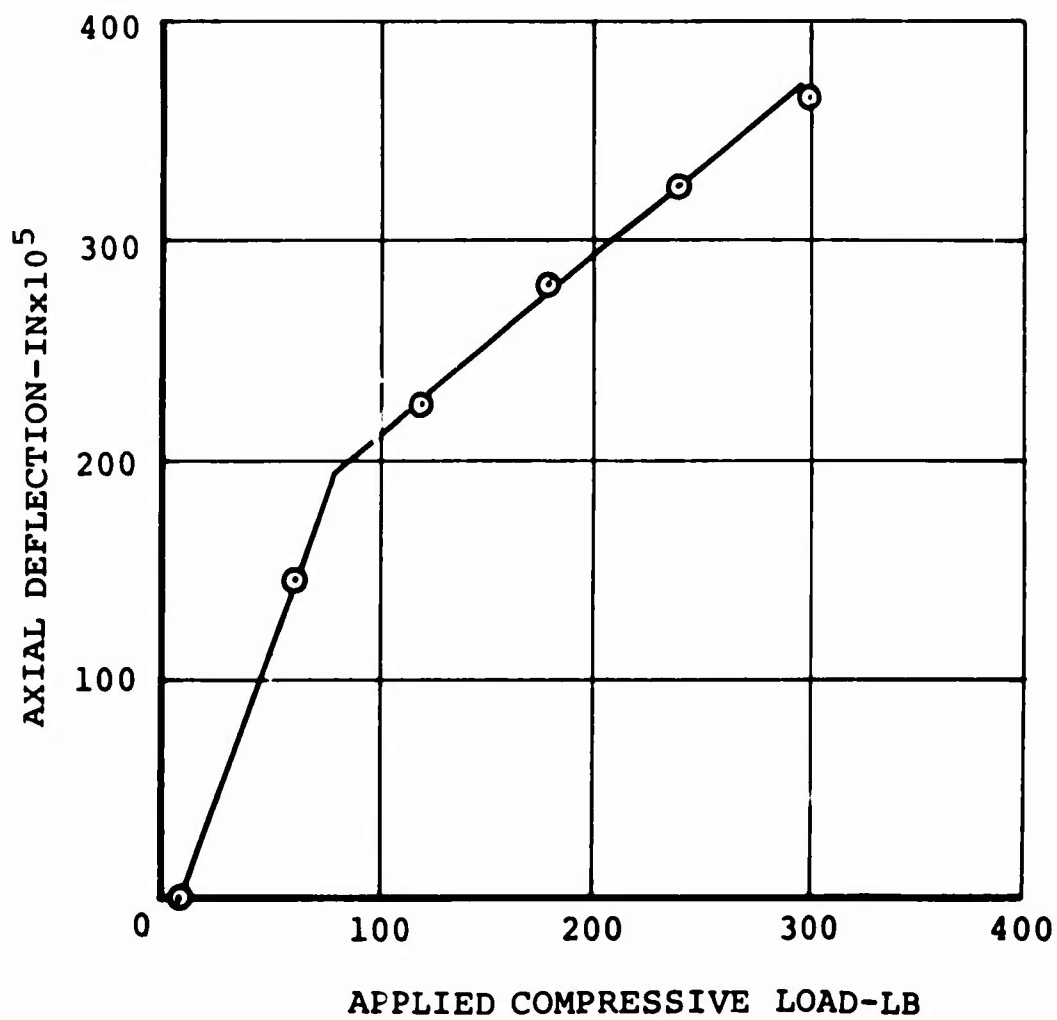
FIGURE 32b. MODIFIED VZ-2 PITCH LINK AXIAL DEFLECTION
IN COMPRESSION.
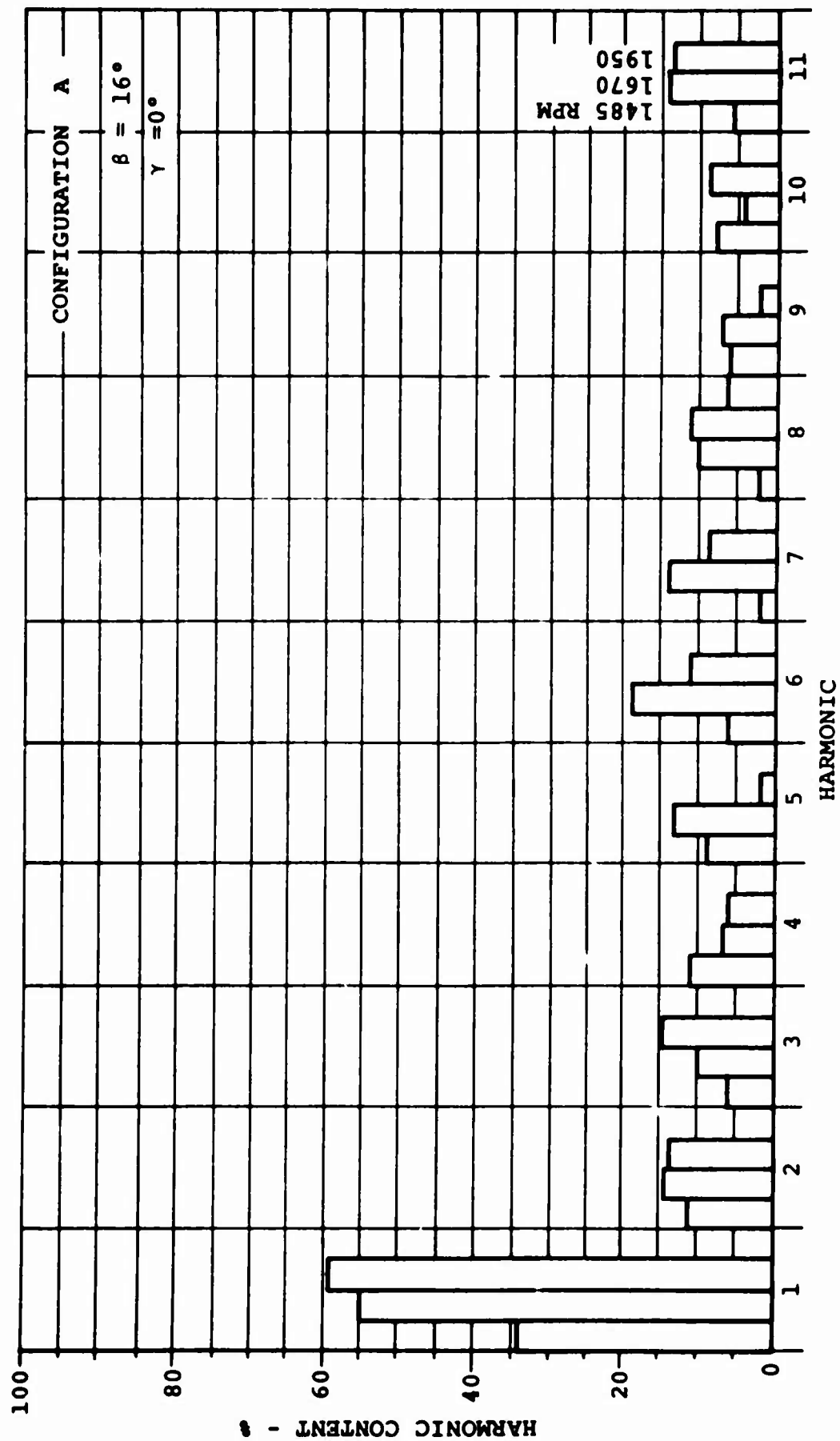
FIGURE 33a.   HARMONIC ANALYSIS OF OSCILLATORY PITCH
LINK LOAD, CONFIGURATION A.
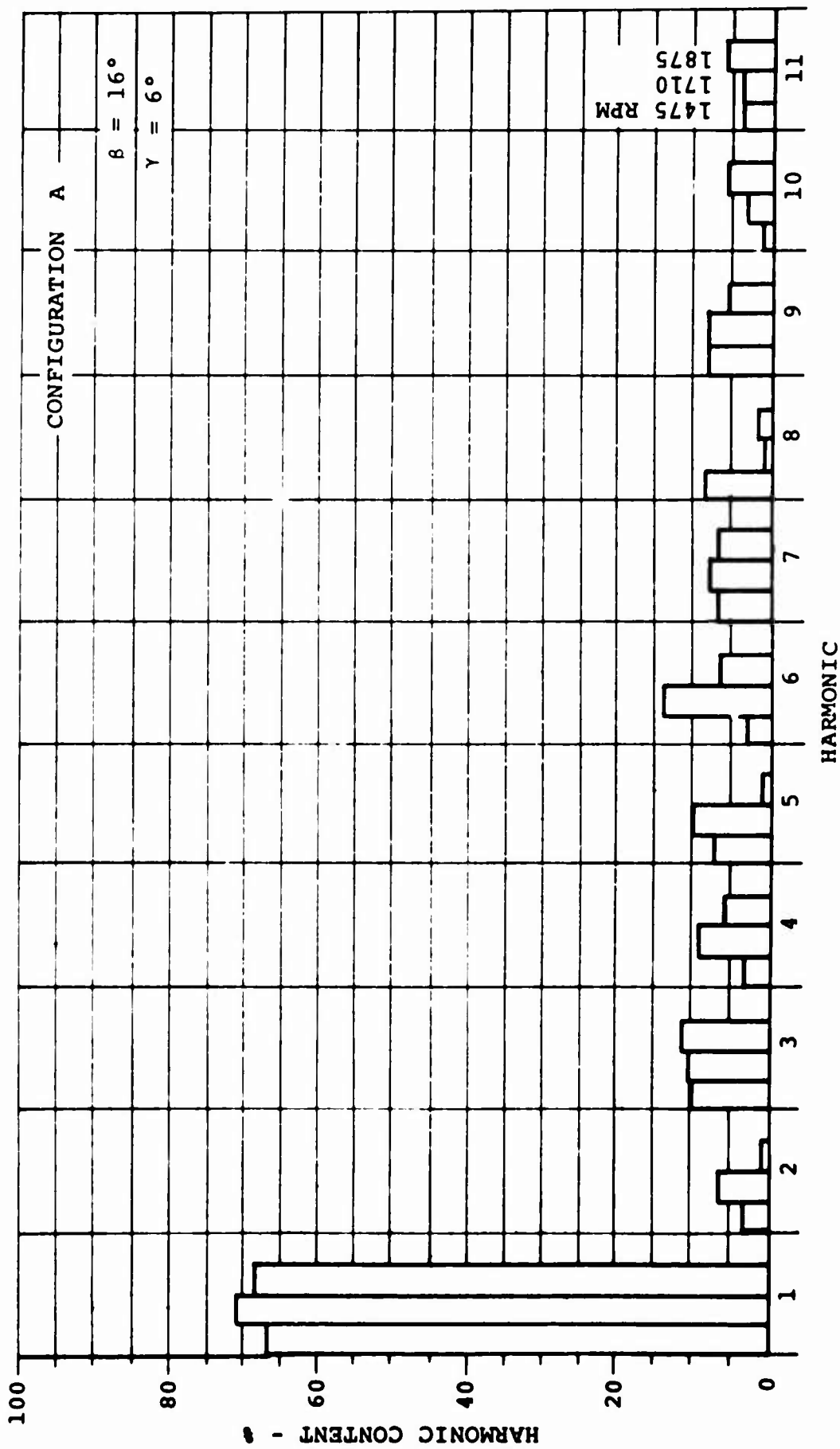
FIGURE 33b. HARMONIC ANALYSIS OF OSCILLATORY PITCH
LINK LOAD, CONFIGURATION A.

83
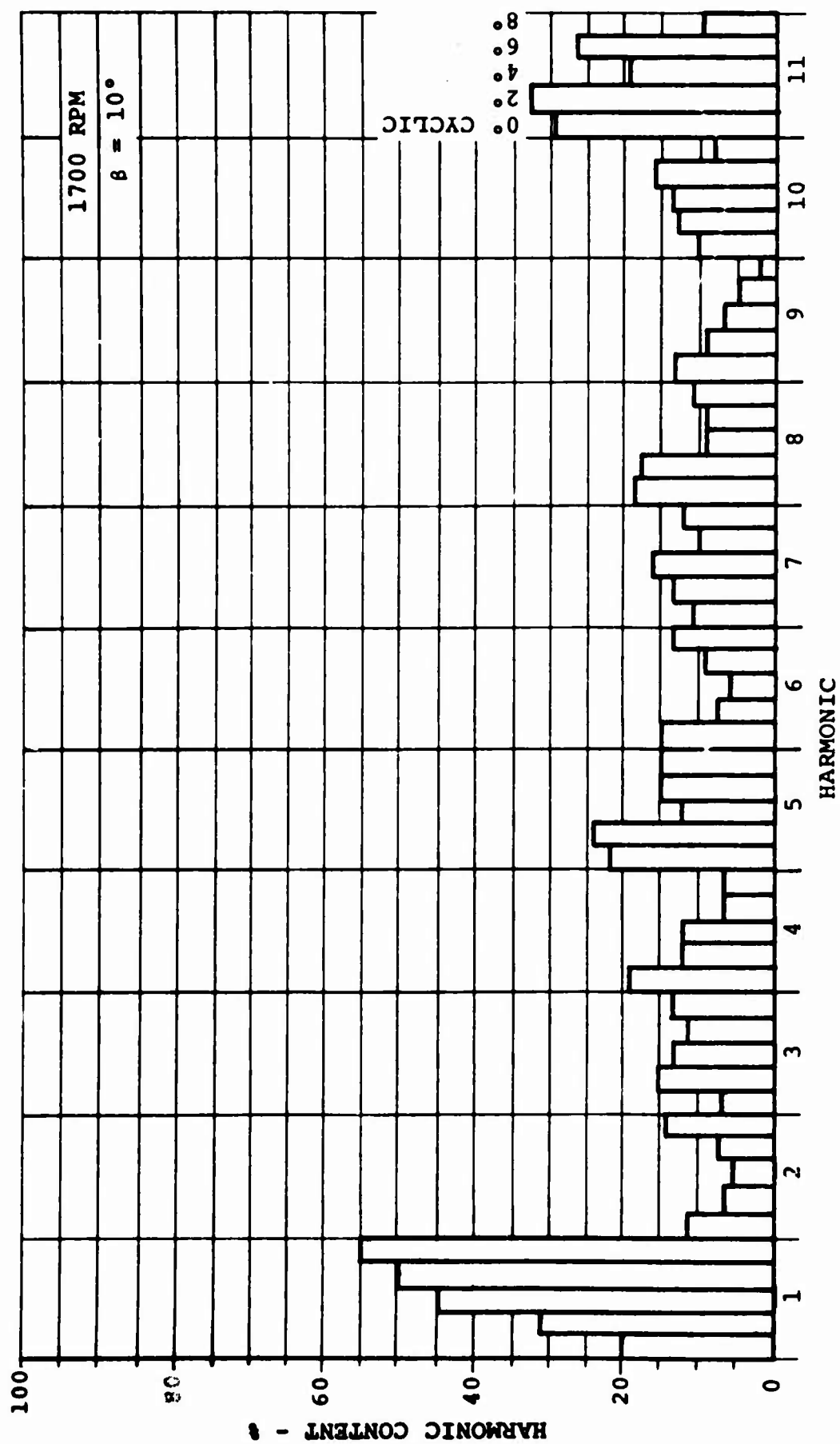
FIGURE 33c.   HARMONIC ANALYSIS OF OSCILLATORY PITCH
LINK LOAD, CONFIGURATION A.
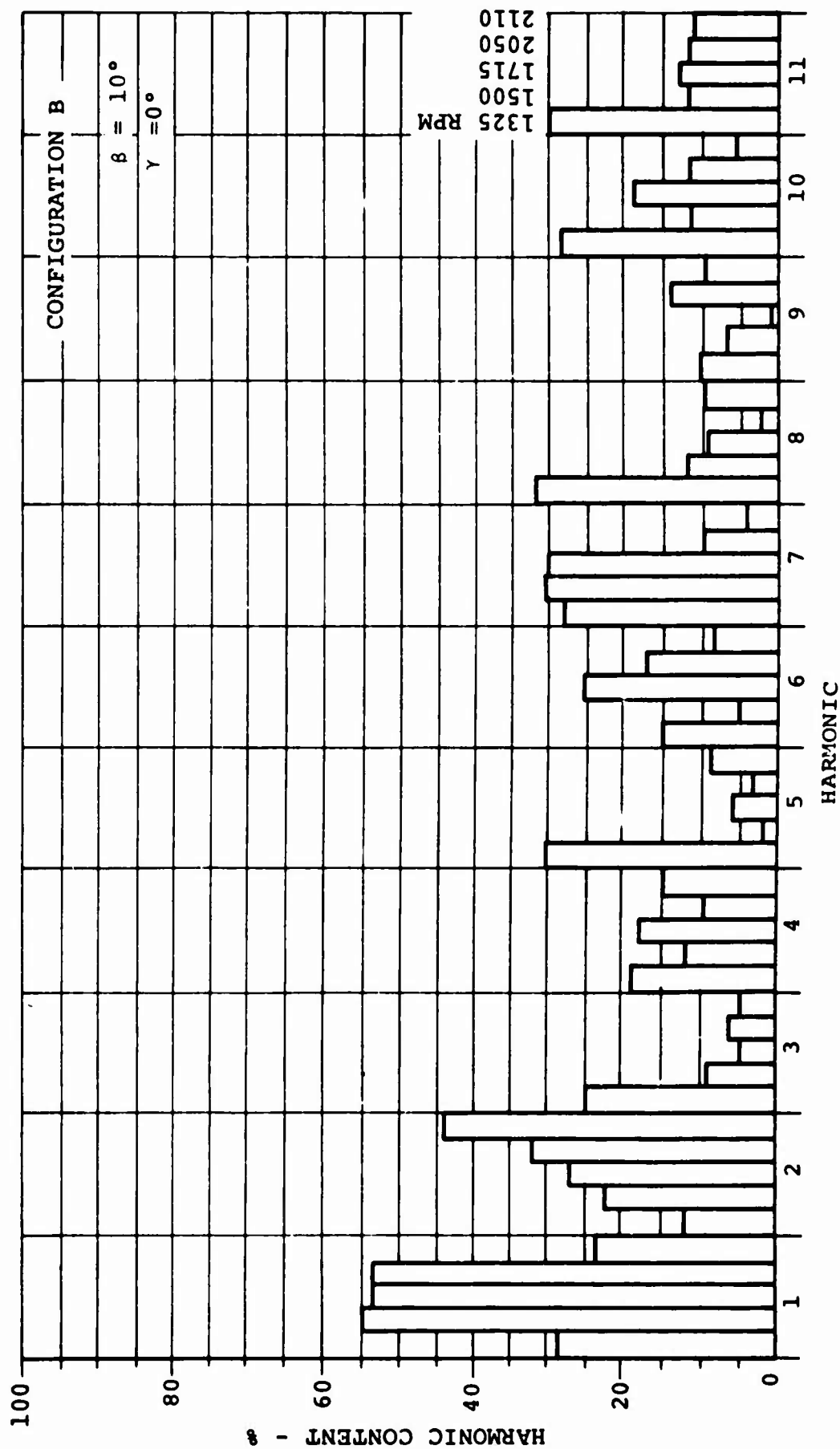
FIGURE 33d. HARMONIC ANALYSIS OF OSCILLATORY PITCH LINK LOAD, CONFIGURATION B.
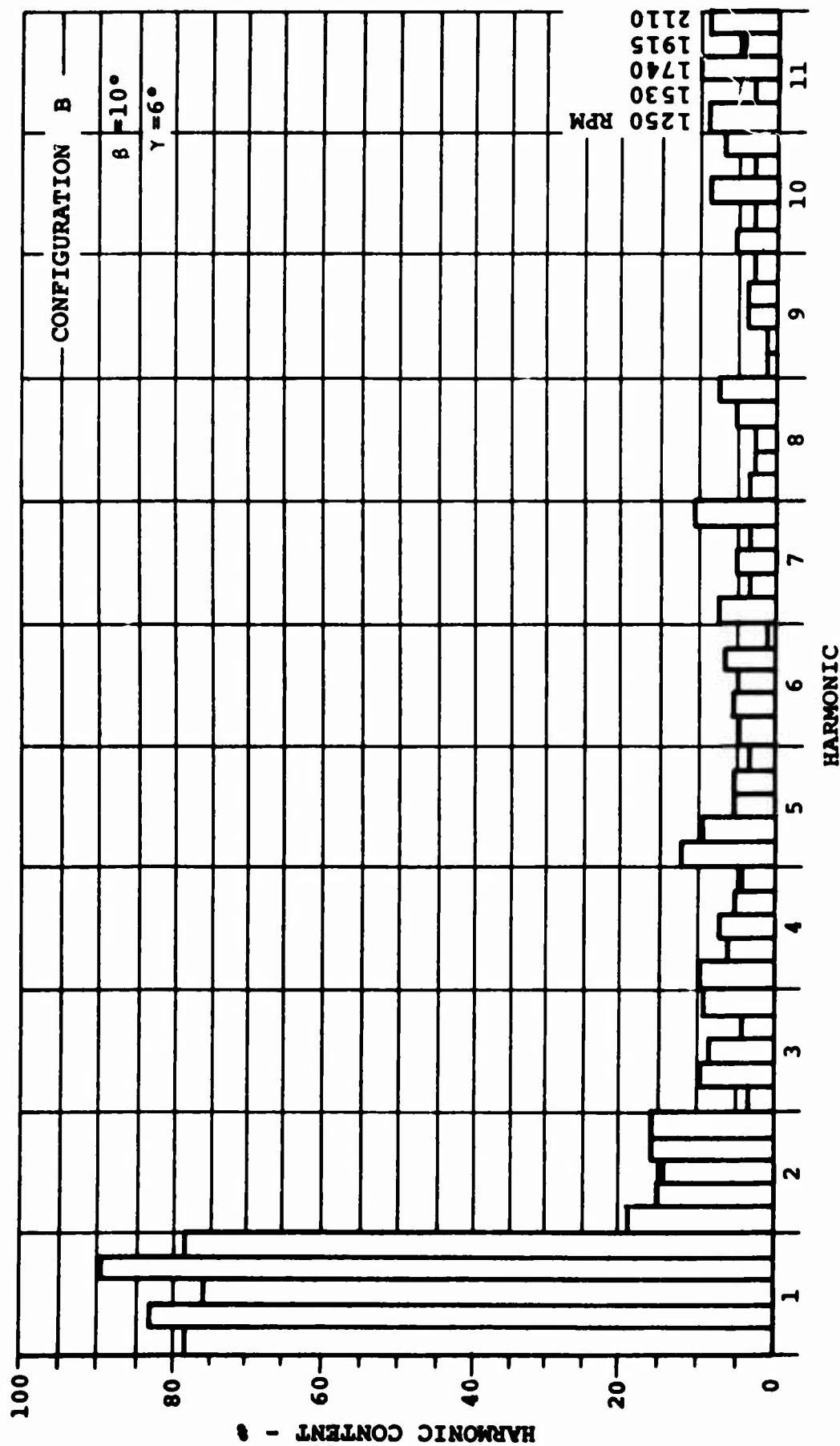
FIGURE 33e. HARMONIC ANALYSIS OF OSCILLATORY PITCH
LINK LOAD, CONFIGURATION B.
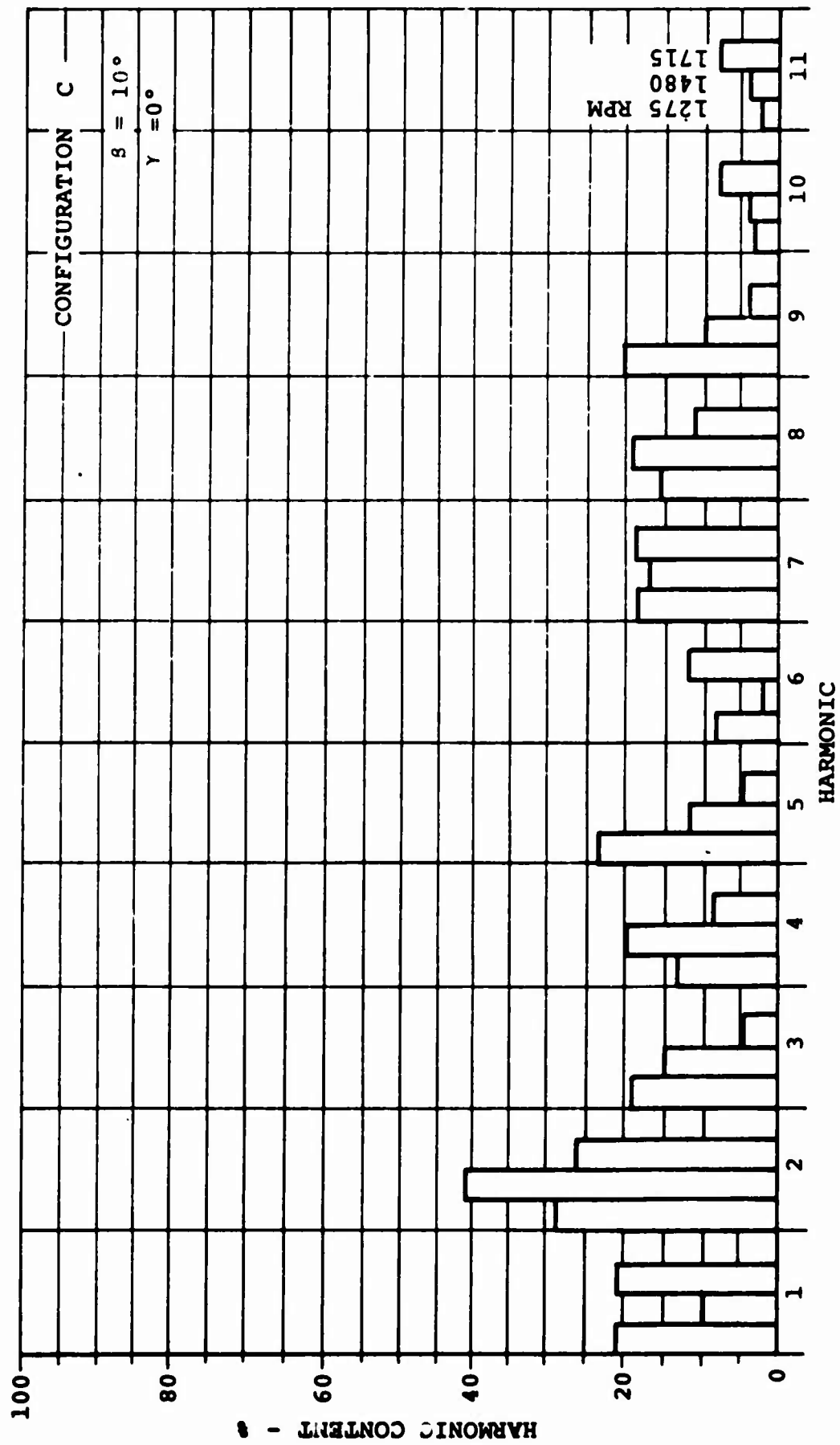
FIGURE 33f. HARMONIC ANALYSIS OF OSCILLATORY PITCH LINK LOAD, CONFIGURATION C.

87
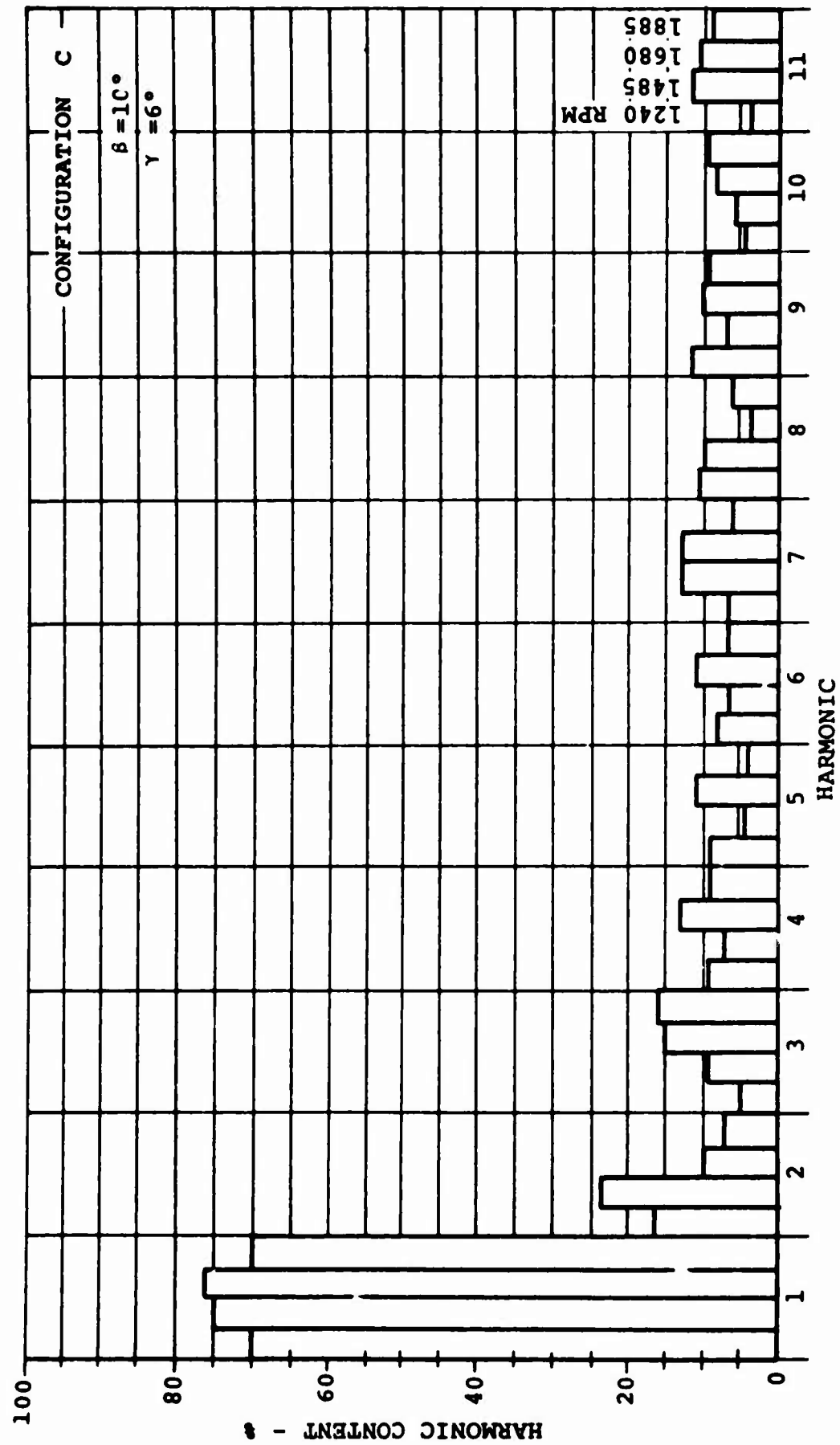
FIGURE 33g. HARMONIC ANALYSIS OF OSCILLATORY PITCH LINK LOAD, CONFIGURATION C.

88
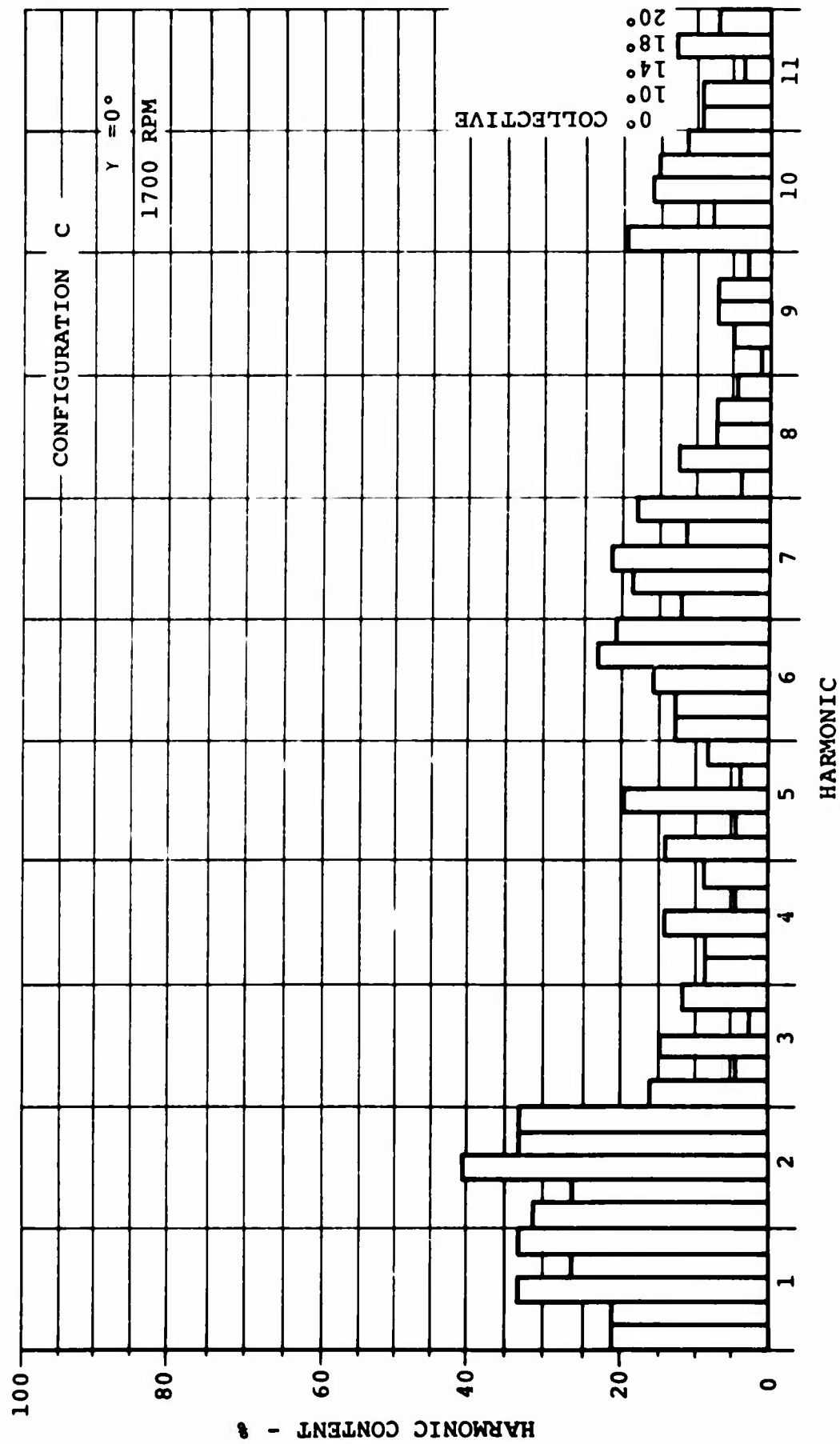
FIGURE 33h. HARMONIC ANALYSIS OF OSCILLATORY PITCH
LINK LOAD, CONFIGURATION C.

89
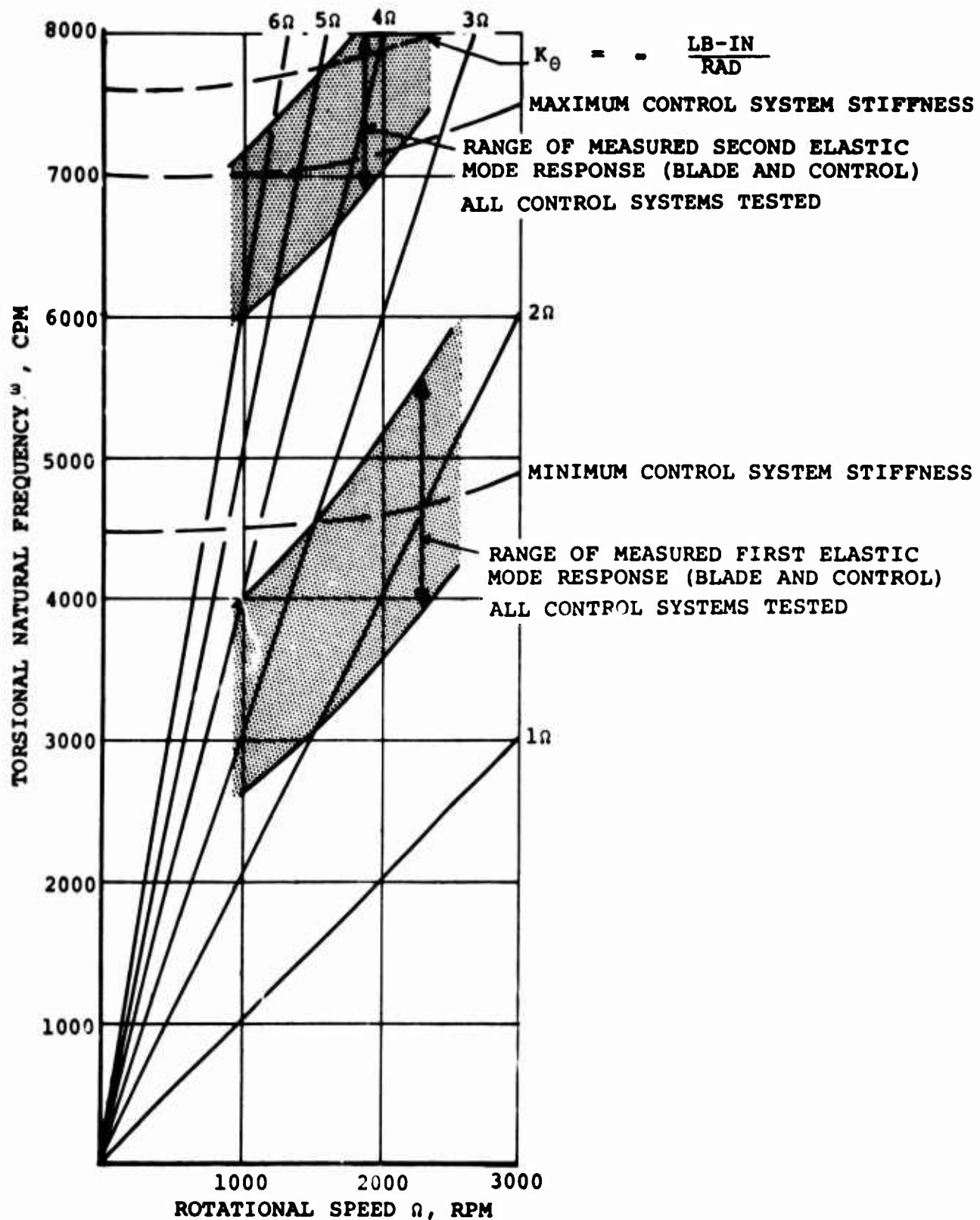
FIGURE 34.   TORSIONAL NATURAL FREQUENCY SPECTRUM-
PREDICTED BLADE-CONTROL SYSTEM FREQUENCIES
AS FUNCTIONS OF CONTROL SYSTEM STIFFNESS
LIMITS, COMPARED WITH MEASURED ELASTIC
MODAL RESPONSE.

90
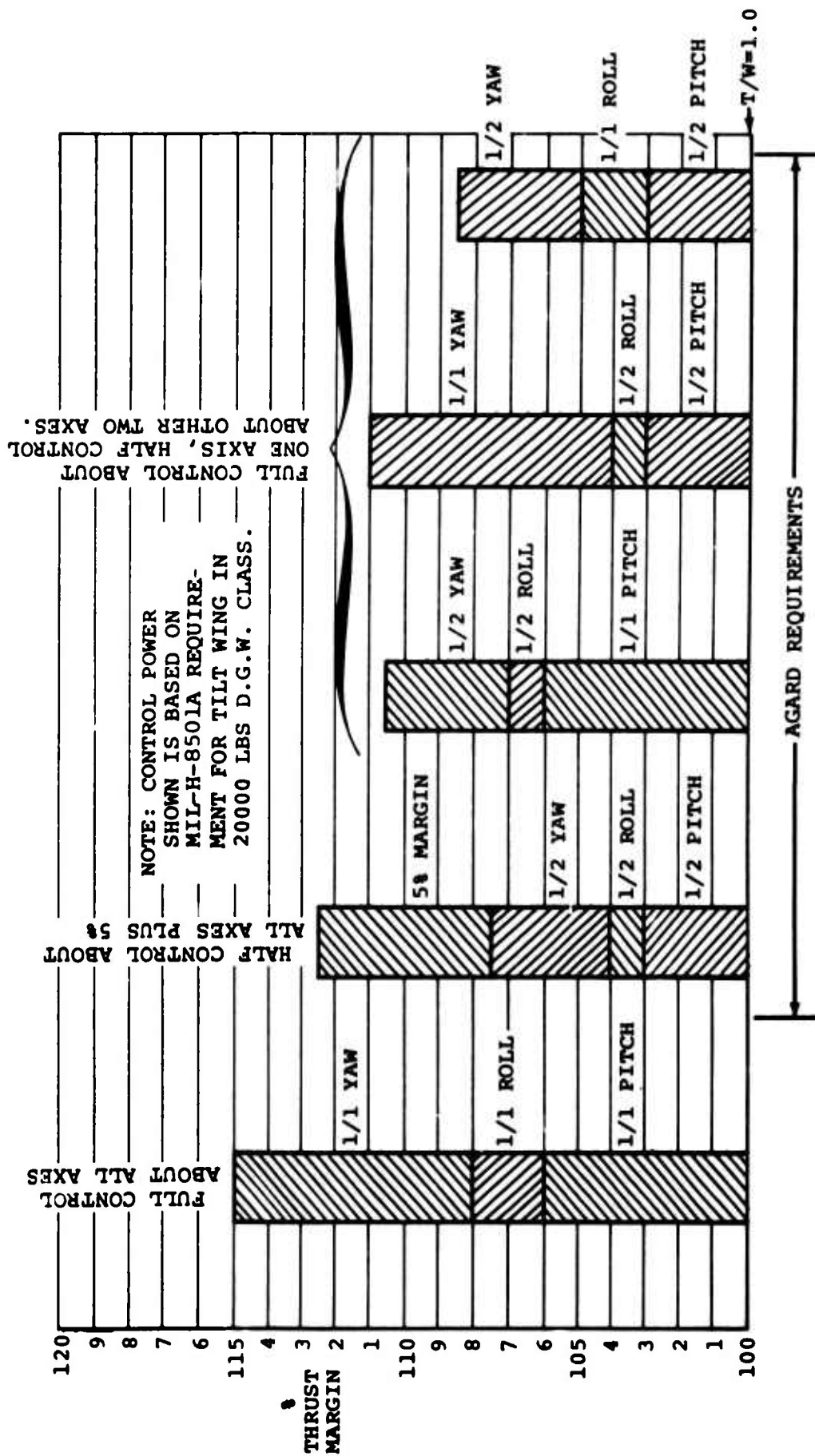
FIGURE 35. REQUIRED THRUST MARGINS FOR CONTROL SYSTEM OPERATION IN HOVER, OUT OF GROUND EFFECT.

91

REFERENCES

1. Miller, R.H., _Rotor Blade Harmonic Air Loading_, I.A.S. paper 62-82, January 1962.

2. _A Test Apparatus For Small Rotorcraft_, Vol. 1, Development and Operational Checkout - ASTIA No. AD235202 - Cornell Aero Lab., Inc., Report No. S6-1195-S-3, November 1959.

3. Fry, B.L., _Static Test of Monocyclic Control on a Full-Scale Boeing-Vertol 76 Rigid Propeller_, The Boeing Company, R-339, Volume I, December 1963.

4. Mort, K.W., and P.F. Yaggy, _Aerodynamic Characteristics of a Full-Scale Propeller Tested With Both Rigid and Flapping Blades and With Cyclic Pitch Control_ - NASA TN-D-1774, April 1963.

5. NASA Conference on V/STOL Aircraft - A Compilation of the Papers Presented. Page 87, Ground Interference Effects - R.O. Shade, November 1960.

6. Davenport, F.J., _Analysis of Propeller & Rotor Performance in Static and Axial Flight by an Explicit Vortex Influence Technique_, The Boeing Company, R-372, February 1965.

7. de Decker, R.W., _An Investigation of Tilt-Wing Hover Yaw Control Devices_, The Boeing Company, R-421, July 1, 1965.

8. AGARD (NATO), _Recommendations for V/STOL Handling Qualities_, R-408, November 1962.

9. Miles, Alfred S., and Joseph S. Newell, _Aircraft Structures_, Volume II, Second Edition, John Wiley and Sons, Inc., 1938.

10. Fry, B.L., _Aerodynamic Tests at Low Speed and in Ground Effect of the Boeing-Vertol 147 Tilt-Wing Powered Model on the Mobile Test Facility_, The Boeing Company, R-339, Volume II.

APPENDIX I

THEORETICAL ANALYSIS

Moment Due to Monocyclic Blade Angle in Hovering Flight

$\Omega = 180°$

$\Omega = 270°$ $\Omega = 90°$

$\Omega = 0°$
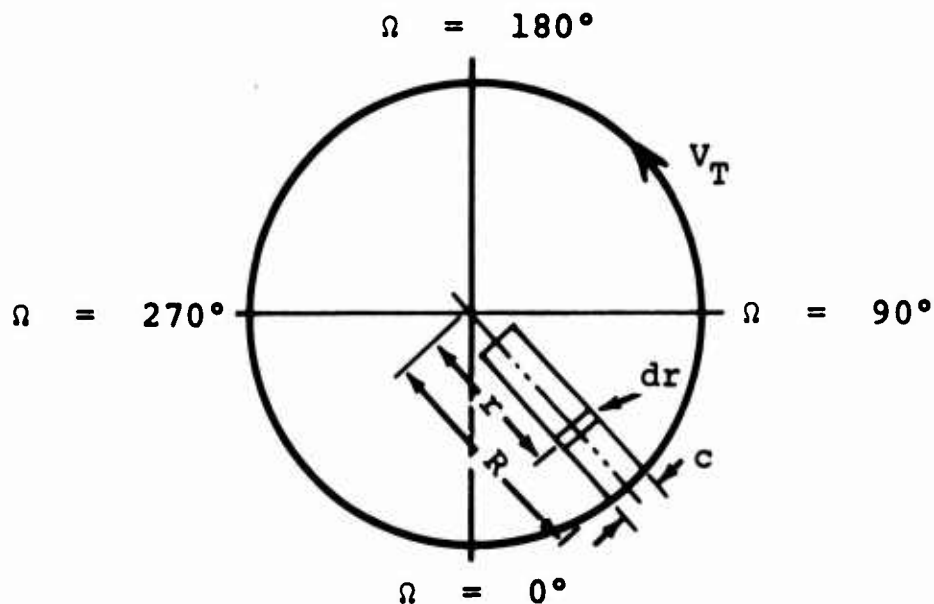
a = average slope of blade lift curve, 1/rad

γ = monocyclic angle, rad

ρ = density, slug/ft^3

B = number of blades

σ = propeller solidity = 0.254

C_T = propeller thrust coefficient = $\dfrac{T}{\rho n^2 D^4}$

Ω = azimuth angle, deg

From simple blade element theory (which neglects induced velocity at the blade):

For a change in blade pitch of $\gamma \sin \Omega$

$$\Delta\text{Lift on element} = (a)\ (\gamma \sin \Omega)\ (\tfrac{1}{2}\rho V_T^2)\ \left(\frac{r^2}{R^2}\right)\ (c)\ (dr)$$

$$\Delta M \text{ due to } \Delta\text{Lift} = (a)\ (\gamma \sin \Omega)\ (\tfrac{1}{2}\rho V_T^2)\ \left(\frac{r^2}{R^2}\right)\ )c)\ (dr)$$

$$(r)\ (\sin \Omega)$$

95

Then integrating over the whole disc:

$$M = (a)\ (\gamma)\ (\tfrac{1}{2}\rho V_T^2)\ (\tfrac{1}{R^2})(\tfrac{1}{2\pi})\ (c)\ (B)\ \int_0^{2\pi}\int_0^R r^3\sin^2\Omega\, dr\, d\Omega$$

$$= \frac{1}{16}\ \rho\ a\ B\ c\ R^2\ V_T^2\ \gamma$$

$$\frac{\delta M}{\delta\gamma} = \frac{1}{16}\ \rho\ a\ B\ c\ R^{\wedge}\ V_T^2$$

Then
$$\frac{\delta C_M}{\delta\gamma} = \frac{a\sigma\ \pi^3}{128}$$

The correction for changes in the induced velocity at the blade is (from unsteady aerodynamics theory, see Reference 1):

$$\frac{M_\gamma\ \text{(unsteady theory)}}{M_\gamma\ \text{(simple theory)}} = \frac{1}{1 + \frac{\sigma a}{8\lambda_0}}, \text{where}\quad \lambda_0 = \sqrt{\frac{2\ C_T}{\pi^3}}$$

Combining the two theories and nondimensionalizing:

$$\frac{\delta C_M}{\delta\gamma} = \left[\frac{a\ \sigma\ \pi^3}{128}\right]\ \left[\frac{1}{1 + \frac{\sigma a}{8\lambda_0}}\right]$$

To obtain the moment offset in percent radius, the previous equation is rearranged:

$$\frac{\frac{\delta M}{\delta\gamma}}{TR} = \left[\frac{\frac{1}{16\pi}\ \rho\ a\ B\ c\ A\ V_T^2}{C_T\ \rho\ n^2\ D^4\ R}\right]\ \left[\frac{1}{1 + \frac{\sigma a}{8\lambda_0}}\right]$$

$$\frac{\frac{\delta M}{\delta\gamma}}{TR} = \left[\frac{c\ a\ B\ \pi^2}{64\ C_T\ R}\right]\ \left[\frac{1}{1 + \sigma\ a/8\lambda_0}\right]$$

96

APPENDIX II

MONOCYCLIC PROPELLER TEST

BEAM COLUMN ANALYSIS

The following analysis was carried out on both sets of
pitch links to determine the axial deflection under dynamic
loading. This was necessary because a static analysis
predicted no change in pitch link loads for the control
systems used, while the dynamic test data showed that there
were differences.

DEFLECTION ON BEAM COLUMN
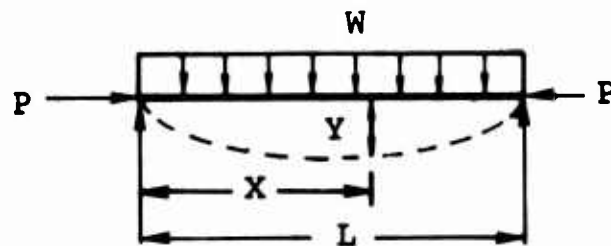
SYMBOLS

M_b = beam bending moment, in -lb
E = modulus of elasticity, lb/in^2
I = moment of inertia, in^4
W = running weight, lb/in
P = axial load on pitch links, lb
y = deflection due to bending, in
L = pitch link length, in
x = distance along pitch link, in
δ = axial deflection of pitch link, in

$$\frac{d^2y}{dx^2} = -\frac{M_b}{EI} \qquad\qquad j = \sqrt{\frac{EI}{P}}$$

$$M_b = Wj^2 \frac{\left[\cos\left(\frac{L}{j}\right) - 1\right]}{\sin\frac{L}{j}} \sin\frac{x}{j} - Wj^2 \cos\frac{x}{j} + W_j{}^2*$$

$$\frac{d^2y}{dx^2} = \frac{1}{EI}\left\{ Wj^2 \frac{\left[\cos\left(\frac{L}{j}\right) - 1\right]}{\sin\frac{L}{j}} \sin\frac{x}{j} - Wj^2 \cos\frac{x}{j} + Wj^2 \right\}$$

$$\frac{dy}{dx} = \frac{1}{EI}\left\{ -Wj^2 \frac{\left[\cos\left(\frac{L}{j}\right) - 1\right]}{\sin\frac{L}{j}} j \cos\frac{x}{j} - Wj^2 \sin\frac{x}{j} + \right.$$

$$\left. Wj^2 x + C_1 \right\}$$

$$y = \frac{1}{EI}\left\{ -Wj^2 \frac{\left[\cos\left(\frac{L}{j}\right) - 1\right]}{\sin\frac{L}{j}} j^2 \sin\frac{x}{j} + \right.$$

$$\left. Wj^4 \cos\frac{x}{j} + \frac{W}{2} j^2 x^2 + C_1 x + C_2 \right\}$$

$$y(o) = 0$$

$$0 = \frac{1}{EI}\left[Wj^4 + C_2 \right]$$

$$C_2 = -Wj^4$$

*Reference 9, pages 90, 91, and 92.

$$y(L) = 0$$

$$0 = \frac{1}{EI}\left\{ -Wj^4\left[\cos\left(\frac{L}{j}\right) - 1\right] + Wj^4 \cos\frac{L}{j} + \right.$$

$$\left. \frac{W}{2}j^2 L^2 + C_1 L - Wj^4 \right\}$$

$$= \frac{1}{EI}\left[\frac{W}{2} j^2 L^2 + C_1 L \right]$$

$$C_1 = -\frac{W}{2}j^2 L$$

$$y = \frac{1}{EI}\left\{ -Wj^4 \frac{\left[\cos\left(\frac{L}{j}\right) - 1\right]}{\sin\frac{L}{j}} \sin\frac{x}{j} + \right.$$

$$\left. Wj^4 \cos\frac{x}{j} + \frac{W}{2}j^2 x^2 - \frac{W}{2}j^2 Lx - Wj^4 \right\}$$

$$y\left(\frac{L}{2}\right) = \frac{1}{EI}\left\{ -Wj^4 \frac{\left[\cos\left(\frac{L}{j}\right) - 1\right]}{\sin\frac{L}{j}} \sin\frac{L}{2j} + \right.$$

$$\left. Wj^4 \cos\frac{L}{2j} + \frac{W}{8}j^2 L^2 - \frac{W}{4}j^2 L^2 - Wj^4 \right\}$$

$$y\left(\frac{L}{2}\right) = \frac{1}{EI}\left\{ -Wj^4 \frac{\left[\cos\left(\frac{L}{j}\right) - 1\right]}{\sin\frac{L}{j}} \sin\frac{L}{2j} + \right.$$

$$\left. Wj^4 \left[\cos\left(\frac{L}{2j}\right) - 1\right] - \frac{W}{8}j^2 L^2 \right\}$$

$$Y\left(\frac{L}{2}\right) = \frac{Wj^2}{EI} \left\{ \frac{-j^2 \left[\cos\left(\frac{L}{j}\right) - 1\right] \sin\frac{L}{2}}{\sin\frac{L}{j}} + \right.$$

$$\left. j^2 \left[\cos\left(\frac{L}{2j}\right) - 1\right] - \frac{L^2}{8} \right\}$$

VZ-2 Pitch Link

$$C.F. = \left(\frac{2\pi}{60}\right)^2 = (RPM)^2 \left(\frac{7.25}{386}\right) \quad (wt/in)$$

$$Wt/In = .052$$

Dist. from center of rotation to pitch link = 7.25 in.

Run 328

$$RPM = 1500$$

$$C.F. = \left(\frac{2\pi}{60}\right)^2 (1500)^2 \left(\frac{7.25}{386}\right) (.052)$$

$$= 26.0 \ lb/in$$

$$I = .00667 \ in^4$$

$$P = 94 \ lb$$

$$j = \sqrt{\frac{EI}{P}} = \sqrt{\frac{10^7 \times .00667}{94}} = 26.6 \ in$$

$$\cos\left(\frac{L}{j}\right) = \cos\frac{12.2}{26.6} = \cos .460 = .896$$

100

$$\sin\left(\frac{L}{j}\right) = \sin .460 = .444$$

$$\sin\left(\frac{L}{2j}\right) = \sin \frac{12.2}{53.2} = \sin .230 = .228$$

$$\cos\left(\frac{L}{2j}\right) = \cos .230 = .974$$

$$y\left(\frac{L}{2}\right) = \frac{710 \times 26}{10^7 \times .00667} \left[\frac{- 710 \ (.896 - 1)(.228)}{.444} + \right.$$

$$\left. 710 \ (.974 - 1) - \frac{(12.2)^2}{8} \right]$$

$$y\left(\frac{L}{2}\right) = .277 \left[38.0 - 18.4 - 18.6 \right]$$

$$= .28 \text{ in}$$

It will now be assumed that the foreshortening of the column, or compressive strain, is negligible under the axial compression load. Therefore, the foreshortening of the column under the combined beam-column loading, x, can be determined for a curved beam whose length along the curved surface is L, and whose maximum lateral displacement is Y(L/2) or 0.28 inch.

$$L \quad = \int\limits_{0}^{L} dS \quad = \int\limits_{0}^{L'} dx \sqrt{1 + \left(\frac{dy}{dx}\right)^2}$$

$$y \quad = \quad .28 \sin \frac{\pi x}{L'}$$

$$\frac{dy}{dx} \quad = \quad .28 \frac{\pi}{L'} \cos \frac{\pi x}{L'}$$

$$\left(\frac{dy}{dx}\right)^2 = \quad .078 \frac{\pi^2}{L'^2} \cos^2 \frac{\pi x}{L'}$$

$$L \quad = \int\limits_{0}^{L} \left(1 + .078 \frac{\pi^2}{L'^2}\cos^2 \frac{\pi x}{L'}\right)^{\frac{1}{2}} dx$$

$$(1+c^2 x^2)^{\frac{1}{2}} = \quad 1 + \tfrac{1}{2} c^2 x^2 - \frac{c^4 x^4}{2 x 4} + \quad \text{(Higher-order terms neglected)}$$

$$L \quad = \int\limits_{0}^{L'} \left\{ 1 + \tfrac{1}{2}\left(.078 \frac{\pi^2}{L'^2}\right) \cos^2 \frac{\pi x}{L'} - \right.$$

$$\left. \frac{1}{8}\left[.078 \frac{\pi^2}{L'^2} \right]^2 \left(\cos^4 \frac{\pi x}{L'}\right) dx \right] \right\}$$

$$L \quad = \left\{ x + .039 \frac{\pi^2}{L'^2}\left[\frac{L'}{2\pi} \left(\frac{\pi}{L'} x + \right.\right.\right.$$

$$\left.\left.\left. \sin \frac{\pi x}{L'} \cos \frac{\pi x}{L'}\right)\right] \right\} \Bigg|_{0}^{L'}$$

$$L = L' + .039 \frac{\Pi^2}{L'^2} \left(\frac{L'}{2}\right), \text{ where } L = 12.2 \text{ in}$$

$$L = L' + .0195 \frac{\Pi^2}{L'}$$

Substituting L = 12.2 in the equation,

$$L'^2 - 12.2 \ L' + .192 = 0$$

Solving for L', using the quadratic formula,

$$L' = \frac{12.2 \pm \sqrt{12.2^2 - 4\ (.192)}}{2}$$

$$= \frac{12.2 \pm \sqrt{148.84 \quad .77}}{2}$$

$$= \frac{12.2 + 12.17}{2}$$

$$= 12.185 \text{ in}$$

$L-L' = \Delta x = .015$ in   (See sketch on page 101.)

$$.015 + \frac{P}{AE} = .015 + \frac{94 \times 12.2}{.112 \times 10^7}$$

$$= .015 + .00104$$

$$= .016 \text{ in}$$

"Beefed Up" Pitch Link

$$C.F. = \left(\frac{2\pi}{60}\right)^2 (RPM)^2 \left(\frac{7.25}{386}\right)^2 (wt/in), \quad wt/in = .0987$$

Run 220

$$RPM = 1500$$

$$C.F. = \left(\frac{2\pi}{60}\right)^2 (1500)^2 \left(\frac{7.25}{386}\right)^2 (.0987)$$

$$= 45.6 \ lb/in$$

$$P = 160 \ lb$$

$$EI = .617 \times 10^6 \ lb\text{-}in^2$$

$$j = \sqrt{\frac{EI}{P}} = \sqrt{\frac{.617 \times 10^6}{160}} = 62.2 \ in$$

$$\cos\left(\frac{L}{j}\right) = \cos\frac{12.5}{62.2} = \cos .201 = .980$$

$$\sin\left(\frac{L}{j}\right) = \sin .201 = .201$$

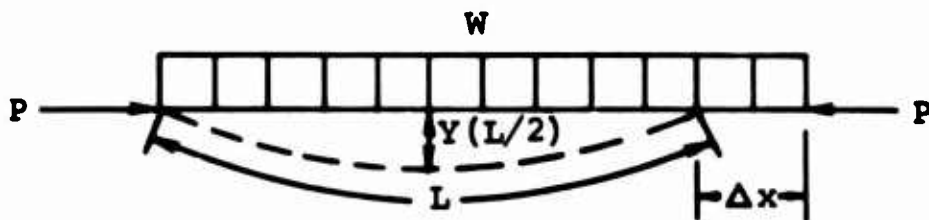$$\sin\left(\frac{L}{2j}\right) = \sin\frac{12.5}{124.4} = \sin .101 = .102$$

$$\cos\left(\frac{L}{2j}\right) = \cos .101 = .995$$

$$y\left(\frac{L}{2}\right) = \frac{3860 \times 45.6}{.617 \times 10^6} \left[\frac{-3860 \ (.980 - 1)(.102)}{.201} + \right.$$

$$\left. 3860 \ (.995 - 1) - \frac{(12.5)}{8}^2 \right]$$

$$y\left(\frac{L}{2}\right) = .286 \left[39.2 - 19.3 - 19.6 \right]$$

$$= .09 \text{ In.}$$

$$y = .09 \sin \frac{\pi x}{L'}$$

$$\frac{dy}{dx} = .09 \ \frac{\pi}{L'} \ \cos \frac{\pi x}{L'}$$

$$\left(\frac{dy}{dx}\right)^2 = .0081 \ \frac{\pi^2}{L'^2} \ \cos^2 \frac{\pi x}{L'}$$

$$L = \int_0^{L'} \left(1 + .0081 \frac{\pi^2}{L'^2} \ \cos^2 \frac{\pi x}{L} \right)^{\frac{1}{2}} dx$$

$$L = \left\{ x + .0041 \frac{\pi^2}{L'^2} \left[\frac{L'}{2\pi} \left(\frac{\pi}{L'} x + \sin \frac{\pi x}{L'} \ \cos \frac{\pi x}{L} \right) \right] \right\} \Big|_0^{L'}$$

$$L = L' + .0041 \frac{\pi^2}{L'^2} \left(\frac{L'}{2} \right)$$

$$L = 12.5 \text{ In.}$$

105

$$L = L' + .0020 \ \frac{\Pi^2}{L'}$$

$$12.5 \ L' = L'^2 + .020$$

$$L'^2 - 12.5 \ L' + .020 = 0$$

$$L' = \frac{12.5 + \sqrt{12.5^2 - 4 \ (.020)}}{2}$$

$$= \frac{12.5 \pm \sqrt{156.25 - .08}}{2}$$

$$L' = \frac{12.5 + 12.49}{2}$$

$$= 12.495$$

$$L-L' = .005 \ \text{in}$$

$$.005 + \frac{P\ell}{AE} = .005 + \frac{160 \ \times \ 12.5}{.224 \ \times \ 10^7}$$

$$= .005 + .00089$$

$$= .006 \ \text{in}$$

THRUST MARGINS REQUIRED IN HOVER DUE TO CONTROL

Application of control power about any axis induces either direct or indirect thrust losses. The thrust losses and control power due to yaw control were found in the test of Reference 7, while those due to roll control were calculated from typical VTOL propeller C_T, C_P, and β curves. The thrust loss due to roll control stems from operation at differential blade angles above and below the blade angle at which maximum figure of merit occurs. The results are summarized in Table IV for hover, out of ground effect. The angular accelerations necessary to meet the requirements of MIL-H-8501A with the specified damping, and the maximum available angular accelerations with zero damping are shown for a tilt-wing aircraft in the 20,000-pound-design-gross-weight class. Thrust losses resulting from each are shown in this table.

	MIL-H-8501A Reqmts (With Damping)		Maximum Available	
Control	Angular Acc (rad/sec^2)	Thrust Loss (deg)	Angular Acc (rad/sec^2)	Thrust Loss (deg)
Roll	0.60	2	0.75	2.5
Pitch*	0.41	6	0.70**	11.5
Yaw	0.58	7	0.62	9.0

TABLE IV

*Pitch control includes the requirement for trimming a $\pm$.05-chord center of gravity shift.

**Maximum available = 25-percent thrust offset with optimum blade efficiency.

The Advisory Group for Aeronautical Research and Development (AGARD) of NATO has formulated requirements for vertical thrust margins in hover, out of ground effect, with various control

power requirements (Reference 8). These requirements are:

    a. Half control power about all axes at $T/W = 1.05$.

    b. Full control about one axis and half control about the other two at $T/W = 1.00$.

The resulting thrust margins are shown in Figure 35. Full control has been assumed to be equal to the MIL-H-8501A requirements with damping. Thrust loss due to full control about all axes is shown for comparison. It can be seen in Figure 35 that to meet the above AGARD recommendations, 12.5-percent and 11-percent thrust margin, respectively, are needed.

DOCUMENT CONTROL DATA - R&D

(Security classification of title, body of abstract and indexing annotation must be entered when the overall report is classified)

1. ORIGINATING ACTIVITY (Corporate author) Vertol Division The Boeing Company Morton, Pennsylvania	2a. REPORT SECURITY CLASSIFICATION Unclassified
	2b. GROUP N/A

3. REPORT TITLE

INVESTIGATION OF AN ISOLATED MONOCYCLIC V/STOL PROPELLER
PERFORMANCE AND OSCILLATORY STRESS

4. DESCRIPTIVE NOTES (Type of report and inclusive dates)

Final

5. AUTHOR(S) (Last name, first name, initial)

de Decker, R. W.

6. REPORT DATE February 1966	7a. TOTAL NO OF PAGES 108	7b. NO OF REFS 10
8a. CONTRACT OR GRANT NO. DA44-177-AMC-319(T) b. PROJECT NO. c. Task 1P121401A14178 d.	9a. ORIGINATOR'S REPORT NUMBER(S) USAAVLABS Technical Report 65-80	
	9b. OTHER REPORT NO(S) (Any other numbers that may be assigned this report) R-432	

10. AVAILABILITY/LIMITATION NOTICES

Distribution of this document is unlimited.

11. SUPPLEMENTARY NOTES	12. SPONSORING MILITARY ACTIVITY U.S. Army Aviation Materiel Laboratories Fort Eustis, Virginia 23604

13. ABSTRACT

This report covers an investigation of single-axis cyclic (mono-cyclic) control of a rigid V/STOL propeller. It discusses control power at high cyclic angles, the effect of control application on power, and the effects on blade dynamic behavior of variations in control system stiffness.

Data were acquired from static tests made on a three-bladed, high-solidity model propeller of six-foot diameter, mounted on the Army-Cornell Apparatus for Rotorcraft Tests (CART).

It was found that control powers generated were completely adequate for longitudinal control of typical tilt-wing aircraft, and that control moment is linear with cyclic input. For trim conditions, the increase in power required is of the order of one percent. Power increases for control become significant only during high-rate maneuver conditions. No unusual control system load conditions were encountered during the course of this investigation.

DD FORM 1473 1 JAN 64

14. KEY WORDS	LINK A		LINK B		LINK C	
	ROLE	WT	ROLE	WT	ROLE	WT
Monocyclic Propeller Performance						

INSTRUCTIONS

1. **ORIGINATING ACTIVITY:** Enter the name and address of the contractor, subcontractor, grantee, Department of Defense activity or other organization (*corporate author*) issuing the report.

2a. **REPORT SECURITY CLASSIFICATION:** Enter the overall security classification of the report. Indicate whether "Restricted Data" is included. Marking is to be in accordance with appropriate security regulations.

2b. **GROUP:** Automatic downgrading is specified in DoD Directive 5200.10 and Armed Forces Industrial Manual. Enter the group number. Also, when applicable, show that optional markings have been used for Group 3 and Group 4 as authorized.

3. **REPORT TITLE:** Enter the complete report title in all capital letters. Titles in all cases should be unclassified. If a meaningful title cannot be selected without classification, show title classification in all capitals in parenthesis immediately following the title.

4. **DESCRIPTIVE NOTES:** If appropriate, enter the type of report, e.g., interim, progress, summary, annual, or final. Give the inclusive dates when a specific reporting period is covered.

5. **AUTHOR(S):** Enter the name(s) of author(s) as shown on or in the report. Enter last name, first name, middle initial. If military, show rank and branch of service. The name of the principal author is an absolute minimum requirement.

6. **REPORT DATE:** Enter the date of the report as day, month, year; or month, year. If more than one date appears on the report, use date of publication.

7a. **TOTAL NUMBER OF PAGES:** The total page count should follow normal pagination procedures, i.e., enter the number of pages containing information.

7b. **NUMBER OF REFERENCES:** Enter the total number of references cited in the report.

8a. **CONTRACT OR GRANT NUMBER:** If appropriate, enter the applicable number of the contract or grant under which the report was written.

8b, 8c, & 8d. **PROJECT NUMBER:** Enter the appropriate military department identification, such as project number, subproject number, system numbers, task number, etc.

9a. **ORIGINATOR'S REPORT NUMBER(S):** Enter the official report number by which the document will be identified and controlled by the originating activity. This number must be unique to this report.

9b. **OTHER REPORT NUMBER(S):** If the report has been assigned any other report numbers (*either by the originator or by the sponsor*), also enter this number(s).

10. **AVAILABILITY/LIMITATION NOTICES:** Enter any limitations on further dissemination of the report, other than those imposed by security classification, using standard statements such as:

(1) "Qualified requesters may obtain copies of this report from DDC."

(2) "Foreign announcement and dissemination of this report by DDC is not authorized."

(3) "U. S. Government agencies may obtain copies of this report directly from DDC. Other qualified DDC users shall request through

_____ ."

(4) "U. S. military agencies may obtain copies of this report directly from DDC. Other qualified users shall request through

_____ ."

(5) "All distribution of this report is controlled. Qualified DDC users shall request through

_____ ."

If the report has been furnished to the Office of Technical Services, Department of Commerce, for sale to the public, indicate this fact and enter the price, if known.

11. **SUPPLEMENTARY NOTES:** Use for additional explanatory notes.

12. **SPONSORING MILITARY ACTIVITY:** Enter the name of the departmental project office or laboratory sponsoring (*paying for*) the research and development. Include address.

13. **ABSTRACT:** Enter an abstract giving a brief and factual summary of the document indicative of the report, even though it may also appear elsewhere in the body of the technical report. If additional space is required, a continuation sheet shall be attached.

It is highly desirable that the abstract of classified reports be unclassified. Each paragraph of the abstract shall end with an indication of the military security classification of the information in the paragraph, represented as (TS), (S), (C), or (U).

There is no limitation on the length of the abstract. However, the suggested length is from 150 to 225 words.

14. **KEY WORDS:** Key words are technically meaningful terms or short phrases that characterize a report and may be used as index entries for cataloging the report. Key words must be selected so that no security classification is required. Identifiers, such as equipment model designation, trade name, military project code name, geographic location, may be used as key words but will be followed by an indication of technical context. The assignment of links, rules, and weights is optional.

916—66